Distinct roles for the endosomal regulators Mtmr5 and Mtmr13 in axon radial sorting and myelination

By

Anna Elizabeth Mammel

A DISSERTATION

the Department of Cell and Developmental Biology
And the Oregon Health & Science University
School of Medicine
In partial fulfillment of
the requirement for the degree of

Doctor of Philosophy

May 2019

CERTIFICATE OF APPROVAL

This is to certify that the PhD Dissertation or Master's thesis of

Anna E Mammel

has been approved on May 22, 2019

_____
Mentor/Advisor, Fred Robinson, Ph.D.

_____
Member and Chair, Peter Mayinger, Ph.D.

_____
Member, Ben Emery, Ph.D.

_____
Member, Michael Cohen, Ph.D.

_____
Member, Kelly Monk, Ph.D.

Table of Contents

List of Figures

List of Abbreviations

CNS	Central Nervous System
PNS	Peripheral Nervous System
SC	Schwann cell
MBP	Myelin basic protein
PLP	Proteolipid protein
P0	Myelin protein zero
PMP22	Peripheral myelin protein 22
PMP2	Peripheral myelin protein 2
CNP	2'3'-cyclic nucleotide 3'-phosphodiesterase
MAG	Myelin associated glycoprotein
Caspr	Contactin-associated protein
Nfasc155	Neurofascin 155
Nfasc186	Neurofascin 186
NrCAM	Neuronal cell adhesion molecule
Na_v	voltage gated sodium channels
SLI	Schmidt-Lanterman incisures
SCP	Schwann cell precursors
Sox10	SRY (Sex Determining Region Y)-Box 10
Oct6/ POU3F1	POU Class 3 Homeobox 1
Krox20/EGR2	Early Growth Response 2
ErbB2/3	Erb-b2/3 receptor tyrosine kinase 2/3
Nrg1-III	Neuregulin 1 type III
Sox2	SRY (Sex Determining Region Y)-Box 2
Erk1/2	extracellular signaling related kinase 1/2
PI3K	phosphoinositide 3-kinase / PI 3-kinase
FAK	Focal adhesion kinase
JNK	c-Jun N-terminal kinase
N-WASP	Neural Wiskott-Aldrich Syndrome Protein
ILK	Integrin Linked Kinase
GTP/GDP	guanosine triphosphate / guanosine diphosphate
RhoA	Ras Homolog Family Member A
Cdc42	Cell Division Cycle 42
Rac1	Ras-Related C3 Botulinum Toxin Substrate 1
ROCK	Rho-Associated Protein Kinase
Arp2/3	Actin related protein 2/3
ERM	Ezrin Radixin Moesin
LIMK	LIM kinase
MLC	Myosin light chain II
MLCK	Myosin light chain kinase
GEF	Guanidine Exchange Factor
INF2	Inverted Formin 2
Dnm2	Dynamin 2
SH3TC2	SH3 Domain and Tetratricopeptide Repeats 2
PI	phosphoinositide
PI3P	phosphatidylinositol 3-phosphate
$PI(3,5)P_2$	phosphatidylinositol 3,5-diphosphate
PI4P	phosphatidylinositol 4-phosphate

$PI(4,5)P_2$	phosphatidylinositol 4,5-diphosphate
$PI(3,4,5)P_3$	phosphatidylinositol 3,4,5-triphosphate
PI5P	phosphatidylinositol 5-phosphate
PI4K	phosphoinositide 4-kinase / PI 4-kinase
FYVE	Fab1, YOTB, Vac1, and EEA1 homology
MVB	multi-vesicular body
VPS34	Vacuolar protein sorting 34
PIKFYVE	Phosphoinositide Kinase, FYVE-Type Zinc Finger Containing
FIG4	Factor-Induced Gene 4
MTMR	Myotubularin related protein
STAT3	Signal transducer and activator of transcription 3
MS	Multiple sclerosis
GBS	Guillain-Barre syndrome
CMT	Charcot-Marie-Tooth disease
MNCV	motor nerve conduction velocities
CMAP	compound muscle action potential amplitudes
LITAF/SIMPLE	lipopolysaccharide-induced tumor necrosis factor-alpha
Cx32	Connexin 32
GDAP1	ganglioside induced differentiation associated protein 1
NDRG1	N-Myc Downstream Regulated 1
PRX	periaxin
HK1	hexokinase 1
FRABIN	FGD1-related F-actin-binding protein
PH-GRAM	Pleckstrin Homology-Glucosyltransferase, Rab-like GTPase Activators and Myotubularins
DENN	differentially expressed in normal verse neoplastic
PDZ	PSD-95/Dlg/ZO-1
MTM1	Myotubularin
Dlg1	Disk large 1
EE	Early endosome
BL	Basal lamina
NF-M	neurofilament medium chain
HEK293	human embryonic kidney 293 cells
EGFP	enhanced green fluorescent protein
SDS-PAGE	sodium dodecyl sulfate polyacrylamide gel electrophoresis
MEF	mouse embryonic fibroblast
EM	electron microscopy
NGF	neuronal growth factor
DAPI	4',6-diamidino-2-phenylindole
DRG	dorsal root ganglion

Acknowledgments

There are a number of people I wish to express gratitude towards, whose support and guidance led to the completion of this dissertation work. I wish to thank my advisor Dr. Fred Robinson whose dedication, expert knowledge, and mentorship made this work possible. The value he places on a well-executed experiment and his attention to detail are traits that I admire. And I plan to adopt these traits as I continue my research journey. Fred has been incredibly helpful and encouraging as I move forward in my career and I wish to thank him for that support. I would also like to thank all the past Robinson lab members for their advice and support. I deeply admire the courage and strength of the graduate student alumni, Annie Logan and Danielle Robinson, and would like to thank them for paving the way forward. I am honored to be a co-author on their papers.

I would also like to express my gratitude to the former technicians in the lab: Alec Condon, Andrea Chin, and Katherine Delgado. Alec always had amazing insight, and I am very thankful he was there to show me the ropes when I first started. Andrea was always willing to listen or lend a helping hand. Katherine and I worked closely to characterize the *Mtmr5*$^{-/-}$ nerve morphology and the manuscript would not have been completed without her. I'm so proud of what we all accomplished together and could not have asked for a better friends or lab mates.

Everyone in the Jungers Center for Neuroscience Research have been helpful and supportive. I want to thank the Unni, Emery, Logan, Banker, and Martin labs for sharing reagents, providing advice, and being an overall wonderful group of people. Jo Hill in the Electron Microscopy core was invaluable in the processing and preparation of sciatic nerves for EM. Stefanie Kaech Petrie and Aurelie Snyder in the advanced light microscopy core assisted in light microscopy imaging and were always willing to offer reagents and invaluable troubleshooting assistance.

I would like to express my gratitude to my committee members, Peter Mayinger, Ben Emery, and Michael Cohen for steering and focusing my research over the years. I would like to thank Ben especially for providing career advice and mentorship, his help was instrumental to completing my PhD. I want to thank the administrative director Lola Bichler for making sure I remembered to sign up for classes, fill out forms, and attend every seminar.

There are so many other people who helped along this journey including my amazing class cohort, your friendship means everything. I would also like to thank my friends, Gina Johnson and Alissa Krumlauf, who kept me grounded and showed me the beauty of the outdoors and the joys of traveling. I would also like to thank my family; even though they don't always understand my work or why I'm still in school, they are always 100% supportive. I would especially like to thank my parents whose love I feel every day and can't ever thank enough.

Lastly, I would like to thank my partner Ben Doron. He pushes and encourages me and keeps me going even during the hard times. He has been there from the first day of our first year and every day since. Thank you, I love you.

Abstract

Nearly half of the proteins linked to demyelinating subtypes of Charcot-Marie-Tooth disease regulate endo-lysosomal trafficking. Most of these proteins are expressed in all human tissues, yet defects caused by loss-of-function mutations are largely isolated to the peripheral nervous system. This observation suggests that myelinating Schwann cells are particularly vulnerable to endosomal trafficking defects, yet the molecular mechanisms that orchestrate this cell-specific vulnerability remain unclear. We hypothesize that endosomal trafficking provides the specific control needed to regulate pro-myelination signals and coordinate cytoskeletal rearrangements during axon sorting and myelination. We demonstrate that three key endosomal regulator proteins, Vps34, myotubularin-related 5 (Mtmr5), and Mtmr13, regulate axon sorting and/or Schwann cell myelination. Loss of the PI 3-kinase Vps34 caused impaired ErbB2/3 receptor signaling, which may contribute to axon radial sorting defects and myelin arrest observed in mutant nerves. Our genetic studies demonstrated that the homologs Mtmr5 and Mtmr13 had unique roles during peripheral nerve development. We provide evidence that Mtmr5 controls axon radial sorting and Mtmr13 regulates Schwann cell myelination to prevent abnormal myelin outfolding formation. We hypothesize that Mtmr5 and Mtmr13 work together with the active PI 3-phosphatase Mtmr2 to tightly regulate the trafficking of receptors such as β1-integrin and ErbB2/3 to control actin assembly and pro-myelination signals. These data may explain why loss-of-function mutations in either Mtmr2, Mtmr5, or Mtmr13 cause Charcot-Marie-Tooth peripheral neuropathy. All cells require the trafficking of membrane receptors, but the work described within this dissertation suggests that Schwann cells rely heavily on endo-lysosomal membrane trafficking for all aspects of their biology. Highlighting why changes in phosphoinositide hydrolysis and endosomal trafficking cause peripheral neuropathy.

Chapter 1

Introduction

1. Evolution of Myelin

Myelin is a specialized, lipid-rich, multilayered membrane that insulates axons and increases the speed of nerve impulses. The evolutionary appearance of myelin is coupled to the acquisition of the hinged jaw; jawless vertebrates (e.g. lampreys) do not have myelinated axons (1). Myelination greatly influences the speed of signals through the nervous system. For example, a non-myelinated 10 μm diameter axon propagates an action potential at about 1 m/s, whereas a myelinated axon of the same diameter conducts at 50-60 m/s. The speed at which non-myelinated axons fire is sufficient for invertebrate animals of relatively small size (0.1 to 30 cm in length) but is insufficient for larger animals (2). Accordingly, large invertebrates such as cephalopods have evolved to have very large axons, up to 1 mm in diameter, to maintain sufficient conduction velocity proportional to their large body size (2). Generation of myelin was transformative for vertebrates because it overcame axon size constraints imposed by the skull and the vertebrae and increases the speed of action potential propagation throughout both the central (CNS) and peripheral nervous systems (PNS) (2).

Two types of myelinating glia arose through convergent evolution: oligodendrocytes in the CNS and Schwann cells (SCs) in the PNS (Fig. 1.1) (3). Myelination most likely arose simultaneously in the PNS and CNS, from adaptations that allowed progenitor ensheathing glia to evolve the ability to wrap axons in a specialized multilayer membrane (2). Mechanistically, myelin functions to cluster sodium ion channels at nodes of Ranvier between myelin sheaths (Fig. 1.1). This allows membrane depolarization to occur exclusively at the nodes, which results in rapid saltatory nerve conduction (4). In addition to myelin production, glial cells also provide support to the axons they ensheath through metabolite exchange (5, 6).

Both oligodendrocytes and SCs serve the vital function of producing myelin but there are fundamental differences between the two cells types. Oligodendrocytes are

derived from neuroepithelial precursors of the neural tube. A mature oligodendrocyte can produce up to 40 myelin segments and enwrap many axons (7). Oligodendrocytes have intrinsic myelination capacity and can enwrap synthetic nanofibers, fixed axons, and micropillars (8, 9). In contrast, SCs are derived from the neural crest and produce a single myelin sheath per axon (Fig. 1.1). PNS myelination is also less stochastic than that of the CNS, with a stringent correlation between axon diameter and myelin thickness (10). Therefore, while CNS and PNS myelinating glia have similar functions, their unique method of myelinating highlights the convergent nature of their evolution.

2. Myelin structure

There are notable similarities and differences in the composition and structure of myelin produced by oligodendrocytes and SCs. Myelin in both the CNS and PNS is lipid rich (70-80%); cholesterol is the major lipid component (4). However, the protein composition is distinct in the CNS and PNS. In mammals, CNS myelin is comprised mainly of myelin basic proteins (MBPs) and proteolipid protein (PLP), which together make up 60-80% of the protein content. MBPs are small, positively charged proteins that localize to the cytoplasmic side of the glial membrane and function to bring the two membrane interfaces together, thereby keeping the myelin compact. PLP is a transmembrane protein that ensures the proper spacing between myelin layers, mice lacking PLP protein have abnormally condensed myelin sheaths (11). In the PNS, myelin protein zero (P0) accounts for more than half of the proteins in myelin. It is a transmembrane glycoprotein that functions analogously to PLP. Compact myelin of the PNS also contains peripheral myelin protein 22 (PMP22), MBP, and peripheral myelin protein 2 (PMP2) (11). In both the CNS and PNS, non-compact myelin regions contain 2’3’-cyclic nucleotide 3’-phosphodiesterase (CNP) and myelin-associated glycoprotein

(MAG), which are thought to maintain the cytoplasmic space and participate in axo-glial signaling (11, 12).

During myelination, the axon and glial cell form junctions at the distal ends of the myelin segment connecting non-compact myelin loops with the axolemma (4). This junction is known as a paranode, which separates the node from the juxtaparanode regions. The paranode is comprised of the axon protein Caspr (contactin-associated protein) and contactin, which interact with their glial partner neurofascin 155 (Nfasc155) (4). The tight interaction between the axon and glial membrane in the paranode leads to the clustering of nodal proteins: Nfasc186, NrCAM, and ankyrin G and subsequent clustering of voltage gated sodium channels (Na_v) (4).

Myelin is devoid of cytoplasm which impedes the transport of metabolites and signals throughout the cell. To circumvent this problem SCs have evolved cytoplasmic pockets in the inner and outer region of the myelin and tunnels between the myelin layers. Underneath the SC plasma membrane, on the abaxonal side, are cytoplasm-filled regions known as Cajal bands (4). These areas are formed through interactions between dystroglycan on the SC surface and laminin 211 in the basal lamina that squeeze out cytoplasm. Cajal bands contain microtubules that deliver mRNA and proteins from the nucleus to lateral glial regions (4). Schmidt-Lanterman incisures (SLIs) are concentric cytoplasm-filled tunnels between individual myelin membrane layers that allow communication between the abaxonal and adaxonal SC surfaces. Gap junctions connect each SLI layers and mediate transport (13). SLIs play an important role in axon maintenance and are rich in actin filament, microtubules, vesicles, and multivesicular bodies. These channels are constantly present in the PNS, and similar cytoplasmic channels appear transiently in the CNS and are thought to serve a similar function (12).

3. Schwann Cell development and myelination

Myelinating and Remak SCs originate from neural crest-derived Schwann cell precursors (SCPs). SCPs further differentiate into immature Schwann cells. Several immature SCs cluster around a group of axons and produce a basal lamina (Fig. 1.2) (14). Immature SCs migrate through the periphery and send actin-rich processes that resemble lamellipodia into axon bundles to determine which axons are large enough to require myelination (>1 μm diameter). The decision to myelinate is dictated to SCs based on the abundance of neuregulin-1 type III (Nrg1-III) on the axon surface, which is proportional to axon caliber (14, 15). Large axons are segregated and form a 1:1 relationship with a pro-myelinating SC (14). The pro-myelinating SC differentiates into a mature myelinating SC (Fig. 1.2). SCs continue to proliferate and sort axons until only small caliber axons remain, in a given axon bundle (by postnatal day 10 in mice). Non-myelinated Remak SCs enwrap groups of small caliber axons forming Remak bundles (Fig. 1.2) (14).

3.1 *Transcriptional Regulators of Schwann cell Myelination*

Three transcription factors, Sox10, Oct6, and Krox20 serve as the central regulators of SC development and myelination (16). Sox10 is an HMG-domain transcription factor that is induced shortly before neural crest cells start to migrate from the neural plate. Sox10 remains throughout the Schwann cell lineage and is required for SC specification (Fig. 1.2) (17). Importantly, Sox10 induces the expression of ErbB2/3, which binds to axonal expressed neuregulin 1 type III to promote further proliferation, differentiation, and pro-myelination signals (18). Sox10 also induces the expression of the POU domain transcription factor Oct6 (also known as Pou3f1) by binding to its downstream enhancer region (16). Expression of Oct6 also depends on chromatin modifications, signaling through the ErbB2/3 heterodimer, and the G protein-coupled receptor Gpr126 (19-22). Oct6 interacts with Sox10 in promyelinating SCs to induce

terminal differentiation by enhancing the expression of Krox20 (Fig. 1.2). Therefore, Oct6 promotes SC progression from promyelinating to myelinating. Both Oct6 and Krox20 are expressed for a short time congruently but Oct6 expression must be turned off for proper myelination to occur (23). Continued expression of Oct6 leads to hypomyelination and axonal loss (23).

Sox10 and Krox20 work together in SCs to promote myelination and myelin maintenance (16). These transcription factors drive myelin gene expression (e.g. MBP, P0, and Connexin 32) and lipid biogenesis (16). They also suppress an immature SC state by inhibiting the expression of Oct6, c-Jun, and Sox2, which are required for both proliferation and induction of immature SCs (16).

3.2 *Role of the ErbB2/3 receptor tyrosine kinase in Schwann cells*

Interactions between the axon and SC are critical to communicate how large an axon is and how thick the myelin should be for optimal conduction. A large diameter axon may have up to 300 layers of myelin around it, but the ratio between axon diameter and total fiber diameter (axon + myelin) is maintained between 0.6 – 0.7 (6). Thus, the larger an axon's diameter the more myelin it requires. The major signal that relays axon size information to the SC is neuregulin-1 type III (Nrg1-III), which is expressed on the axon surface (24). The abundance of Nrg1-III is proportional to the axon size. Nrg1-III binds to ErbB2/3 tyrosine kinase receptors expressed on the surface of SCs. ErbB3 binds to Nrg1 then heterodimerizes with ErbB2. ErbB2 auto-phosphorylates and also phosphorylates ErbB3 to mediate a downstream signaling cascade in the SC to activate the kinases: Erk1/2, PI 3-kinase/Akt, FAK, and JNK. These kinases promote SC survival, proliferation, motility, and myelination (Fig. 1.3) (24).

The interaction between Nrg1-III and ErbB2/3 is crucial for SC proliferation, migration, axon sorting, and myelination, as evident by a near absence of SC

progenitors in the peripheral nerves of *Nrg1*, *ErbB2,* and *ErbB3* deficient mice (18, 21, 25). Heterozygous Nrg1 mutant mice (*Nrg1*$^{+/-}$) have reduced myelin thickness, and increased myelin thickness is observed in transgenic mice which overexpress Nrg1 (24). *Nrg1*$^{+/-}$ mice also have axon radial sorting defects. *Nrg1*$^{+/-}$ bundles had increased number of axons, and an increased frequency of large caliber axons (> 1 μm) retained in these bundles (21). These data suggest that Nrg1-ErbB2/3 signaling provides a mechanism for axon recognition and ensheathment. Communication between Nrg1-III and ErbB2/3 provides a model for how SCs in the PNS detect the size of a given axon (26).

3.3 *Schwann cell metabolism supports axon survival*

Axons are incredibly long structures. A single neuron can have a total axon length of 100 meters, which requires a high level of metabolic support (13). Emerging evidence indicates that axon integrity is maintained in part by the metabolic support of SCs. Liver kinase B1 (LKB1) activates the downstream kinase AMPK, and acts as a metabolic sensor in energy deficient conditions (27). SC specific depletion of LKB1 in adult mice does not impact myelin morphology but leads to axonal loss, particularly the loss of sensory axons in Remak bundles. LKB1 loss leads to the accumulation of dysfunctional mitochondria in SCs, which may generate reactive oxygen species, disrupt lipid homeostasis, and compromise axonal health (27). LKB1 in SCs promotes long-term axon survival through metabolic support rather than myelin maintenance (27).

Additionally, SC specific deletion of the mitochondrial transcription factor A gene (Tfam) causes progressive peripheral neuropathy in mice. The absence of Tfam impacts small unmyelinated c-fibers first then causes demyelination and secondary axon degeneration (28). Together these data suggest that maintaining mitochondrial function is essential not only for the health of the SC but also the axon the glial cell supports.

3.4 *Role of actin dynamics during radial sorting and myelination*

SCs undergo dramatic cytoskeletal rearrangements in order to segregate and subsequently wrap around axons (29). In myelinating cells, F-actin is absent from compact myelin except for the inner most myelin layer at the leading edge of the growing myelin sheath (29). Myelin is produced by the spiral wrapping of the glial cell membrane around the axon (Fig. 1.3). The glial cell pushes between the layers of compacting myelin and the axon itself. It has been proposed that actin polymerization at the leading edge of the enwrapping glial cell, followed by immediate actin disassembly behind the leading edge, is the driving forc needed for both myelin wrapping and compaction (30). Mouse models and *in vitro* myelination studies have identified several cytoskeletal proteins critical for PNS myelination: Rho GTPases, N-WASP, Profilin 1, and Pmp22 (Fig. 1.3). While Pmp22 is actually a myelin protein, increased expression of this protein leads to increased F-actin at SC paranodes where abnormal hypermyelination occurs (31). Our understandings of the factors that drive this actin assembly/disassembly process are still limited. However, recently developed live cell image techniques used to visualize myelin wrapping in zebrafish make this an exciting new area of study (29).

Radial sorting requires the establishment of SC polarity, remodeling of the cytoskeleton, interactions with axons, proliferation, and differentiation (10). For radial sorting of axons to occur, SCs must extend actin-rich lamellipodia between axons and segregate the larger axons to the periphery. Axon radial sorting is regulated in part by extracellular matrix components including: Laminin 2, Laminin 4, Collagen XV. As well as the SC receptors: Integrin α6β1 and Dystroglycan (14). Radial sorting is also controlled by downstream SC cytoskeleton signaling molecules, such as FAK, ILK, N-WASP, Profilin, Merlin, and Rho GTPases (14).

Rho GTPases are important for the coordinated remodeling of the actin cytoskeleton during SC polarization and myelination. Rho GTPases act as molecular

switches that rapidly exchange from a GTP bound (active) to a GDP bound (inactive) state to control signaling from membrane receptors to the cytoskeleton (32). Rho GTPases include RhoA, Cdc42, and Rac1. RhoA signals through the Rho-kinase, ROCK, to mediate stress fiber formation. Cdc42 and Rac1 activate N-WASP and Arp2/3 to promote actin-rich filopodia and lamellipodia formation, respectively (32).

ROCK is a serine-threonine kinase that regulates actin polymerization and myosin activity through the activation of the downstream effectors, Ezrin Radixin Moesin (ERM), LIM Kinases, Adducin, Myosin Light Chain II (MLC), and Myosin Light Chain Kinase (MLCK) (33). ROCK is activated at the onset of SC myelination. Pharmacological inhibition of ROCK in myelination cultures results in the formation of numerous short myelin segments that also show abnormal branching (33). Inhibition of ROCK also leads to a decrease in MLC phosphorylation and ERM mislocalization. MLC and ERM proteins are normally concentrated at either end of the SC before myelination and enriched in actin microfilaments at the paranodes of compact myelin sheaths (34). Chapter 4 will discuss the role of RhoA/ROCK and ERM during SC myelination.

Rac1 and Cdc42 are also critical for SC differentiation, axon radial sorting, and myelination. Rac1 is activated downstream of β1-integrin in SCs. Conditional knockout of Rac1 in mouse SCs causes radial sorting defects and myelination arrest due to decreased merlin phosphorylation (35). Cdc42 is required for normal SC proliferation, and conditional SC deletion in mice leads to aberrant axon sorting and abnormal myelin outfoldings (36). Cdc42 activation depends in part on FRABIN, a Cdc42 specific guanidine exchange factor (GEF). Human loss-of-function mutations in FRABIN cause peripheral nerve demyelination and abnormal myelin outfoldings (CMT4H) (37). In addition, mutations in the Cdc42 interacting protein INF2 also leads to demyelinating peripheral neuropathy (CMTDIE) (38). Together, these results highlight the important

roles of Rho GTPases in generating actin-rich structures required for both radial axon sorting and myelination.

3.5 *Regulation of Schwann cell receptor signaling by endosomal trafficking*

Axonal radial sorting and myelination require the control of signaling and adhesion proteins expressed on the plasma membrane of SCs. Endosomal trafficking of receptors regulates this process, fine tuning the extrinsic signals a SC receives. Several *in vitro* and *in vivo* studies have demonstrated the essentiality of SC endocytosis for myelination (39, 40). Dynamins are membrane-associated GTPases that mediate the separation of endocytic vesicles from the plasma membrane (41). Mutations in Dynamin 2 (Dnm2) cause dominate intermediate Charcot-Marie-Tooth disease. In SC-dorsal root ganglion co-cultures, expression of disease-causing variants of Dnm2 impairs the endocytosis of key membrane proteins (β_1-integrin, ErbB2, and transferrin receptor) and suppresses myelination (39). SH3 Domain and Tetratricopeptide Repeats 2 (SH3TC2) is involved in ErbB2/3 receptor internalization through direct ErbB2 interaction and causes demyelinating peripheral neuropathy when mutated (40). Phosphatidylinositol 3-phosphate PI3P is an early endosome signature. We and others have shown that maintenance of normal PI3P levels is critical to controlling ErbB2/3 trafficking and downstream signaling in SCs to regulate radial sorting and myelination (42, 43). These results suggest that SCs utilize endosomal trafficking to tightly control ErbB2/3 receptor signaling and may use this mechanism to control other critical signaling molecules (Fig. 1.3).

Bulk membrane production and trafficking is critical for myelination because of the extreme amount of myelin membrane required to enwrap an axon. It has been proposed that regulating the balance between endocytosis and exocytosis provides an

additional mode of myelin production from the canonical transportation from the Golgi (44). In immature oligodendrocytes, the major myelin protein PLP accumulates in late endosome membranes and axon signals trigger exocytosis of PLP-laden membranes into growing myelin membranes (45). In SCs, myelin protein zero (P0), the most abundant myelin protein, is enriched in late endosomes/lysosomes at the onset of myelination (46). This suggests that SCs and oligodendrocytes both use endosomes as a myelin membrane storage compartment to provide the membrane needed for myelination.

3.6 *Role of PI kinases and PI phosphatases in Schwann cells*

Phosphoinositides (PI) are small lipid signaling molecules that regulate membrane trafficking throughout the cell (47). PIs have a *myo*-inositol headgroup that can be reversibly phosphorylated at positions D3, D4, and D5 to generate seven distinct species. The various PI species can be interconverted through the activity of PI kinases and phosphatases (47). PIs serve to distinguish membrane compartments within the cell, and function by recruiting specific proteins that display the appropriate PI binding domains. The ability of PIs to be interconverted quickly and specifically make them ideally suited to control membrane trafficking and signaling (47).

Different PI species have distinct subcellular localization and sets of binding proteins. Golgi membranes are enriched in phosphatidylinositol 4-phosphate (PI4P), and other phosphorylated derivatives $PI(4,5)P_2$ and $PI(3,4,5)P_3$ are enriched at the plasma membrane (Fig. 1.4). PI4P is generated by four different PI 4-kinases (PI4Ks) depending on subcellular compartment, and PI4KA is responsible for generating PI4P at the plasma membrane (48). PI4P generated at the plasma membrane is critical for myelination; mice with a SC-specific *Pi4ka* deletion displayed reduced myelin thickness due to changes in actin-polymerization and impaired lipid metabolism (48). Interestingly, loss of *Pi4ka* does

not affect the levels of $PI(4,5)P_2$ or $PI(3,4,5)P_3$. $PI(3,4,5)P_3$ is generated at the plasma membrane by class I PI3Ks, which are stimulated by Nrg1-ErbB2/3 signaling. $PI(3,4,5)P_3$ recruits the kinase Akt, which plays a critical role in regulating myelin sheath thickness (49). Therefore $PI(3,4,5)P_3$ levels are a critical factor in determining the number of myelin wraps a SC produces.

Early endosomes are enriched in PI3P, which is generated by class II and class III PI 3-kinases (Fig. 1.4) (47). PI3P is recognized by proteins containing FYVE (Fab1, YOTB, Vac1, and EEA1 homology) domains that sort endosomal cargo for recycling or into multi-vesicular bodies (MVBs) which fuse with lysosomes for protein degradation (43). The majority of PI3P is generated by the PI 3-kinase, Vps34. Myotubularin proteins dephosphorylate PI3P to generate PI (Fig. 1.4). We have shown that Vps34 is critical for both axon radial sorting and myelination (43). Work done to demonstrate the role of Vps34 in SCs will be discussed further in Chapter 2.

PI3P is further phosphorylated by the PI 5-kinase PIKFYVE to produce $PI(3,5)P_2$, which is enriched on MVB/late endosomes and lysosomes and is critical for SC myelination (50). FIG4 is a PI 5-phophsatase, but its primary function is to promote the activity of PIKFYVE (Fig. 1.4). Therefore, loss of either PIKFYVE or FIG4 leads to decreased $PI(3,5)P_2$ levels (50). Concordantly, mutations in FIG4 cause demyelinating peripheral neuropathy in humans (CMT4J) (Fig. 1.4). Loss of Fig4 in mice causes demyelination, defects in autophagy-mediated protein degradation, and impaired endo-lysosomal homeostasis in the PNS (51). The dephosphorylation of $PI(3,5)P_2$ to PI5P is mediated by the PI 3-phosphatase myotubularin-related 2 (MTMR2) in SCs (Fig. 1.4). Loss of MTMR2 or bindings partners, MTMR5 and MTMR13, causes demyelinating peripheral neuropathy (Fig. 1.4) (52).

There is evidence that FIG4 and MTMR2 functionally interact to maintain appropriate levels of $PI(3,5)P_2$ during myelination. FIG4 heterozygosity was able to

rescue dysmyelination in *Mtmr2*-null mouse nerves (53). This suggests that the balance of $PI(3,5)P_2$ is critical to maintain the regulated endo/lysosomal trafficking required to generate a functional myelin sheath. These findings make it clear that a variety of PI signaling pathways are critical to produce and maintain a myelin sheath. Radial sorting and myelination require precise signal outputs. PIs provide an excellent means to quickly, precisely, and reversibly control promyelination signaling, either directly or through membrane trafficking.

4. Peripheral nervous system injury and regeneration

Peripheral nerve injury can be caused by compression, laceration, infection, inflammation, or toxins (e.g. chemotherapy drugs). The PNS has the amazing ability to regenerate, a process that is extremely limited after CNS injuries. This is because SCs are able to undergo an adaptive response to prevent neuronal death and support axon regrowth/guidance after injury (54). Both Remak and myelinating SCs, distal to the nerve damage, pull away from the axons undergoing Wallerian degeneration (Fig. 1.5). The loss of axon contact leads to a change in signals received by the SC, which, until the time of injury, were coming from the axon and basal lamina (54). This triggers conversion of Remak and myelinating SCs into repair SCs (Fig. 1.5). Repair SCs upregulate the transcription factors STAT3 and c-Jun and employ autophagy/phagocytosis to degrade their myelin sheaths (55, 56). Repair SCs also release cytokines to recruit macrophages, which aid in the later stages of myelin and axon debris clearing. Repair SCs elongate up to three times the size of myelin or Remak SCs, and branch to form tracks (Fig. 1.5). These tracks, known as Bunger bands, facilitate axon navigation during regrowth (57). Axon regeneration in humans can take months to several years due to the slow rate of axon regrowth. Once axons have successfully regenerated, repair SCs are induced to adopt either a Remak or

myelinating phenotype depending on the size of the newly formed axons (Fig. 1.5). Repair SCs are a transient population that appears only as needed, highlighting the incredible plasticity of SCs.

5. Demyelinating disease and peripheral neuropathy

Demyelination results from diseases that affect myelinating glial cells, which leads to myelin loss and the relative axon retention. Axons lacking myelin sheaths become atrophic and eventually degenerate. However, this axon loss is secondary to myelin disruption (58). Demyelinating diseases that affect the CNS can be caused by inflammation, viral infection, metabolic derangement, hypoxic-ischemia, or focal compression (58). In the PNS, axonal or demyelinating neuropathy can be caused by heritable mutations, diabetes, infection (e.g. *Mycobacterium leprae*), inflammation, or chemical toxins (59). Multiple sclerosis (MS) is a chronic neuroinflammatory disease that impacts myelination in the CNS, whereas Guillain-Barré syndrome (GBS) is an acute inflammatory disease that attacks PNS myelin (59). Both MS and GBS are progressive disorders that cause muscle weakness, difficulty walking, and numbness in the legs and arms. Most treatments for MS and GBS target or suppress a patient's immune system to stop it from attacking the myelin sheath and causing further damage to the patient's nervous system (59). Demyelinating peripheral neuropathies are also caused by genetic mutations, as discussed below.

6. Charcot-Marie-Tooth disease

6.1 *Inheritance and clinical presentation*

Charcot-Marie-Tooth (CMT) is a heterogeneous genetic disorder that affects peripheral nerves. This disorder was first described by three neurologists, Jean Martin Charcot, Pierre Marie, and Howard Henry Tooth (60). CMT is the most common

inherited neurological condition, affecting 1 in 2500 people. Recent sequencing advances have identified over 80 distinct genes that are known to cause CMT when mutated (61). While the majority of CMT patients have autosomal dominant inheritance, autosomal recessive, and X-linked inheritance also occur. CMT is clinically heterogeneous, patients present with a range of onset age, progression, and electrodiagnostics. The “classic” phenotype affects both motor and sensory nerve function, causing gait defects, “foot drop”, sensory loss, and muscle atrophy. Symptoms are usually slow to progress but can move quickly in early onset cases (60).

Examination of nerve conduction is the conventional means to classify CMT into demyelinating, axonal, or intermediate subtypes. This classification is based on both motor nerve conduction velocities (MNCV) and compound muscle action potential amplitudes (CMAP). For reference, a MNCV around 50 m/s is considered normal. The determining value for demyelinating CMT is a MNCV <38 m/s at the extremities. An MNCV between 35 m/s and 45 m/s is considered intermediate. Readings greater than 45 m/s are classified as axonal CMT provided the patient’s CMAP is decreased (60). Based on electrodiagnostic and mutational inheritance patterns, CMT is divided into four major subtypes. Patients with CMT type 1 (CMT1) and 2 (CMT2) have demyelinating or axonal presentation, respectively. CMT type 4 (CMT4) is inherited in an autosomal recessive pattern and usually affects the myelin sheath. Patients with X-linked inheritance have CMT type X (CMTX) (60). Lastly, dominant intermediate CMT (DI-CMT) shows both demyelination and axonal degeneration with intermediate nerve conduction velocity (NCV). Each of these types can be further subdivided genetically based on the mutated gene.

Genes mutated in CMT are critical in maintaining the structure or function of SCs and axons in the PNS. Four genes are known to cause CMT1: duplication in *PMP22*, and loss-of-function mutations in *P0*, *SIMPLE*, and *EGR2* (encoding KROX20). This

group of genes accounts for over 70% of CMT cases (60). These proteins are critical for SC differentiation, or comprise major components of PNS myelin. CMTX is caused by mutations in *GJB1*, which encodes the SC specific gap junction protein Connexin 32 (Cx32). CMT2 is typically less severe than the demyelinating forms and affects various structural, metabolic, and trafficking proteins important for axon health (62). Thus far, eleven genes have been determined to cause CMT4: *GDAP1* (CMT4A), *MTMR2* (CMT4B1), *MTMR13* (CMT4B2), *MTMR5* (CMT4B3), *SH3TC2* (CMT4C), *NDRG1* (CMT4D), *EGR2* (CMT4E), *PRX* (CMT4F), *HK1* (CMT4G), *FRABIN* (CMT4H), and *FIG4* (CMT4J) (63). Unlike the other CMT subtypes it is less clear, based on protein function, why loss-of-function mutations in these genes cause peripheral neuropathy.

6.2 *Demyelinating CMT: Roles of Endosomal trafficking proteins in Schwann cells*

The majority of genes known to cause demyelinating forms of CMT encode endosomal/lysosomal regulatory proteins (64). These include Dynamin 2 (*DNM2*), SH3 domain and tetratricopeptide repeats 2 (*SH3TC2*), FGD1-related F-actin-binding protein (*FRABIN*), N-Myc Downstream Regulated 1 (NRG1), lipopolysaccharide-induced tumor necrosis factor-alpha (*LITAF)/SIMPLE,* factor-induced gene 4 (*FIG4*), and myotubularin-related protein 2 (*MTMR2*), *MTMR13,* and *MTMR5*. While expressed in tissues throughout the body, mutations in these proteins cause few phenotypic defects outside peripheral neuropathy (61). This suggests that SCs are particularly sensitive to disruptions in endosomal/lysosomal trafficking, yet the reason for this vulnerability remains unclear.

Mutations in Dnm2 cause dominant intermediate CMT (DI-CMT). Dynamins are membrane-associated GTPases which facilitate the scission of endocytic vesicles from the plasma membrane (41). The expression of Dnm2 CMT-causing variants in SC-dorsal

root ganglion co-cultures causes impaired endocytosis, and reduced myelination (39). SH3TC2 regulates the endocytosis of activated ErbB2 receptor through direct interaction. Mutations in SH3TC2 are thought to disrupt PM localization, ErbB2 activation, and cause CMT4C (40). FRABIN is a CDC42 exchange factor that causes CMT4H when mutated. Knockdown of Frabin in rat RI4 SCs leads to inhibition of transferrin receptor internalization (37). Truncating mutations in NDRG1 are responsible for most CMT4D cases. These NDRG1 mutations are unable to mediate early endosome recycling (65). CMT1C is caused by mutations in LITAF/SIMPLE, which is localized to early endosomes and regulates the sorting of endocytic cargo for lysosome degradation by the ESCRT machinery (66). Mutations in FIG4 cause CMT4J. Loss of FIG4 decreases $PI(3,5)P_2$ levels, causing endo/lysosome enlargement and disrupts normal lysosome protein degradation (51). Lastly, three members of the myotubularin protein family cause demyelinating CM4B when mutated: MTMR2, MTMR5, and MTMR13 (52, 67, 68).

MTMR2 is an active PI 3-phosphatase that dephosphorylates the endosomal/lysosomal lipids PI3P and $PI(3,5)P_2$. While MTMR5 and MTMR13 lack catalytically active phosphatases domains, they bind directly to MTMR2 (69, 70). Additionally, MTMR5 and MTMR13 both contain DENN domains predicted to activate Rab GTPases that regulate endosomal trafficking (71). It was been proposed that MTMR2 works with MTMR5 or MTMR13 to control early endosomal recycling through PI3P hydrolysis and Rab21 activation (72). The propensity for endosomal trafficking proteins to cause CMT when mutated suggests that SCs are vulnerable to endosomal trafficking disruptions.

7. Peripheral neuropathy caused by mutations in MTMR2, MTMR5, and MTMR13

7.1 *Myotubularin-related protein family of PI 3-phosphatases*

Myotubularins are a large, 14-member family of phosphoinositide (PI) phosphatases. They share the catalytic signature (Cys-$(X)_5$-Arg) of protein tyrosine phosphatases, but through biochemical approaches it has been determined that they are specific for PIs (73, 74). The myotubularin family consists of both active and inactive members that lack the cysteine residue required for dephosphorylation (Fig. 1.6). The active members dephosphorylate PI3P and PI(3,5)P_2 at the D3 position of *myo*-inositol to generate PI and PI5P (75-77). Myotubularins contain several other domains that mediate either protein-protein or protein-lipid interactions. The PH-GRAM (Pleckstrin Homology-Glucosyltransferase, Rab-like GTPase Activators and Myotubularins) domain binds to PIs and is N-terminal to the phosphatase domain (78). The majority of myotubularins contain a C-terminal coiled-coil domain which mediates homomeric and heteromeric interaction between myotubularin proteins (79-81). Specific myotubularins contain additional domains, such as a DENN (Differentially Expressed in Normal verse Neoplastic) domain which activates Rab GTPases, a FYVE domain that binds to PI3P, and PDZ (PSD-95/Dlg/ZO-1) binding domains that mediate protein interactions (Fig. 1.6) (71, 75).

A common theme within the myotubularin family is that active members form heteromeric interactions with inactive members (Fig. 1.6). The inactive member functions to increase the active binding partner's catalytic activity, substrate specificity, or subcellular localization (69, 82-84). For example MTMR8/MTMR9 complex preferably dephosphorylates PI3P, whereas MTMR6/MTMR9 complex dephosphorylates PI(3,5)P_2 to control autophagy and apoptosis respectively (85).

Four myotubularin family members cause genetic disorders when mutated. MTM1 causes X-linked centronuclear myopathy; and loss-of-function mutations in MTMR2, MTMR5, or MTMR13 cause CMT peripheral neuropathy (86). The following sections will explore the roles of each of these proteins in the PNS.

7.2 *Role of MTMR2 in the peripheral nervous system*

CMT4B1 is a recessive disorder caused by loss-of-function mutations in MTMR2 (52). CMT4B1 shows early childhood onset, decreased MNCV (9-20 m/s), distal sensory impairment, and redundant loops of myelin known as myelin outfoldings. Myelin outfoldings are thought to arise from excessive longitudinal myelin growth (Fig. 1.7). The thickness of the myelin remains unaltered by MTMR2 loss, suggesting that MTMR2 controls myelination rather than facilitate its formation (52). MTMR2 has ubiquitous expression throughout the body, yet loss of MTMR2 primarily affects myelinating SCs in the PNS (87, 88). In Mtmr2-null mice, myelin outfoldings begin to appear at three weeks of age (89). Mtmr2 conditional knockout mouse models have shown that loss of Mtmr2 in SCs but not motor neurons leads to myelin abnormalities (90). Mtmr2-null mice also have impaired spermatogenesis potentially due to loss of adhesion between Sertoli and germ cells (89). Consistent with this result, a single CMT4B1 patient has been reported to have azoospermia (89).

In SCs, Mtmr2 interacts with Disk large 1 (Dlg1) to coordinate vesicle endocytic trafficking of Sec8 targeted membranes. This was originally proposed as a mechanism to regulate bulk myelin production directly by membrane transport from early endosomes to the plasma membrane (91). However, a recent study demonstrated that loss of Mtmr2 alters pro-myelination signaling, likely through abnormal recycling of the receptor from the early endosome back to the plasma membrane (42). Mtmr2-null sciatic nerves showed a transient but significant increase in activated ErbB2 (pErbB2) at the onset of myelination (42). Importantly, CMT4B1-like myelin abnormalities were reduced *in vitro* when ErbB2/3 activation was suppressed pharmacologically with the Nrg1 inhibitor Niacin (Vitamin B3) (42). This suggests that Mtmr2 controls ErbB2/3 receptor activation

through endosomal trafficking to modulate the amount of pro-myelination signal and regulate myelination.

7.3 *Role of MTMR13 in the peripheral nervous system*

MTMR13 has a catalytically inactive phosphatase domain and is ubiquitously expressed in tissues throughout the body (88). However, loss-of-function mutations in MTMR13 largely affect the PNS and cause CMT4B2 demyelinating neuropathy (92). In some cases, loss of MTMR13 function also causes glaucoma (93). CMT4B2 shows autosomal recessive inheritance and is similar to CMT4B1 in terms of nerve pathology. Both CMT4B1 and CMT4B2 are characterized by early onset, demyelinating neuropathy, and myelin outfoldings (93) (Fig. 1.7). Our lab has shown that MTMR2 and MTMR13 depend on one another to maintain their normal protein abundance in the PNS, and their levels are unaltered in the CNS (94). This mutual protein dependence may explain the strikingly similar nerve pathologies when either protein is mutated. Consequently, we were able to partially rescue CMT4B2-like dysmyelination by re-expressing MTMR2 at physiological levels in *Mtmr13*$^{-/-}$ myelinating cultures (95). This suggests that MTMR2 and MTMR13 likely function together to regulate SC myelination.

MTMR13 is a large 208 kDa protein containing an N-terminal DENN domain which enhances Rab protein GDP to GTP exchange. Rab21, Rab28, and Rab27a have all been proposed as potential MTMR13 targets (71, 72). The first reported MTMR13 mutation was an in-frame deletion in the DENN domain, which may suggest that Rab activation by MTMR13 is a requirement for normal SC myelination (92). *Drosophila* orthologs of MTMR2, MTMR5/13, and RAB21 function in a complex to promote the recycling of proteins from endosomes in fly macrophage cells. This recycling is thought to influence macrophage cell shape by controlling actin remodeling in filipodia (72).

However, the role of MTMR13-mediated endosomal trafficking and actin remodeling has yet to be elucidated in myelinating Schwann cells.

7.4 *Role of MTMR5 in the peripheral nervous system*

MTMR5 shares a 59% protein identity with MTMR13, and they are the only two proteins in the human genome that share their unique set of protein domains (Fig. 1.6). MTMR5 is an inactive PI phosphatase, contains an N-terminal DENN domain, and binds to MTMR2 (69). Mutations in *MTMR5* were shown to cause CMT4B3 neuropathy in 2013 (67). Three members of a Korean family show pure demyelinating neuropathy with myelin abnormalities that closely resemble the myelin outfoldings observed in CMT4B1 and CMT4B2 patients (67). None of the siblings show cognitive impairment consistent with other CMT4B subtypes. Since the original description, four additional families with *MTMR5*-linked neuropathy have been identified with distinct mutational signatures (96-99). These four families have more complex syndromic phenotypes than the original description: predominantly axonal neuropathy with multiple cranial features, denervation, cognitive delay, and in some cases, brain atrophy (96-99). Nerve biopsies were analyzed for two of the four patient families and show no evidence of the myelin outfoldings characteristic of MTMR2 and MTMR13 loss-of-function mutations. Instead, the MTMR5 mutant nerve biopsies show axon loss, thin myelin, and Bungner's bands indicating axon de/regeneration (96, 97). This suggests that *MTMR5*-linked neuropathy might be distinct from CMT4B1/2 subtypes.

The generation and initial characterization of an *Mtmr5* knockout mouse has been described, but peripheral nervous system defects were not assessed (100). A splicing mutation in rat *Mtmr5* was described in 2016 (101). Neurological impairment was not observed in *Mtmr5* mutant rats, but the authors admitted that subclinical neurological impairment was not investigated. Both of these rodent models documented

in detail the primary male infertility phenotype associated with loss of *Mtmr5*. However, both rodent models lacked in-depth neurological assessment required to determine the role of Mtmr5 in the PNS. Therefore, we generated a novel *Mtmr5* knockout mouse to comprehensively characterize *Mtmr5*-associated neuropathy.

How SCs determine which axons to myelinate and produce enough myelin for rapid nerve conduction remains an open question. This dissertation work seeks to determine how SCs utilize endosomal trafficking to regulate signals critical for axon sorting and myelination. The conclusions from this dissertation work identify how three key endosomal regulatory proteins, Vps34, Mtmr5, and Mtmr13 control radial sorting and/or SC myelination. This work also provides insight into why SCs are venerable to endosomal trafficking disruptions and provides a frame work for understanding the demyelinating CMT to develop future therapies.

FIGURES AND LEGENDS

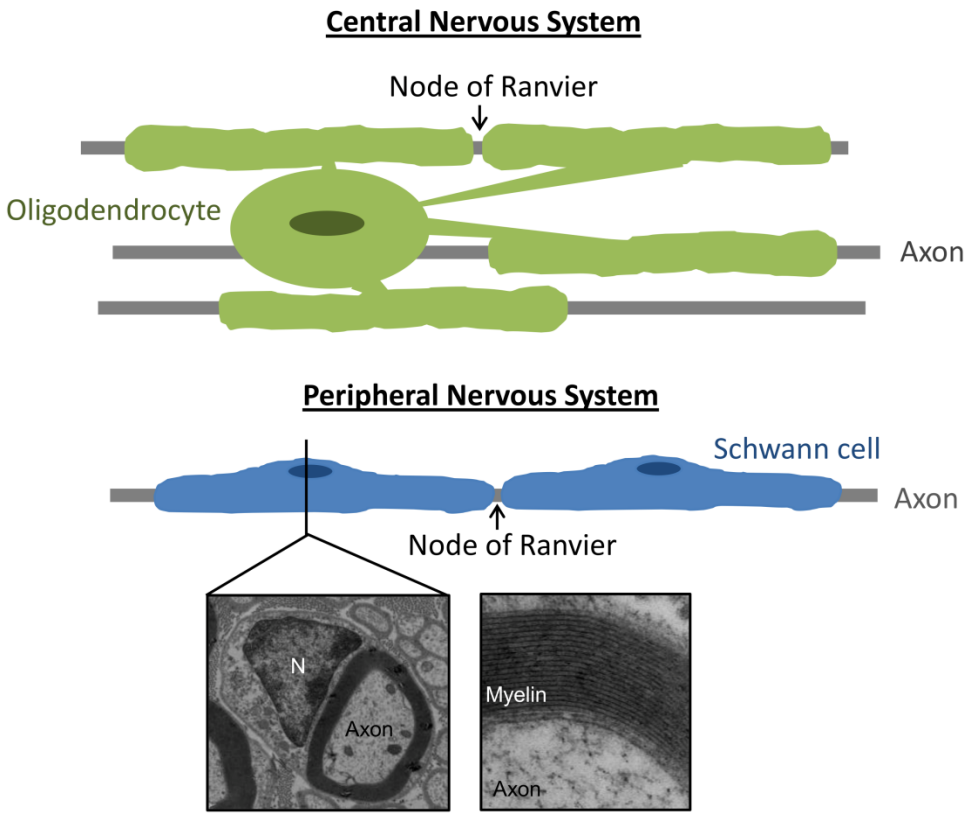

Figure 1.1: Myelination in the central and peripheral nervous systems. Myelin is a multilayer, specialized membrane that enwraps axons. Myelin clusters ion channels at nodes of Ranvier to mediate saltatory conduction. Oligodendrocytes produce myelin in the central nervous system and Schwann cells produce myelin in the peripheral nervous system. Oligodendrocytes generate multiple myelin segments and enwrap several different axons. Schwann cells produce a single myelin segment and form a 1:1 relationship with an axon. Electron microscopy images of compact SC myelin show the multiple myelin membrane layers. Abbreviations: N, nucleus.

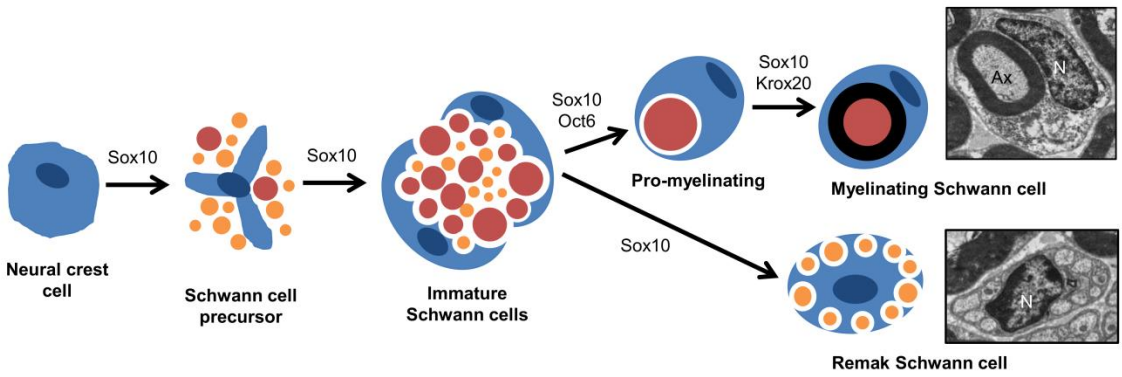

Figure 1.2: Schwann cell development. Schwann cells are derived from the neural crest. The transcription factor Sox10 is expression throughout the SC linage. Schwann cell precursors (SCPs) differentiate into immature Schwann cells. Several immature Schwann cells surround a bundle of mixed caliber axons. Large axons (> 1μm in diameter) are sorted into a 1:1 relationship with a pro-myelinating Schwann cell that expresses the transcription factor Oct6. Oct6 is downregulated and Krox20 is upregulated to generate a terminally-differentiated myelinating Schwann cell. Small caliber axons (<1μm diameter) remain unmyelinated and are supported by a Remak Schwann cell. Electron micrographs of myelinating and Remak Schwann cells are shown (3-month-old mouse sciatic nerve). Abbreviations: Ax, axon; N, nucleus.

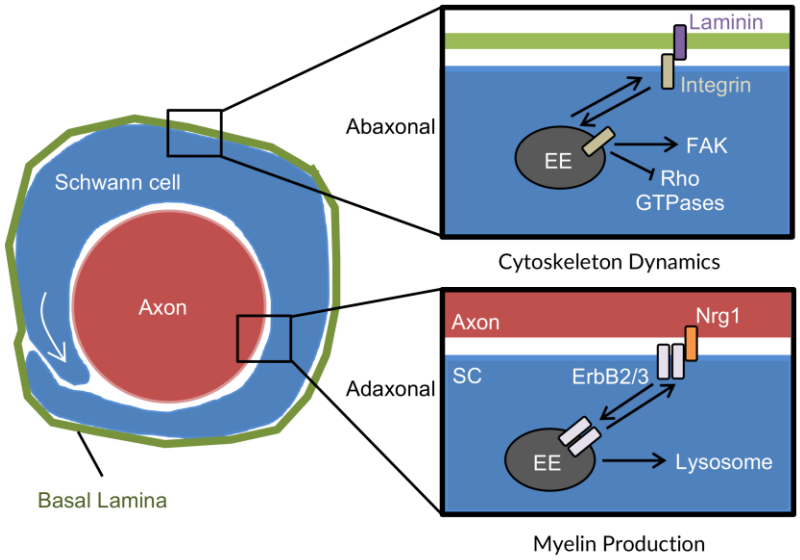

Figure 1.3: Endosomal trafficking is critical for Schwann cell myelination. Schwann cells spirally wrap myelin membrane around the axon by extending their inner tongue inwards against the axon. This process is known as myelination and is mediated by cytoskeleton changes, membrane production, and cytoplasmic receptors. Signals from receptors on both the abaxonal (Schwann cell-basal lamina) and adaxonal (Schwann cell-axon) interface are regulated by endosomal trafficking. At the abaxonal interface $\alpha_6\beta_1$-integrin interacts with laminin 211 in the Schwann cell basal lamina (BL) and signals from both the cytoplasm and early endosome (EE) to control Rho GTPase, FAK, and other actin-associated proteins to control cytoskeletonal dynamics. At the adaxonal interface, the tyrosine kinase receptor ErbB2/3 interacts with axonal Nrg1-III. ErbB2/3 pro-myelination signals are controlled by endosome recycling and lysosome degradation.

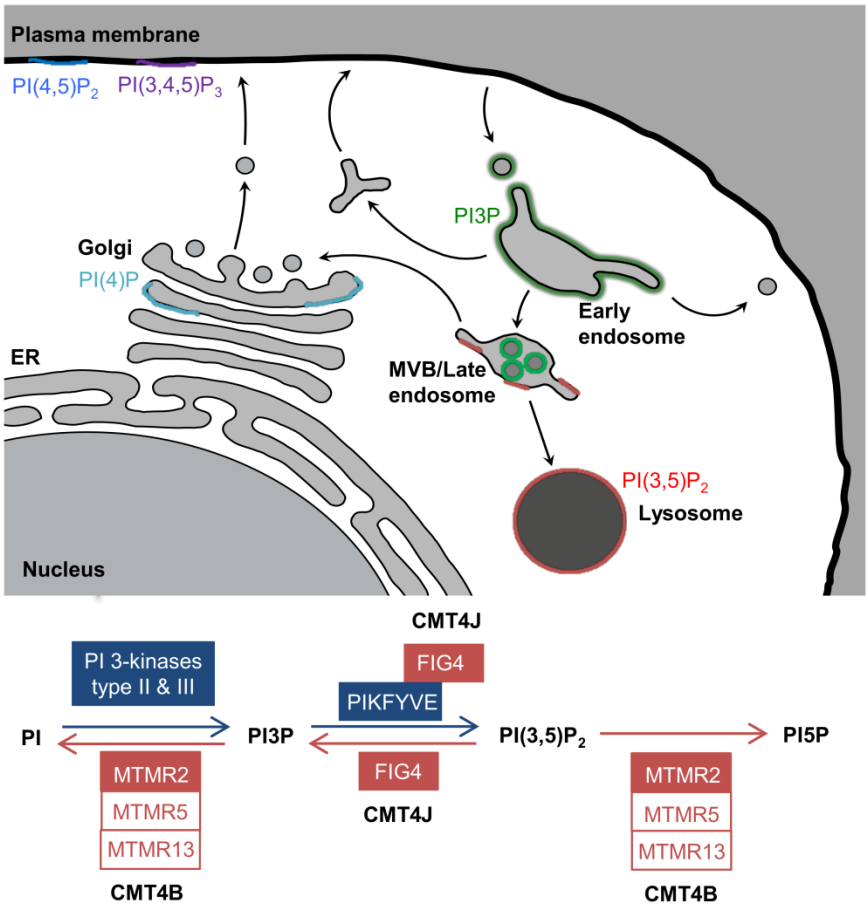

Figure 1.4: Phosphoinositide regulation of membrane trafficking. Phosphoinositides (PIs) are lipids that regulate membrane trafficking and signaling. Seven distinct PI species can be interconverted by specific PI kinases and phosphatases. PI3P and $PI(3,5)P_2$ are early endosome and late endosome/lysosomal signatures, respectively. PI3P is generated by PI 3-kinases and turned over by MTMR2 along with its binding partners MTMR5 and MTMR13 in Schwann cells. PI3P is converted to $PI(3,5)P_2$ by PIKFYVE and FIG4. FIG4 is a PI 5-phosphatase but regulates PIKFYVE and leads to decreased $PI(3,5)P_2$ levels when mutated. MTMR2 along with MTMR5 and MTMR13 dephosphorylates $PI(3,5)P_2$ to generate PI5P. Loss of function mutations in FIG4 cause the inherited peripheral neuropathy CMT4J, and mutations in MTMR2, MTMR5, or MTMR13 cause CMT4B.

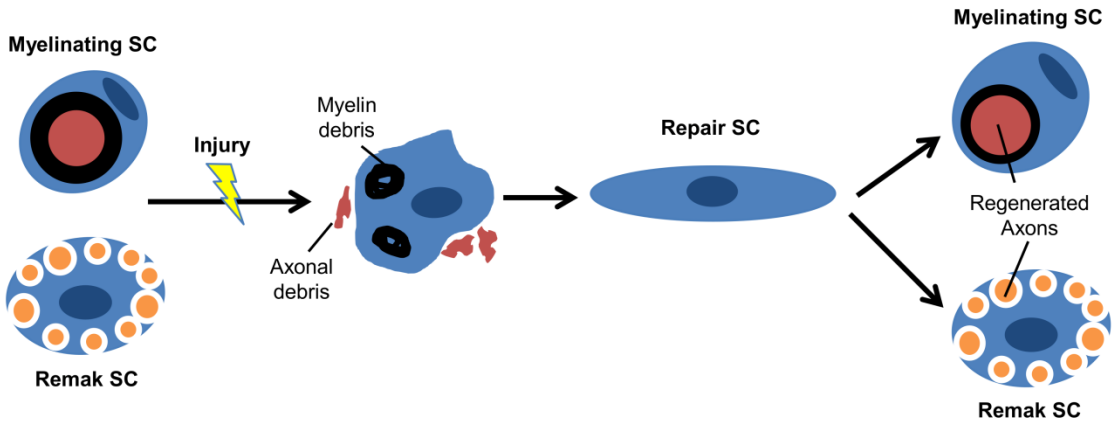

Figure 1.5: Schwann cell response to peripheral nerve injury. Both myelinating and Remak Schwann cells respond to peripheral nerve injury. Axons undergo Wallerian degeneration distal to the injury site. Myelinating Schwann cells undergo autophagy and phagocytosis to degrade their myelin. Schwann cells transdifferentiate into repair Schwann cells, which elongate to from a bridge between the site of injury and the distal stump. Repair Schwann cells provide tracks for the regenerating axons. Once the axons have reformed Schwann cells differentiate into either myelinating or Remak Schwann cells. Abbreviation: SC, Schwann cell.

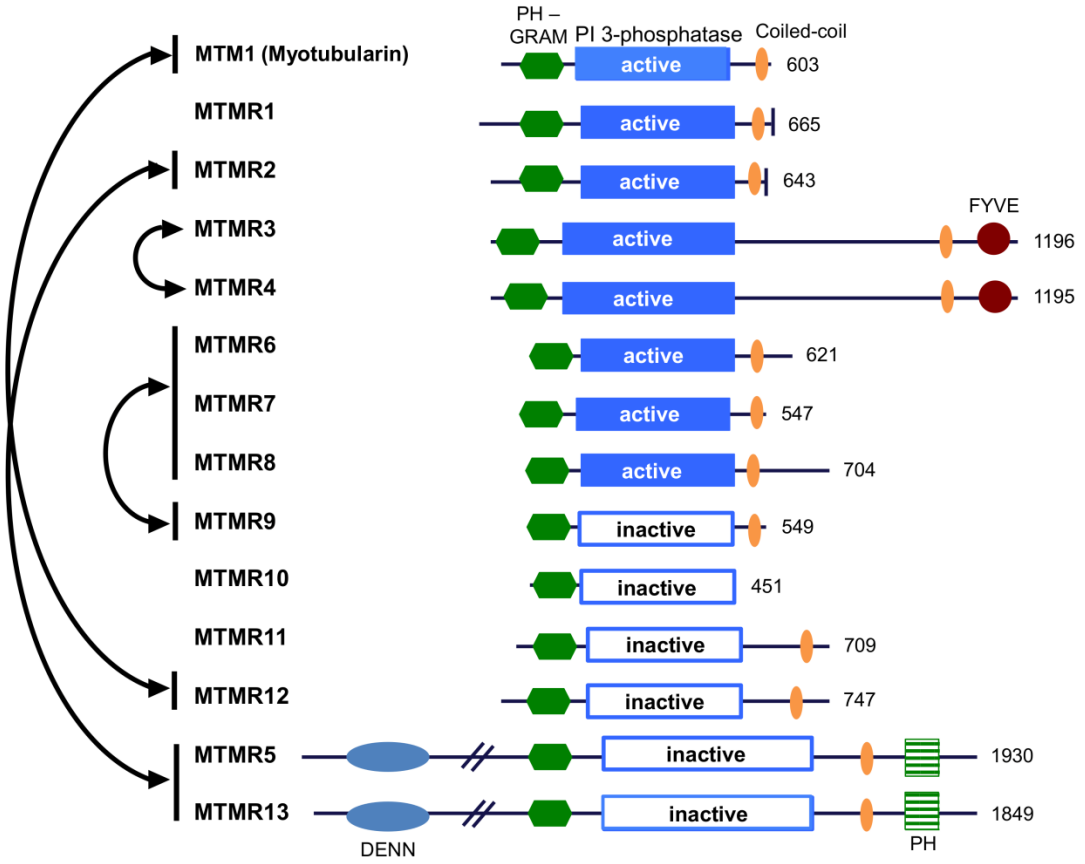

Figure 1.6: Myotubularin protein structures and interactions. Myotubularin (MTMR) family of PI 3-phosphatase is comprised of 14 members. About half of the MTMRs contain a catalytically-active phosphatase domain. The other half are pseudophosphatases that interact with catalytically active members. All MTMR proteins contain a PH-GRAM domain, and the majority contain a coiled-coil domain that mediates homomeric and heteromeric interactions. Several MTMR proteins contain other PI- and protein-interacting domains including FYVE, PDZB (vertical line), PH, and DENN. Arrows indicate interactions that have been reported between MTMR members.

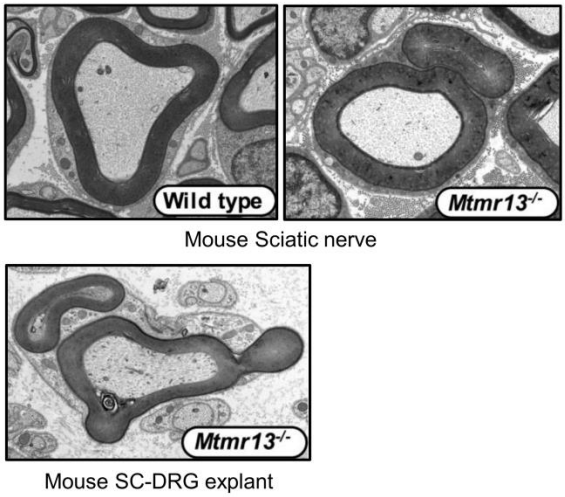

Figure 1.7: Dysmyelination caused by loss of Mtmr13. Loss of function mutations in MTMR13 cause the inherited peripheral neuropathy CMT4B2. Patients with MTMR13 mutations have characteristic myelin outfoldings. *Mtmr13*-null mouse sciatic nerves contain CMT4B2-like myelin outfoldings. Schwann cell-dorsal root ganglia (SC-DRG) cultures generated from *Mtmr13*$^{-/-}$ mice have similar myelin outfoldings (95). The myelin outfoldings observed in human patients, mouse models, and explant cultures are morphologically similar.

Chapter 2

Schwann cell-specific deletion of the endosomal PI 3-kinase Vps34 leads to arrested myelination and abnormal ErbB2-ErbB3 tyrosine kinase signaling

Anne M. Logan,[1,2] **Anna E. Mammel**,[1,3] Danielle C. Robinson,[1,2] Andrea L. Chin,[1] Alec F. Condon,[1,2] and Fred L. Robinson[1,4,*]

[1]The Jungers Center for Neurosciences Research, Department of Neurology, Oregon Health & Science University, 3181 SW Sam Jackson Park Road, Portland, OR 97239, USA.

[2]Neuroscience Graduate Program, Oregon Health & Science University

[3]Cell, Developmental & Cancer Biology Graduate Program, Oregon Health & Science University

[4]Vollum Institute, Oregon Health & Science University

[*]Corresponding Author: The Jungers Center for Neurosciences Research, Department of Neurology, Oregon Health & Science University, Mail Code L623, 3181 SW Sam Jackson Park Road, Portland, OR 97239, USA. Tel 503-494-8783; Fax 503-494-9161; Email: robinsof@ohsu.edu

PREFACE

This work is published in *Glia.*

Anne Logan designed and performed the majority of the experiments and data analysis in the manuscript. Anna Mammel made a substantial intellectual contribution though the identification of ErbB2/3 signaling abnormalities in Vps34 conditional knockout mouse nerves. Anna Mammel also edited the manuscript. Danielle C. Robinson and Alec F. Condon assisted with morphology analysis.

Fred Robinson contributed to the concept of the project and wrote the manuscript with Anne Logan

The contents of chapter two are modified from the following publication:
Anne M. Logan, Anna E. Mammel, Danielle C. Robinson, Andrea L. Chin, Alec F. Condon, and Fred L. Robinson. Schwann cell-specific deletion of the endosomal PI 3-kinase Vps34 leads to delayed radial sorting of axons, arrested myelination, and abnormal ErbB2-ErbB3 tyrosine kinase signaling. *Glia* 2017 Sep;65(9):1452-1470.

ABSTRACT

The PI 3-kinase Vps34 (Pik3c3) synthesizes phosphatidylinositol 3-phosphate (PI3P), a lipid critical for both endosomal membrane traffic and macroautophagy. Human genetics have implicated PI3P dysregulation, and endosomal trafficking in general, as a recurring cause of demyelinating Charcot-Marie-Tooth (CMT) peripheral neuropathy. Here, we investigated the role of Vps34, and PI3P, in mouse Schwann cells by selectively deleting *Vps34* in this cell type. *Vps34*-Schwann cell knockout (*Vps34*^{SCKO}) mice show severe hypomyelination in peripheral nerves. *Vps34*$^{-/-}$ Schwann cells interact abnormally with axons, and there is a delay in radial sorting, a process by which large axons are selected for myelination. Upon reaching the promyelinating stage, *Vps34*$^{-/-}$ Schwann cells are significantly impaired in the elaboration of myelin. Nerves from *Vps34*^{SCKO} mice contain elevated levels of the LC3 and p62 proteins, indicating impaired autophagy. However, in the light of recent demonstrations that autophagy is dispensable for myelination, it is unlikely that hypomyelination in *Vps34*^{SCKO} mice is caused by impaired autophagy. Endosomal membrane traffic is also disturbed in *Vps34*$^{-/-}$ Schwann cells. We investigated the activation of the ErbB2/3 receptor tyrosine kinases in *Vps34*^{SCKO} nerves, as these proteins, which play essential roles in Schwann cell myelination, are known to traffic though endosomes. In *Vps34*^{SCKO} nerves, ErbB3 was hyperphosphorylated on a tyrosine known to be phosphorylated in response to Nrg1 exposure. The overall level of ErbB2 was also decreased during myelination. Our findings suggest that the loss of Vps34 alters the trafficking of ErbB2/3 through endosomes. Abnormal ErbB2/3 signaling may contribute to the hypomyelination observed in *Vps34*^{SCKO} mice.

INTRODUCTION

In eukaryotic cells, phosphoinositides (PIs) are regulated by PI kinases, phosphatases and lipases, a network of enzymes that control localization and turnover, thereby orchestrating compartmentalized membrane signaling. Phosphorylation and dephosphorylation of PIs both play important roles in the regulation of acute cellular signaling, membrane trafficking and cytoskeletal dynamics (41, 102). PIs function as inducible binding sites on membranes, as specific phosphorylation states on the inositol head group trigger the recruitment of specific effector proteins (41, 102).

PI signaling plays an important role in myelination in both the central and peripheral nervous systems (CNS and PNS). Myelin is a multilayer wrapping of specialized plasma membrane that surrounds axons and makes possible efficient saltatory impulse propagation (59). Oligodendrocytes and Schwann cells are the specialized glial cells which produce myelin in the CNS and PNS, respectively. Phosphatidylinositol 3,4,5-trisphosphate (PI[3,4,5]P_3), 3,5-bisphosphate (PI[3,5]P_2), and 3-phosphate (PI3P) have each been demonstrated to play important roles in myelination (21, 53, 103, 104). Moreover, mutations in four PI phosphatases, myotubularin-related (*MTMR*) *2*, *MTMR5*, *MTMR13* and *FIG4*, have been identified as the causes of specific forms of demyelinating Charcot-Marie-Tooth (CMT) peripheral neuropathy (52, 67, 68, 105) (Fig. 1A).

PI3P plays an important role in both endosomal trafficking and autophagy (41, 106). Highly enriched on early endosomes, PI3P recruits specific effector proteins, many of which contain FYVE or PX domains (107). Depletion of PI3P delays the traffic of proteins through endosomes (41). PI3P also plays a key role in autophagosome formation (106). In mammalian cells, the majority of PI3P is thought to be generated via the phosphorylation of PI by the class II and III PI 3-kinases (PI3Ks) (41, 108) (Fig. 1A).

CMT-causing mutations and studies with gene knockout mice have indicated that PI3P dysregulation and endosomal-lysosomal dysfunction may be a common trigger for dysmyelination in the PNS (61). However, it is unclear which isoforms of PI3K are involved in generating PI3P in Schwann cells (Fig. 2.1A). Moreover, a number of distinct pools of PI3P may be present in these cells. To begin to elucidate the roles of PI3P, endosomal trafficking, and autophagy in myelinating Schwann cells, we have examined the role of the PI3K Vps34 (*Pik3c3*) in mice. Vps34 is the sole member of the class III PI3K sub-family; a homolog has been identified in most eukaryotes (107, 109). Vps34 is involved in endosomal-lysosomal trafficking, autophagy, and cellular responses to nutrient availability (109). The role of Vps34 in specialized mammalian cells and tissues, however, remains unclear. Recently, investigators have begun using conditional alleles of *Vps34* to examine protein function in specific mouse cell types (108, 110-113).

Given the potential roles of PI3P, endosomal trafficking, and autophagy in myelinating Schwann cells, we sought to determine the function of Vps34 in this unique cell type. We generated a mouse line in which *Vps34* is specifically deleted in Schwann cells and show that this mutation leads to delayed radial sorting of axons and arrested myelination. Despite reaching the promyelinating stage, Schwann cells that lack Vps34 are inefficient at generating myelin sheaths. We also found that both the autophagic and endosomal pathways are disturbed in Schwann cells that lack Vps34. Lastly, we assessed the impact of Vps34 loss on the activation of the ErbB2/3 receptor tyrosine kinases, which play essential roles in Schwann cell myelination, and are known to traffic though endosomes. ErbB2/3 showed abnormal posttranslational modifications in Vps34-deficient nerves, suggesting that deranged endosomal trafficking of these kinases has altered their signaling output, a change that may contribute to the observed hypomyelination.

RESULTS

Schwann cell-specific deletion of *Vps34/Pik3c3*

To selectively inactivate *Vps34* in Schwann cells, *Vps34*$^{flox/flox}$ mice (110) were crossed with myelin protein zero (P0)-Cre transgenic mice, which express Cre recombinase in Schwann cells beginning at embryonic (E) day 14.5 (114) (Fig. 2.1B-C). *Vps34*$^{flox/flox}$ *P0-Cre*$^{+}$ mice are hereafter referred to as *Vps34*-Schwann cell knockout (*Vps34*^{SCKO}). Loss of Vps34 protein in sciatic nerve extracts was confirmed by immunoblotting (Fig. 2.1C). Vps34 protein was reduced to about 37% of control levels in *Vps34*^{SCKO} sciatic nerves (Fig. 2.1C). The remaining Vps34 protein in *Vps34*^{SCKO} nerves can be accounted for by cell types other than Schwann cells, including axons, fibroblasts, and endothelial cells. A similar degree of targeted protein persistence in sciatic nerves has been reported when using Schwann cell-specific Cre drivers and whole nerve extracts (56, 104, 115-117). Vps34 protein levels in mutant brain tissue were similar to controls (Fig. 2.1D), consistent with the documented Schwann cell specificity of the P0-Cre transgene (114).

Loss of Schwann cell Vps34 leads to arrested myelination

To evaluate the role of Vps34 in myelination, we examined sciatic nerves from control and *Vps34*^{SCKO} mice at postnatal (P) days 3, 7, 21 and 56 (Fig. 2.2A). In control nerves examined at P3, significant radial sorting has occurred, a majority of the large caliber axons are in 1:1 relationships with Schwann cells, and many large axons have thin myelin sheaths (116, 118) (Fig. 2.2A). At P3, *Vps34*^{SCKO} nerves were similar to those from control animals (Fig. 2.2A). Neither myelin thickness (g ratio), nor the number of myelinated axons in the nerve were significantly altered (*data not shown*). Nerve pathology becomes apparent in *Vps34*^{SCKO} mice at P7, when vacuoles are observed in the cytoplasm of many Schwann cells (Fig. 2.2A & B). Accumulation of

large, late endosomal/lysosomal vacuoles is a well-established hallmark of Vps34 loss and PI3P depletion (119-121).

We next examined *Vps34*^{SCKO} nerves at 21 days, when myelination is normally complete, with nearly all axons 1 μm or larger myelinated. At P21, most *Vps34*^{SCKO} Schwann cells contain cytoplasmic vacuoles, and myelin sheaths are thinner than in controls (Fig. 2.2A. Nerve pathology progressively worsens in adult *Vps34*^{SCKO} mice; at 56 days, myelin sheaths are thinner, and about 56% of the large axons are completely unmyelinated (Fig. 2.2A & *data not shown*).

Altered ErbB2/3 signaling in the absence of Schwann cell Vps34

As endosomal-lysosomal abnormalities are first observed in *Vps34*$^{-/-}$ Schwann cells at P7, we reasoned that the initial deficits in the trafficking of membrane proteins might be discernable at P7. Further, given the stalled myelination and altered axo-glial interactions which we observed at this developmental stage, we considered whether the loss of Vps34 might alter the trafficking and signaling of Schwann cell membrane proteins critical to myelination, such as ErbB2/3 and integrins, which are known to traffic through endosomes (14, 15).

Given the critical role of the ErbB2-ErbB3 receptor tyrosine kinases (RTK) in myelination, we investigated whether the activation or trafficking of these kinases might be altered in *Vps34*^{SCKO} mice. Phosphorylation of ErbB3 on Tyr1289, which correlates with Nrg1 exposure and ErbB2 activation, was significantly increased in *Vps34*^{SCKO} nerves (Fig. 2.3A-D). Consistently, the relative phosphorylation of ErbB2 on Tyr1248 was increased, albeit not to a statistically significant extent (Fig. 2.3A,E). A more notable change in ErbB2 was a decrease of about 50% in the overall abundance of the protein at P7, consistent with altered kinase turnover (Fig. 2.3A & F). Strikingly, both

ErbB2 and ErbB3 possessed higher apparent molecular weights in mutant nerves, a feature which was subtle at P7, but readily apparent at P21 (Fig. 2.3A & B).

Collectively, our findings suggest that the loss of Vps34 has altered the trafficking of ErbB2/3 through endosomes. In *Vps34*$^{-/-}$ Schwann cells, PI3P-depleted endosomes likely allow the persistence of hyper-phosphorylated forms of ErbB2/3, which would normally be sorted into multivesicular bodies (MVBs) by the PI3P-dependent Hrs/Vps27-ESCRT pathway for degradation in the lysosome (107, 120) (Fig. 2.4). Other posttranslational modifications, such as ubiquitination, might also be partially responsible for the increased apparent molecular weights of ErbB2/3 in *Vps34*^{SCKO} nerves. The endosomal sorting of ErbB receptors into the MVB/LE pathway to the lysosome involves the tagging of receptors with ubiquitin (122). Hrs/Vps27, which binds simultaneously to PI3P and ubiquitin, recruits the ESCRT complex to drive sequestration of activated receptors in the lumen of the MVB, thus terminating kinase signaling and routing the receptor to the lysosome (122) (Fig. 2.4). Lastly, impaired recycling of ErbB receptors could also contribute to the abnormal posttranslational modifications we observe, perhaps by preventing the normal dephosphorylation of ErbB2/3 (Fig. 2.4) (122).

As a downstream target of ErbB2/3, the PI3K-Akt kinase pathway plays a key role in Schwann cell myelination (*reviewed in* (6, 123, 124)). However, we found that Akt activation, as reported by phosphorylation of Thr308 and Ser473, was not significantly altered in *Vps34*^{SCKO} nerves (Fig. 2.3A, B; Fig. 2.5). The activation of another downstream signaling pathway, Erk1/2, was also unaltered in *Vps34*^{SCKO} nerves (Fig. 2.5).

Given the crucial role of the integrin pathway in radial sorting (*reviewed in* (14, 125)), we considered whether deranged endosomal trafficking in *Vps34*$^{-/-}$ Schwann cells might lead to abnormal integrin trafficking and reduced focal adhesion kinase (FAK) activation. However, we found that FAK phosphorylation on Tyr397, which correlates

with kinase activation, was similar in *Vps34*^{SCKO} and control nerves (Fig. 2.5), suggesting that the FAK pathway is not affected by the loss of Vps34 and associated trafficking defects. In summary, our results suggest that the loss of Vps34 alters the trafficking of a subset of Schwann cell membrane proteins through endosomes.

DISCUSSION

Relatively little is known about how the endosomal trafficking of proteins and lipids regulates Schwann cell myelination. However, mutations in eight different genes encoding the endosomal proteins cause demyelinating CMT (61). Although the specific functions of FRABIN/FGD4, SH3TC2, MTMR2, MTMR5, MTMR13, FIG4, SIMPLE/LITAF, and Dynamin 2 are still being determined, their association with human disease suggests that Schwann cell myelination is susceptible to subtle disturbances in endosomal-lysosomal trafficking (61, 66, 126). To explore this enigmatic aspect of myelination, we examined the role of a key endosomal phosphoinositide, PI3P, by selectively deleting the PI 3-kinase Vps34 in mouse Schwann cells. Vps34 is believed to be responsible for generating about 65% of cellular PI3P (108). To our knowledge, our study is the first investigation of the role of Vps34 in glia. *Vps34*^{SCKO} mice show abnormal Schwann cell-axon interactions and persistent hypomyelination in peripheral nerves. Immature, non-myelinating Schwann cells proliferate dramatically in mutant nerves, likely because of their poor capacity for myelination. Endosomal-lysosomal membranes accumulate in *Vps34*$^{-/-}$ Schwann cells during initial myelination, indicating abnormal trafficking. In addition, *Vps34*^{SCKO} nerves show altered post-translational modification of ErbB2/3, a tyrosine kinase heterodimer known to traffic through endosomes (122). Here, we discuss cellular mechanisms by which Vps34 deletion may cause the observed peripheral nerve pathology.

Endosomal trafficking of transmembrane signaling receptors

One mechanism by which endocytic trafficking may regulate myelination is by controlling which signaling and adhesion proteins Schwann cells express on their plasma membranes before and during myelination. This "tuning" of the extracellular face of the cell membrane will likely influence both the nature and amplitude of proliferation and differentiation signals that Schwann cells receive from axons, and from the basal lamina. Such signals will also likely influence the cells capacity for elaborating myelin membranes after committing to this phenotype (6).

There is *in vitro* evidence for the essentiality of Schwann cell endocytosis for myelination (39). Mutations in Dynamin 2 (Dnm2) cause dominant intermediate CMT (DI-CMT). Dynamins are membrane-associated GTPases which facilitate the scission of endocytic vesicles from the plasma membrane (41). The expression of DI-CMT-causing variants of Dnm2 in Schwann cell-dorsal root ganglion co-cultures was shown to impair endocytosis, and to suppress myelination (39). Moreover, the endocytosis of several key membrane proteins (β_1-integrin, ErbB2, and transferrin receptor) was reduced following the expression of disease-causing variants of Dnm2 in Schwann cell lines.

We explored how the *in vivo* signaling of surface receptors might be affected when Schwann cell endosomal trafficking is disturbed by Vps34 deletion. In mutant nerves, we observed hyperphosphorylation of ErbB3 on a tyrosine residue known to be phosphorylated by its binding partner, ErbB2, following exposure to axonal Nrg1 (122). ErbB2 levels and post-translational modifications were also altered in *Vps34*^{SCKO} nerves. We propose that these alterations to ErbB2/3 result from abnormal trafficking of the heterodimer through endosomes.

The described alterations to ErbB2/3 were observed both during initial myelination (P7) and when myelination is normally complete (P21). Thus, in *Vps34*$^{-/-}$ Schwann cells, the ErbB2/3 heterodimer may have signaled abnormally during a period

when its activity is critical for myelination (P7 and before) (15). We have not yet determined whether the overall biological activity of ErbB2/3 is up- or down-regulated in *Vps34*$^{-/-}$ Schwann cells. The persistent hyperphosphorylation of ErbB3 suggests that the heterodimer may be hyperactive. However, the activation of several downstream targets of ErbB2/3, the Akt and Erk1/2 kinases, was not significantly changed in mutant nerves. Conversely, ErbB2 protein levels are decreased by about 50% at P7. Moreover, altered trafficking of ErbB2/3 might have prevented access to key downstream targets, thereby causing an overall decrease in ErbB2/3 biological activity. We speculate that it is more likely that ErbB2/3 signaling is decreased (rather than increased) in *Vps34*$^{-/-}$ Schwann cells, and suggest that this feature contributes to the hypomyelination observed in mutant mice.

Given the importance of ErbB2/3 signaling to Schwann cell myelination, abnormal trafficking of these receptors has been proposed as a common pathogenic mechanism linking multiple subtypes of demyelinating CMT (66). An example of such dysregulation is found in SH3TC2, a likely endosomal scaffold protein which is mutated in CMT4C. SH3TC2 has been shown to bind to ErbB2 and alter ErbB2/3 signaling (40). We anticipate that *Vps34*^{SCKO} mice will be useful for learning more about ErbB2/3 trafficking and activation in Schwann cells, as altered trafficking of the receptor complex in these mice appears to have trapped ErbB2/3 in specific states of post-translational modification.

We also noted altered Schwann cell-axon interactions and moderately delayed radial sorting in *Vps34*^{SCKO} nerves, suggesting that endocytosis of receptors critical for interactions with the basal lamina might be altered. Accordingly, we postulated that FAK activation, which is triggered by integrin signaling, might be altered in *Vps34*$^{-/-}$ Schwann cells, particularly since endocytosis of the $\alpha_6\beta_1$ integrin dimer potentates FAK activation in cancer cell lines (127). However, FAK activation was not altered in *Vps34*^{SCKO} nerves.

Thus, Vps34 may not regulate the trafficking of integrins through Schwann cell endosomes. Alternatively, integrin trafficking might be disturbed, but in a manner that affects downstream targets other than FAK; we have yet to examine the impact of loss of Vps34 on ILK, Rac1 and p38 MAP kinase (125). Finally, additional adhesion molecules known to be involved in radial sorting, such as dystroglycan or Gpr126, could potentially be affected by the altered endosomal trafficking of *Vps34*$^{-/-}$ Schwann cells (20, 128). It is important to note that the delayed radial sorting we observe in *Vps34*^{SCKO} mice is less significant than the radial sorting arrest caused by Schwann cell-specific deletion of ILK, FAK, β1-integrin, or Gpr126 (20, 118, 129, 130), suggesting that these signaling pathways may be more subtly affected in our mutant mice.

In summary, our findings suggest that the loss of Vps34, and the associated depletion of PI3P, affects the trafficking of a subset of Schwann cell membrane proteins through endosomes. Abnormal post-translational modification of ErbB2/3, consistent with altered endosomal trafficking, was observed. In contrast, FAK phosphorylation, which is influenced by the trafficking of integrins through endosomes, was not discernibly altered in *Vps34*^{SCKO} nerves. Our study with *Vps34*^{SCKO} mice provides an *in vivo* complement to *in vitro* work on Dynamin 2, which demonstrated the importance of endocytosis for myelination (39). Loss of Vps34 disrupts or delays several steps in the flow of cargo proteins through endosomes, all of which are downstream of Dynamin's function in liberating endocytic pits from the plasma membrane (Fig. 9) (41). Continued study of *Vps34*^{SCKO} mice will likely provide additional insights into the role of endosomal trafficking in myelination.

Bulk endosomal-lysosomal transport of myelin membranes

A second mechanism by which Vps34 deletion may inhibit myelination is by disturbing the overall balance of endocytosis and exocytosis of myelin membranes,

which are enriched in specialized lipids and proteins. This aspect of myelin biogenesis has been largely studied in oligodendrocytes, and it remains to be determined if similar mechanisms operate in Schwann cells (44). Proteolipid protein (PLP) is the most abundant protein in CNS myelin. In oligodendrocytes, some myelin membrane components, such as PLP, cholesterol, and galactosylceramide are preassembled into small membrane domains as they traffic though the Golgi apparatus (44). Such membranes are thought to be delivered to the growing myelin sheet by secretory vesicular trafficking. This vectorial delivery of partially assembled myelin membranes from the *trans*-Golgi to the plasma membrane is believed to occur in Schwann cells as well (44). After delivery to the plasma membrane, small myelin domains are thought to be clustered together through the action of MBP (44).

It has been proposed that regulating the balance of endocytosis and exocytosis provides an additional mode of myelin production (44). In immature oligodendrocytes, plasma membrane-associated PLP is endocytosed and accumulates in late endosomes (45). Exposure of these cells to axons suppresses endocytosis and triggers exocytosis of PLP-laden membranes from late endosomes into growing myelin membranes (45).

It is unclear whether an analogous mechanism for endosomal regulation of myelination operates in Schwann cells. However, myelin protein zero (P0), the most abundant myelin protein in the PNS, has been reported to be enriched in late endosomes/lysosomes at the onset of myelination (P1) (46). The same study found that elevating intracellular Ca^{2+} triggers exocytosis of lysosomes in cultured Schwann cells. Lysosome exocytosis in Schwann cells was found to be regulated by the Rab27a GTPase; loss of Rab27a in mice inhibited remyelination in injured adult nerves (46). Thus, secretory lysosomes containing P0 may contribute to myelin delivery to the plasma membrane; this mechanism may be analogous to the regulated delivery of PLP from late endosomes in oligodendrocytes (45, 46).

The altered endosomal-lysosomal membranes that we observe in *Vps34*$^{-/-}$ Schwann cells suggest that the endocytosis of myelin components, such as lipids and P0, might be impaired. Moreover, the transport of endocytosed myelin components from early endosomes to late endosomes/lysosomes would very likely be suppressed in *Vps34*$^{-/-}$ Schwann cells, given the established role of PI3P in MVB formation and endosome maturation (41) (Fig. 2.4). Consistently, we observe accumulation of EEA1, an early endosomal protein that appears to accumulate when MVB formation is impaired (Fig. 2.4). If the transport of myelin membranes and proteins to late endosomal/lysosomal depots was inadequate in *Vps34*$^{-/-}$ Schwann cells, such components would be unavailable for exocytosis into growing myelin membranes. We speculate that such a mechanism could contribute to the hypomyelination we observe in *Vps34*^{SCKO} nerves. However, further studies will be required to clarify the roles of Vps34 and PI3P in the trafficking of myelin membrane components.

In summary, we demonstrate that Vps34, a kinase that generates PI3P, is essential for Schwann cell myelination. Depletion of PI3P leads to enlarged late endosomal/lysosomal vacuoles and suppressed trafficking in Schwann cells. Suppressed endosomal trafficking likely causes changes in the abundance and posttranslational modification of ErbB2/3, a signaling defect that may contribute to arrested myelination in *Vps34*^{SCKO} nerves. The observed defects in endosomal-lysosomal membranes, when considered in the light of established roles of Vps34 in trafficking, suggest that Vps34 could also be key to controlling bulk membrane myelin production by maintaining a balance between endo- and exocytosis. Our study has yielded a novel disease-relevant model that will likely provide further insight into those forms of demyelinating CMT that involve endosome dysfunction.

MATERIALS AND METHODS

Schwann cell-specific inactivation of Vps34. The mouse *Pik3c3* (*Vps34*) gene consists of 25 exons strung over about 75 kilobases (kb) on the forward strand of chromosome 18. *Pik3c3/Vps34*$^{flox/flox}$ mice were a generous gift from Fan Wang. This line of mice contains an engineered allele of *Pik3c3* in which exons 17 and 18, which encode the ATP binding sequences of the kinase, are flanked with *loxP* sites (110). In the presence of Cre recombinase, exons 17 and 18 are removed and the Vps34 protein is not expressed (108, 110). Genotyping of *Vps34*$^{flox/flox}$ mice was carried out using PCR (40 cycles) using primers ALO-18 (Vps34 F; GCCACCCATTGCTGCCT) and ALO-21 (Vps34 R; CCCTCACTGGCTGTGGC). To generate mice with a Schwann cell-specific deletion of *Vps34, Vps34*$^{fl/fl}$ mice were crossed with mP$_0$TOTA(Cre) (P0-Cre) transgenic mice (114). The P0-Cre transgene was detected by PCR with oligonucleotides ALO-5 (P0-F; CACCACCTCTCCATTGCAC) and ALO-6 (P0-R; GCTGGCCCAAATGTTGCTGG). *Vps34*$^{fl/fl}$ mice were previously found to be indistinguishable from wild type mice (110). Control mice were either *Vps34*$^{fl/fl}$ (*P0-Cre*$^{-}$*)* or *Vps34*$^{+/fl}$ (*P0-Cre*$^{-}$*)* littermates of *Vps34*$^{fl/fl}$ *P0-Cre*$^{+}$ (*Vps34*^{SCKO}) mutant mice. Mice of either sex were used in all experiments. All work with animals was approved by and conformed to the standards of the Oregon Health & Science University Institutional Animal Care and Use Committee.

Morphology. Preparation of mouse sciatic nerves for electron microscopy (EM), or for light microscopy of toluidine blue-stained nerve sections, was as previously described (94). EM and light microscopy imaging were also as previously described (94). Toluidine blue sections were imaged at 63x on a Zeiss ApoTome microscope. Two cross sections of the sciatic nerve (one each from the left and right nerve) were analyzed per mouse, and 4-7 mice of each genotype were analyzed at each time point. The entire

sciatic nerve cross-section was imaged using a tiling function and the acquired images were stitched together into a single file.

Toluidine blue stained cross-sections were used to determine g ratio by measuring the axonal circumference and dividing that number by the circumference of the outer edge of the myelin sheath. The diameter of each corresponding axon was found by dividing axon circumference by π. For g ratio analysis, axons from throughout the entire nerve cross-section were sampled; 50 round axons were measured (100 total per mouse). In P3 nerves, g ratio on all possible round, myelinated axons was measured (60-100 axons per mouse).

For total axon counts, toluidine blue stained cross sections were analyzed. At P56, four cross sectional areas (2 each from the left and right nerve) of 100 μm^2 per animal were analyzed (4-5 animals of each genotype). Axons ≥ 1 μm in diameter and in a 1:1 relationship with a Schwann cell were counted, whether myelinated or not. For P56, about 20-28% of the entire transverse fascicular area (TFA) was counted. For P21 axon counts, total axons ≥ 1 μm were counted in ~30% of the complete TFA of each mouse (n = 4) on two cross sections (left and right sciatic nerve). For axon counts in P3 and P7 mice, the entire TFA was counted in 4-7 mice per genotype. Every axon that was in a 1:1 relationship with a Schwann cell was counted in two cross-sections (right and left sciatic nerve), and the average of the two sections was calculated. An additional analysis of total large caliber axon number at P7 was performed using EM images (890x magnification; 8-16 images per animal) (Fig. 3D). The total number of axons in 1:1 relationships with Schwann cells (myelinated or not) was determined. On average, 42% of the TFA was analyzed for each mouse (n = 5 for control; n = 4 for *Vps34*^{SCKO}). Once the axon count for a significant fraction of the nerve was established, this number was scaled based on total nerve area to generate a predicted total axon count for the nerve.

Immunoblotting. Immunoblotting of sciatic nerve and brain extracts were performed as previously described (94). Rabbit monoclonal antibodies (mAb) for Vps34, ErbB3, pErbB3 (Tyr1289), ErbB2, pAkt (Ser473), and pAkt (Thr308) were from Cell Signaling Technology. Rabbit polyclonal antibodies (pAb) for pErbB2 (Tyr1248), Akt, and Erk1/2 were from Cell Signaling Technology. Additional antibodies used were mouse mAb to FAK (BD Bioscience), rabbit pAb to ppErk1/2 (pTpY(185/187) (Invitrogen) and mouse mAb to β-tubulin (E7) (Developmental Studies Hybridoma Bank), rabbit pAb to LC3 (Novus Biologicals), mouse mAbs to GAPDH and rabbit pAb to pFAK (Tyr397) (Millipore). Sciatic nerve and brain extracts were prepared as previously described (94). For each P3 and P7 nerve lysate, three mice of the same genotype (6 nerves total) were pooled. For P21 and P56, a single mouse was used (2 nerves) for each lysate. Each time point/antibody combination was run in triplicate (3 lysates per genotype per time point). 17-25 µg of protein per lane was resolved in 4-12% NuPAGE Bis-Tris gels (Invitrogen), and chemiluminescent quantitation of immunoblots was as previously described (94).

Statistics. GraphPad Prism 5 was used for all statistical analyses. Unpaired t tests (two-tailed) were used to evaluate significance, except in Figure 8, where unpaired t tests with Welch's correction were used.

ACKNOWLEDGEMENTS

Deconvolution microscopy and analysis were carried out in OHSU's Advanced Light Microscopy Core at The Jungers Center for Neurosciences Research. The authors wish to thank Aurelie Snyder and Stefanie Kaech Petrie of the Advanced Light Microscopy Core for expert advice. The DeltaVison CoreDV microscope was purchased with a Shared Instrumentation Grant from the National Institutes of Health-National

Center for Research Resources (S10-RR023432 to Thomas Keller). The authors wish to thank Robert Kayton, Lisa Dirling Vecchiarelli, Mellissa Williams and Sue Aicher for assistance with electron microscopy, nerve preparation and expert advice. The electron microscope was purchased through a grant from the Murdock Charitable Trust (to Sue Aicher). The authors wish to thank Dr. Michael Wegner for the Sox10 antibody. The 1D4B (LAMP-1) and E7 (β-tubulin) monoclonal antibodies, developed by Drs. J. Thomas August and Michael Klymkowsky, respectively, were obtained from the Developmental Studies Hybridoma Bank developed under the auspices of the National Institutes of Health-National Institute of Child Health & Human Development and maintained by The University of Iowa, Department of Biology, Iowa City, IA 52242.

This work was supported by National Institutes of Health – National Institute of Neurological Disorders and Stroke grants NS057903 and NS086812 (to F.L.R.) and the OHSU Neuroscience Imaging Center P30 grant (NS061800; To Sue Aicher), as well as an Oregon Brain Institute Neurobiology of Disease Graduate Fellowship (to A.M.L.), and through the philanthropy of Frank and Julie Jungers.

Conflict of Interest Statement. None declared

FIGURES AND LEGENDS

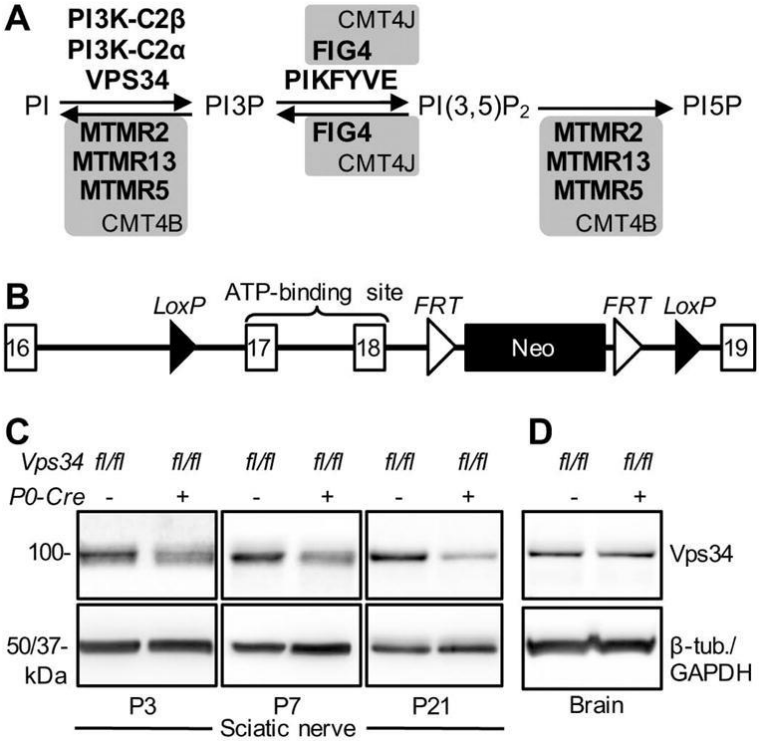

Figure 2.1: Schwann cell-specific deletion of *Pik3c3/Vps34*. **(A)** Biochemical pathway for the regulation PI3P, PI(3,5)P_2 and PI5P abundance by PI kinases and PI phosphatases. Loss-of-function mutations in those kinases and phosphatases in grey boxes cause the indicated forms of demyelinating CMT. Although the PI 5-phosphatase FIG4 is capable of dephosphorylating PI(3,5)P_2, the predominant role of this enzyme in mammalian cells is the promotion of PIKFYVE kinase activity. **(B)** The mouse *Pik3c3/Vps34* conditional deletion allele used in this study (110) (See *Supplemental Material*). Schwann cell-specific expression of *Cre* Recombinase from the *P0-Cre* transgene (*Tg*) triggers deletion of *Pik3c3/Vps34* exons 17 and 18, as well as the neomycin expression cassette. **(C)** Immunoblot analysis of Vps34 protein abundance in sciatic nerve extracts from $Vps34^{fl/fl}$ (control) and $Vps34^{fl/fl}$;$P0\text{-}Cre^{+}$ ($Vps34^{SCKO}$) mice at P56, using an antibody specific for the amino terminus. Arbitrary Vps34 protein levels:

100 ± 14.22% in *Vps34*$^{fl/fl}$ vs. 37 ± 4.07% in *Vps34*$^{fl/fl}$*;P0-Cre*$^{+}$, $p = 0.01$, n = 3 mice. Vps34 levels were normalized to β-tubulin. **(D)** Immunoblot analysis of brain extracts from control and *Vps34*^{SCKO} mice at 14 weeks indicated no significant change in Vps34 protein levels (n = 3 mice).

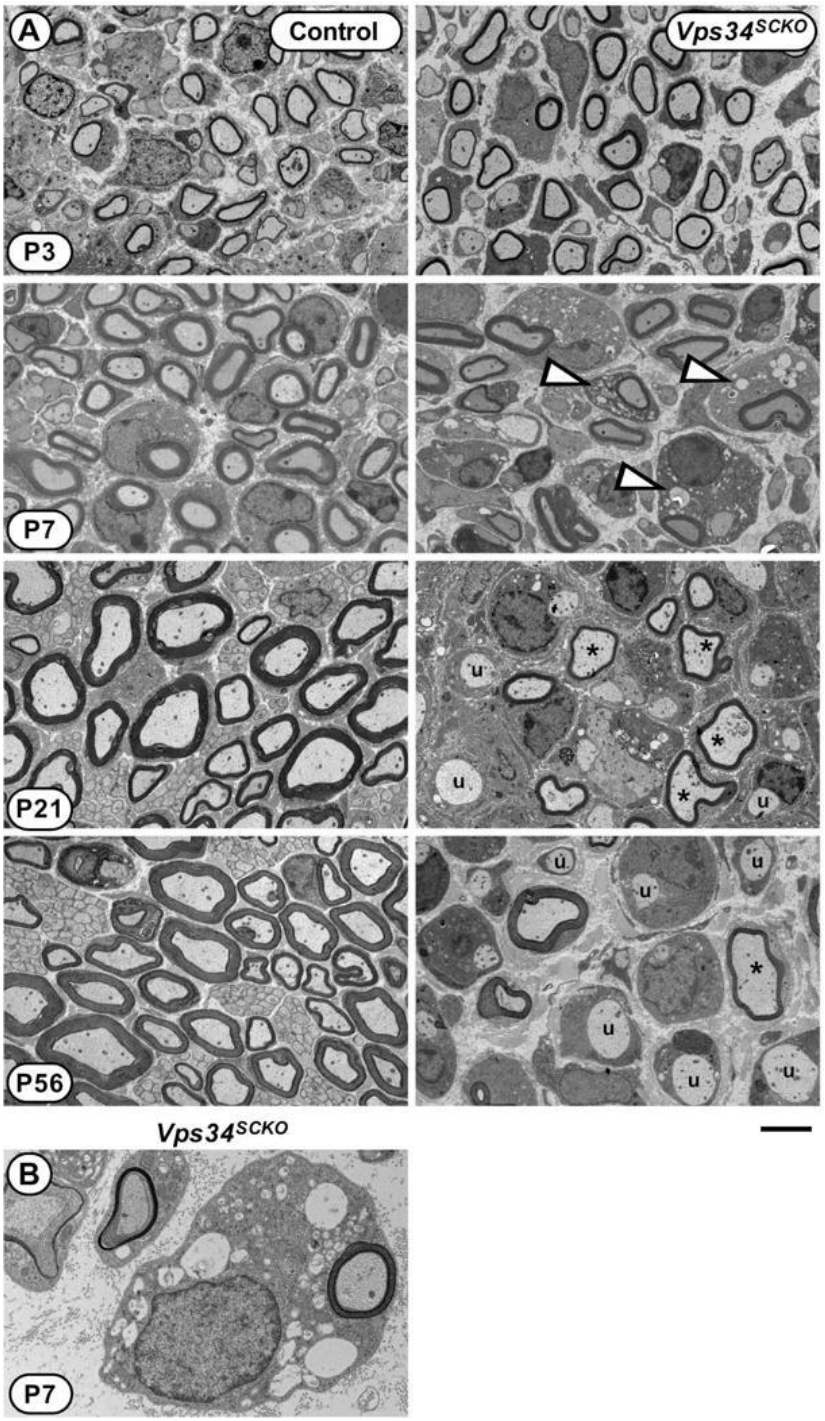

Figure 2.2: Defective myelination in *Vps34*^{SCKO} nerves. **(A)** EM analysis of mid-sciatic nerve cross sections of control and *Vps34*^{SCKO} mice at P3, P7, P21, and P56. At P3, *Vps34*^{SCKO} nerves appear normal when compared to controls (n = 7 mice). By P7, nerve pathology is evident, notably vacuoles (*white arrowheads*) in the cytoplasm of

some Schwann cells (n = 4 or 5 mice). At P21 and P56, hypomyelinated (*asterisks*) and unmyelinated (*u*) axons are evident in mutant nerves (n = 4 or 5 mice). **(B)** An example of a *Vps34*$^{-/-}$ Schwann cell with numerous endosomal-lysosomal vacuoles within its cytoplasm. Scale bar: 4 μm (A), 1.3 μm (B).

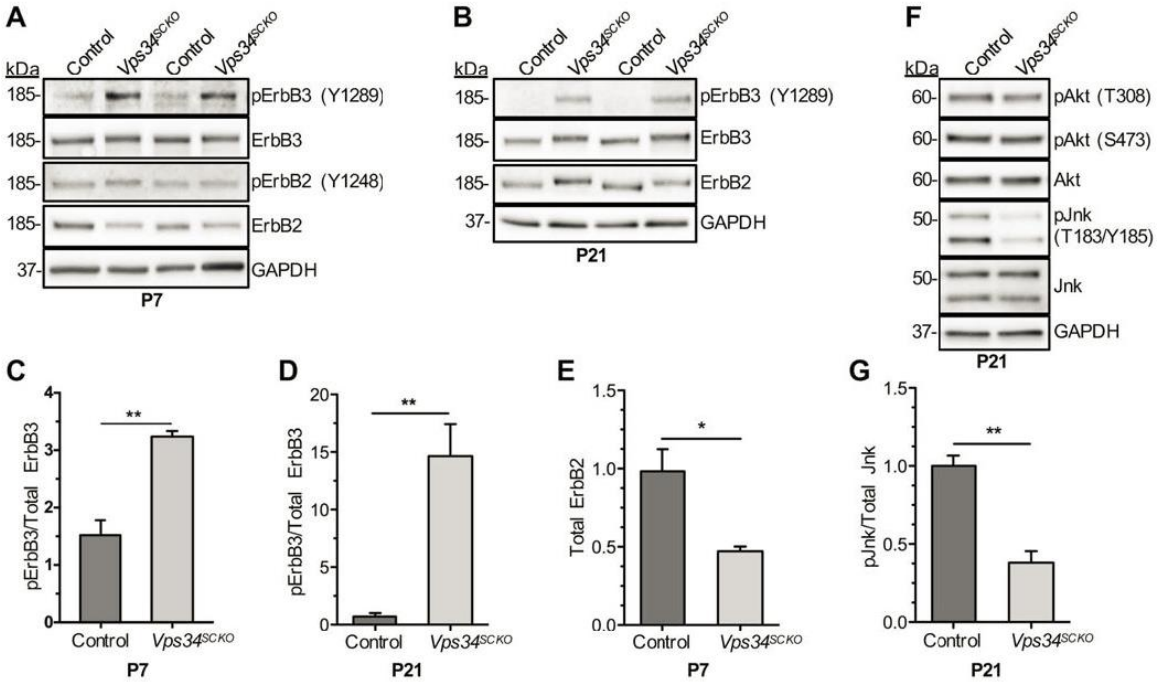

Figure 2.3: Altered ErbB2/3 receptor signaling in *Vps34*^{SCKO} nerves. **(A & B)** The activation of ErbB2/3 and a downstream target, Akt, was assessed by immunoblotting P7 and P21 sciatic nerve extracts with the indicated antibodies and quantifying the relative amounts of activated (phosphorylated) forms compared to total protein levels. Two (replicate) lanes for each genotype are shown. At P7 and P21, the ErbB2 and ErbB3 proteins from *Vps34*^{SCKO} nerve extracts migrated more slowly in SDS-PAGE gels than the same proteins from control extracts, suggesting altered post-translational modifications. Akt kinase activation, which was assessed by monitoring phosphorylation at T308 and S473, was not significantly changed in *Vps34*^{SCKO} nerves at P7 or P21. **(C & D)** The ratio of activated ErbB3 (pY-1289) to total ErbB3 was significantly increased in *Vps34*^{SCKO} nerve extracts at both P7 and P21. **(E)** The ratio of activated ErbB2 (pY-1248) to total ErbB2 was increased in mutant nerves at P7, albeit not to a statistically significant degree; phospho-ErbB2-Y1248 was undetectable in P21 nerve extracts. **(F)** *Vps34*^{SCKO} nerves contained significantly decreased levels of total ErbB2 protein at P7.

For P7, n = 4 and 3 nerve extracts from control and *Vps34*^{SCKO} mice, respectively. For P21, n = 3 and 4 nerve extracts from control and *Vps34*^{SCKO} mice, respectively (*n.s.*, not significant; *$p < 0.05$; **$p < 0.01$; mean ± SEM).

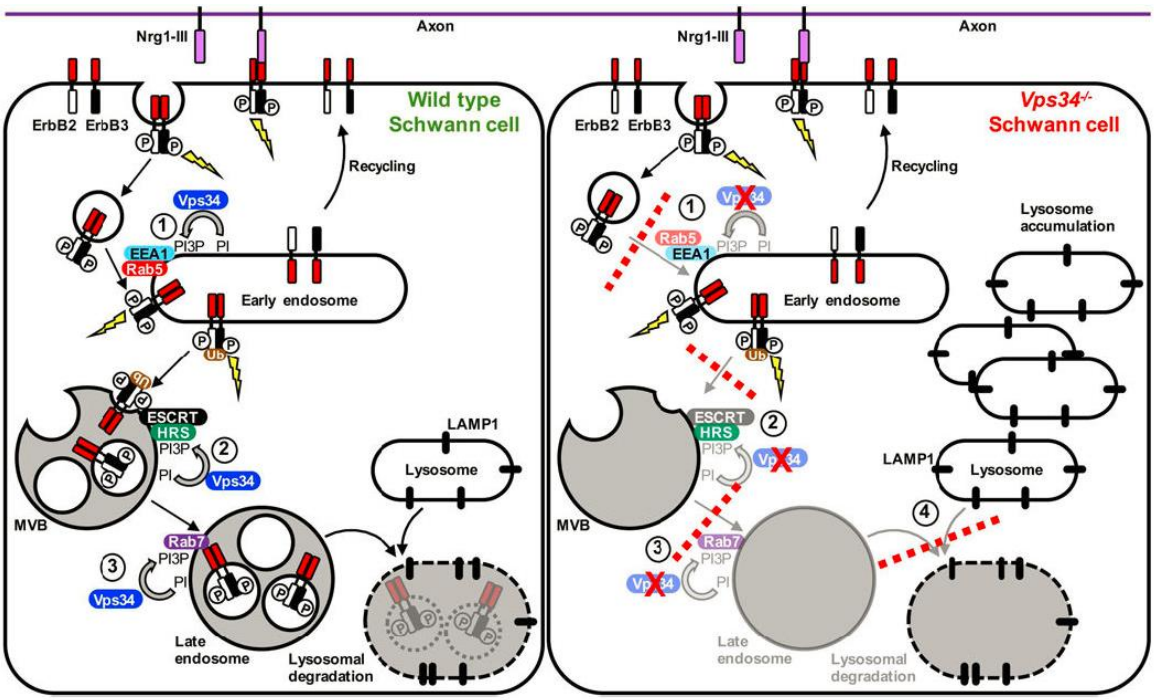

Figure 2.4: Proposed model for the role of Vps34 in endo-lysosomal trafficking of ErbB2/3 in Schwann cells. Binding of axonal Nrg1-III to ErbB3 induces receptor heterodimerization and stimulates ErbB2 kinase activity. ErbB2 phosphorylates both itself and ErbB3, creating phosphotyrosine-based docking sites for downstream signaling proteins (*lightning bolt*). Activation of ErbB2/3 triggers internalization by clathrin-mediated endocytosis. Fusion of ErbB2/3 containing vesicles with early endosomes requires PI3P, which is produced by Vps34, and requires EEA1 and Rab5 (Step 1) (131). Internalized ErbB2/3 heterodimers likely continue to signal from endosomal compartments and can be recycled from endosomes to the cell membrane. On endosomes, ubiquitination (Ub) of ErbB2/3 targets the heterodimer for sorting into multivesicular bodies (MVBs). In a second Vps34-dependent step, PI3P recruits Hrs, which binds concomitantly to ubiquitin on ErbB2/3. Hrs recruits the ESCRT complex, which drives the budding event that generates the receptor-containing internal vesicles of MVBs (Step 2) (132). Once in MVBs, ErbB2/3 signaling is terminated (66). PI3P also

mediates early-to-late endosome maturation through the recruitment of Rab7 (133) (Step 3). ErbB2/3 receptors are degraded when late endosomes fuse with LAMP1-positive lysosomes (66). We propose that, in *Vps34*$^{-/-}$ Schwann cells the depletion of PI3P results in a slowing or blockade of trafficking Steps 1, 2, and 3 (*red dashed lines*). Such trafficking defects are predicted to reduce the fusion of ErbB2/3-bearing endocytic vesicles with early endosomes (Step 1) and prevent the sorting of phosphorylated ErbB2/3 into MVBs (Step 2). This proposed abnormal trafficking of ErbB2/3 is consistent with our observations of both enhanced phosphorylation of ErbB3 on Y1289 and altered posttranslational modification of ErbB2 in *Vps34*^{SCKO} peripheral nerves. *Vps34*$^{-/-}$ Schwann cells are also likely deficient in Rab7-dependent late endosome maturation (Step 3). Finally, abnormal MVBs/late endosomes may fuse inefficiently with lysosomes (Step 4), resulting in lysosome accumulation.

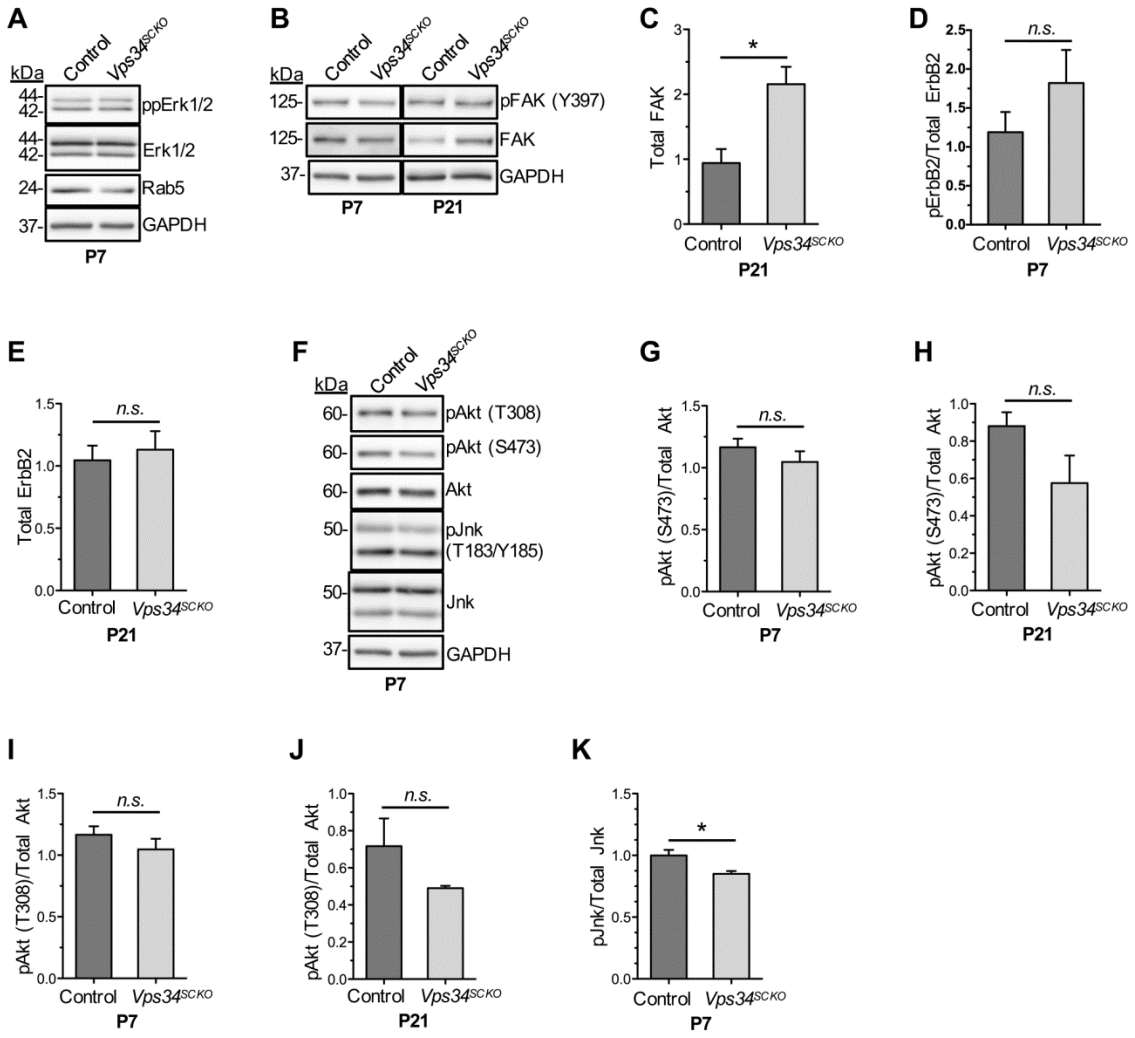

Figure 2.5: **Evaluation of kinase signaling pathways downstream of Nrg1-ErbB2/3, and FAK activation in sciatic nerves from control and *Vps34*^{SCKO} mice**. **(A)** P7 *Vps34*^{SCKO} nerves showed no change in the activation of Erk1/2, or the level of the early endosome protein Rab5. **(B)** The effect of Vps34 loss on FAK activation was determined by immunoblotting P7 and P21 sciatic nerve extracts and quantifying the relative amounts of phosphorylated protein (pFAK-Y397). The level of activated FAK was not significantly different at P7 in *Vps34*^{SCKO} nerves compared to controls. **(C)** By P21, the level of total FAK was increased in *Vps34*^{SCKO} nerves, while the level of phospho-FAK-Y397 was unchanged. Increased total FAK levels at P21 may result from the significant

hyperproliferation of Schwann cells that occurs after P7 in *Vps34*^{SCKO} nerves, as FAK has been shown to be important for Schwann cell proliferation (134). **(D)** Phospho-ErbB2 levels were not significantly changed in *Vps34*^{SCKO} nerves at P7 ($p = 0.2362$). **(E)** The amount of total ErbB2 protein was unchanged in P21 nerves ($p = 0.67$). **(F)** Evaluation of the activation of Akt and Jnk kinases in control and *Vps34*^{SCKO} sciatic nerves at P7 using immunoblotting. **(G–J)** Activation of Akt was assessed at two phosphorylation sites (T308 and S473). T308 is downstream of ErbB2/3 receptor signaling; S473 is believed to be phosphorylated by mTORC2 or ILK. (G & I) In P7 nerves, there is no difference in Akt activation at residue S473 ($p = 0.33$) or T308 ($p = 0.60$). (H & J) By 21, the amount of Akt phosphorylation was slightly decreased at residue S473 ($p = 0.11$) and residue T308 ($p = 0.21$) in *Vps34*^{SCKO} nerves. **(K)** Jnk activation was assessed by monitoring phosphorylation of residues T183 and Y185, both of which are phosphorylated downstream of ErbB2/3 signaling. Jnk phosphorylation was modestly decreased at P7 in *Vps34*^{SCKO} nerves. For P7, n = 4 and n = 3 independent extracts for control and *Vps34*^{SCKO}, respectively. For, P21 n = 3 and n = 4 independent extracts for control and *Vps34*^{SCKO}, respectively. Each sciatic nerve extract (the biological replicate) was prepared by homogenizing the (pooled) nerves from three mice of the same genotype at P7, and one or two mice at P21. Graphed data are mean ± SEM; *n.s.,* not significant; *$p < 0.05$; unpaired t-tests were used to evaluate significance.

Chapter 3

Distinct roles for Charcot-Marie-Tooth disease-causing endosomal regulators Mtmr5 and Mtmr13 in axon radial sorting and Schwann cell myelination

Anna E. Mammel[1,2], Katherine C. Delgado[1], Andrea L. Chin[1], Alec F. Condon[1,3], and Fred L. Robinson[1,4,*]

[1]The Jungers Center for Neurosciences Research, Department of Neurology, Oregon Health & Science University, 3181 SW Sam Jackson Park Road, Portland, OR 97239, USA.

[2]Cell, Developmental & Cancer Biology Graduate Program, Oregon Health & Science University

[3]Neuroscience Graduate Program, Oregon Health & Science University

[4]Vollum Institute, Oregon Health & Science University

[*]Corresponding Author: The Jungers Center for Neurosciences Research, Department of Neurology, Oregon Health & Science University, Mail Code L623, 3181 SW Sam Jackson Park Road, Portland, OR 97239, USA. Tel 503-494-8783; Fax 503-494-9161; Email: robinsof@ohsu.edu

PREFACE

This work is in preparation for submission for publication.

Anna Mammel designed and performed the majority of the experiments and data analysis in the manuscript. Anna wrote this manuscript draft. Katherine Delgado assisted with nerve morphology analysis and manuscript editing. Alec Condon designed gRNA for generation of the *Mtmr5*$^{-/-}$ mouse. Andrea Chin assisted with sequence analysis of the *Mtmr5*$^{-/-}$ founder mice.

Fred Robinson contributed to the concept of the project, experimental design, and edited the manuscript.

ABSTRACT

Charcot-Marie-Tooth type 4B (CMT4B) disease caused by myotubularin-related 5 (*MTMR5*; *set binding factor 1* (*SBF1*)) mutations show a spectrum of axonal and demyelinating nerve phenotypes. In contrast to other CMT4B subtypes caused by *MTMR2* or *MTMR13* (*SBF2*) mutations which are characterized by myelin outfoldings and pure demyelinating neuropathy. Therefore, it remains unclear whether MTMR5 has an analogous or distinct role from its homolog MTMR13 in the peripheral nervous system (PNS). MTMR5 and MTMR13 are pseudophosphatases predicted to regulate endosomal trafficking by activating Rab GTPases and binding to the catalytically-active phosphoinositide phosphatase MTMR2. In the mouse PNS, Mtmr2 was required to maintain wild type levels of Mtmr5 and Mtmr13. Suggesting that avid binding of Mtmr2 to both Mtmr5 and Mtmr13 may be critical for normal endosomal trafficking and nerve development. Loss of Mtmr5 in mice did not cause abnormal CMT4B-like myelin outfoldings. However, *Mtmr5*$^{-/-}$ adult mouse nerves had fewer myelinated axons likely resulting from axon radial sorting defects. Genetic elimination of both Mtmr5 and Mtmr13 in mice led to perinatal lethality, indicating that the two proteins have particularly-redundant function during embryogenesis. Mtmr5 levels were highest during axon radial sorting, whereas Mtmr13 increased as myelin formed and remained high through adulthood. Our findings suggest that in the PNS Mtmr5 and Mtmr13 bind avidly to Mtmr2 to ensure proper axon radial sorting and Schwann cell myelination, respectively. This lays the ground work for understanding the non-redundant roles that the endosomal regulators MTMR5 and MTMR13 have during normal peripheral nerve development and disease.

INTRODUCTION

During the development of the peripheral nervous system (PNS), Schwann cells associate with bundles of mixed diameter axons. During a process known as radial sorting, Schwann cells segregate large diameter axons (>1 μm) from smaller axons, which remain in bundles (10, 14). Once sorted into a 1:1 association with a Schwann cell, large caliber axons are enwrapped in a specialized multilayer membrane sheath called myelin (6). Myelin facilitates rapid saltatory nerve conduction by clustering sodium channels at nodes of Ranvier (135). Small caliber axons (<1 μm) remain unmyelinated and are supported by Schwann cells in Remak bundles (10). Both myelinating and Remak Schwann cells provide metabolic support to maintain axon integrity (5, 6, 27, 28, 136). Radial sorting and subsequent myelination require coordinated cytoskeleton reorganization and receptor signaling from both the adaxonal and abaxonal Schwann cell surfaces (6, 14). The precise control of downstream signaling is thought to be mediated in part by receptor trafficking through the endo-lysosomal pathway (39, 40, 43).

Genomic studies have suggested a link between abnormal endosomal trafficking and multiple subtypes of demyelinating Charcot-Marie-Tooth (CMT) disease (64). CMT is the most common inherited neurological disorder, affecting 1 in 2500 people (61). Genetic mutations that cause CMT are typically subdivided into either axonal or demyelinating forms, which affect the axon or Schwann cell, respectively (137). CMT type 4 (CMT4) is characterized by autosomal recessive inheritance and demyelination (63). Nearly half of the human proteins that cause CMT4 when mutated are proposed to regulate membrane trafficking through endo-lysosomal compartments. These proteins include dynamin 2 (*DNM2*), factor-induced gene 4 (*FIG4*), FGD1-related F-actin- binding protein (*FRABIN*), lipopolysaccharide-induced tumor necrosis factor-alpha factor (*LITAF*), SH3 domain and tetratricopeptide repeats 2 (*SH3TC2*), myotubularin- related 2 *(MTMR2), MTMR5,* and *MTMR13* (64). Several of these proteins including FIG4,

FRABIN, MTMR2, MTMR5, and MTMR13 control endo-lysosomal trafficking by generating or binding phosphoinositides (PIs) localized to early endosomes and lysosomes. Despite the broad expression of these genes in mammalian tissues, mutations primarily impact the PNS. This suggests that myelinating Schwann cells are highly sensitive to disruptions in endo-lysosomal PI levels and membrane trafficking defects (64, 66).

CMT4B results from mutations in MTMR2, MTMR5 (also known as Set Binding Protein 1, SBF1), or MTMR13 (SBF2) (Fig. 3.1) (52, 67, 68). Myotubularins are a large family of phosphatidylinositol (PI) 3-phosphatases that control membrane trafficking through endosomes and lysosomes (138). This family of proteins includes both catalytically active and inactive phosphatase enzymes. MTMR2 contains an active phosphatase domain whereas MTMR5 and MTMR13 contain catalytically inactive phosphatase domains (68, 73, 139). MTMR5 and MTMR13 share 59% protein identity and possess the same unique set of protein domains, including a DENN domain which actives Rab GTPases and a coiled-coil motif that facilitates association with MTMR2 (Fig. 3.1). MTMR2 and MTMR13 are thought to function as a membrane-associated complex that regulates PI levels and drives Rab GTPase activation to influence the trafficking of key Schwann cell receptors through endosomes (42, 53, 94, 95). However, it remains unclear if MTMR5, which also binds avidly to MTMR2 (69), has an analogous role to MTMR13 in the PNS.

The human nerve pathology associated with homozygous mutations in MTMR2 or MTMR13 has been well characterized. Loss-of-function mutations in MTMR2 or MTMR13 cause distinctive myelin outfoldings, which are thought to arising from excessive longitudinal myelin growth, and severe axon loss secondary to demyelination (52, 68). In contrast, MTMR5-associated neuropathies show a broader clinical presentation including myelin outfoldings, axon loss, thin myelin, and/or Schwann cell

bands (67, 97, 98). To date, five families have been identified with CMT-causing mutations in *MTMR5*; most are missense mutations within or near the DENN-domain (Fig. 3.1) (67, 97, 98, 140, 141). Thus, it remains unclear whether MTMR5 loss-of-function causes myelin outfoldings analogous to those observed in the nerves of CMT4B1 (MTMR2) and CMT4B2 (MTMR13) patients.

To elucidate the role of Mtmr5 in the PNS, we generated an *Mtmr5* knockout mouse model using CRISPR-mutagenesis and assessed the pathological consequences of Mtmr5 loss on peripheral nerves. We used biochemical approaches to determine how the three CMT-causing myotubularin proteins interact and the functional significance of these interactions in relation to disease. Our study indicated that homologous proteins, Mtmr5 and Mtmr13, both require Mtmr2 to maintain their protein levels in the PNS but have distinct roles during axon radial sorting and myelination.

RESULTS

A novel deletion allele of *Mtmr5*

The function of Mtmr5 in the peripheral nervous system is unclear due to the variability in CMT4B3 patient nerve pathology (67, 97, 98). To assess the role of Mtmr5 in the peripheral nervous system a knockout mouse model (*Mtmr5*$^{-/-}$) was generated and assessed for nerve defects. Initial characterization of an *Mtmr5* deletion allele in mice was described prior to the discovery that mutations in human MTMR5 cause CMT4B3 disease (100). The previously described *Mtmr5* deletion causes male infertility, but whether these mice develop peripheral nerve defects was not examined (100). We attempted to reestablish this mouse line to define nerve pathology by intracytoplasmic injection of *Mtmr5*$^{-/-}$ mouse sperm into a fertilized egg, however, this approach was unsuccessful. Therefore, a novel *Mtmr5* knockout mouse model was generated using CRISPR-Cas9 mutagenesis. To delete the *Mtmr5* gene, guide RNAs (gRNAs) were

designed to target exon 1 and exon 25 (Fig. 3.2A). Founder mice were screened for mutations in exon 1 and/or large deletions that remove the sequence spanning exon 1 to exon 25. A founder mouse was determined to be mosaic for two distinct deletions between exon 1 and exon 25 (mutation 1 and 2) (Fig. 3.2A). Only mutation 2 was passed on to the founder mouse progeny (Fig. 3.2B). This novel *Mtmr5* allele was predicted to yield a frame-shit containing a premature stop codon in exon 25; translation would result in a non-functional six amino acid peptide (Fig. 3.2B; Supp. Fig. 3.9).

Consistent with the predicted gene disruption, the 208 kDa Mtmr5 protein was undetectable in sciatic nerve and brain exacts from *Mtmr5*$^{-/-}$ mice (Fig. 2C & D). However, a truncated Mtmr5 protein of 84.8 kDa was detected at a low level in brain extracts of from P7 *Mtmr5*$^{-/-}$ mice (Supp. Fig. 3.10). We predict that translational initiation from an ATG codon in exon 26 led to low-levels of this truncated Mtmr5 protein, at least in neonatal mouse brains. The described N-terminally truncated Mtmr5 protein was not detected in adult brain or sciatic nerve extracts (Fig. 3.2, Supp. Fig. 3.10). When expressed, the truncated protein may be non-functional because the protein lacks both the DENN and PH-GRAM domains (Fig. 3.1).

Mtmr5$^{-/-}$ mice were viable and observed at the frequency predicted by Mendelian genetics. Homozygous mutants of both sexes were about 30% smaller than wild type and *Mtmr5*$^{+/-}$ controls (Supp. Fig. 3.11). This weight difference was observed at weaning and continued throughout the life of the animal. Overt motor or gait deficiencies were not observed in *Mtmr5*$^{-/-}$ mice examined at P38 and 17-months (*data not shown*). *Mtmr5*$^{-/-}$ males were sterile (Table 1), consistent with previous observations made using a distinct deletion allele (100). Sterility of the *Mtmr5*$^{-/-}$ mouse along with lack of protein expression demonstrated successful generation of a *null* allele.

Biochemical relationships amongst CMT-linked myotubularins

MTMR5 and MTMR13 are known to bind MTMR2 avidly via their coiled-coil motifs, however it is unclear whether the pseudophosphatases also interact with each other (69, 70). To test their physical association, we overexpressed epitope-tagged MTMR5 with MTMR13 and/or MTMR2 in HEK293 cells. MTMR5 and MTMR13 formed a very weak interaction that did not require coiled-coil dimerization or their mutual binding partner MTMR2 (Fig. 3.3). The weak interaction between MTMR5 and MTMR13 had no impact on their mutual protein abundance. In contrast, binding to MTMR2 greatly increased the protein levels of both MTMR5 and MTMR13 (Fig. 3.3A, B). These data suggest that MTMR5 and MTMR13 form a very weak association that does not equate to their avid binding of MTMR2.

We previously demonstrated that Mtmr2 and Mtmr13 require each other to maintain wild type protein levels in mouse sciatic nerves (94). To determine if Mtmr2 and/or Mtmr13 proteins were required to regulate Mtmr5 levels, we examined mutant mouse brain and sciatic nerve lysates. Both Mtmr5 and Mtmr13 proteins were significantly reduced in *Mtmr2*$^{-/-}$ nerves (Fig. 3.4A, B). However, the requirement of Mtmr2 to maintain Mtmr5 at wild type levels was not reciprocal; *Mtmr5*$^{-/-}$ sciatic nerve lysates had comparable Mtmr2 levels to wild type nerves (Fig. 3.4D, E). Mtmr13 loss had no impact on Mtmr5 levels in mouse brain or sciatic nerves, demonstrating that these pseudophosphatases do not require one another to maintain wild type protein levels (Fig. 3.4A, C). The stabilization of Mtmr5/13 levels by Mtmr2 was unique to the PNS, loss of Mtmr2 had no impact on the levels of Mtmr5 or Mtmr13 in brain extracts (Fig. 3.4C). Loss of both Mtmr5 and Mtmr13 protein in *Mtmr5*$^{-/-}$; *Mtmr13*$^{-/-}$ mouse embryonic fibroblasts (MEFs) did not impact Mtmr2 abundance (Fig. 3.4F, G). In summary, these data demonstrate the requirement of Mtmr2 to maintain both Mtmr5 and Mtmr13 protein abundance specifically in the PNS, where CMT disease manifests.

Reduced sciatic nerve axons and normal myelination in the absence of Mtmr5

The nerve pathology of Mtmr13 loss has been well characterized through the use of mouse models, while the pathology resulting from Mtmr5 loss remains relatively undefined. Loss-of-function mutations in *Mtmr13* cause distinct Schwann cell myelin abnormalities known as “myelin outfoldings” in human CMT patients and mouse models (92, 142, 143). The role of Mtmr5 in the PNS remains unclear due to the variation in patient nerve biopsies. Through examination of *Mtmr5*$^{-/-}$ mouse nerves we sought to determine whether Mtmr5 has a distinct or analogous role to Mtmr13 in the PNS. At age 3 months, the morphology of *Mtmr5*$^{-/-}$ sciatic nerves appeared grossly normal compared to wild type controls by light microscopy (Fig. 3.5A-D). Loss of Mtmr5 did not cause CMT4B-like myelin outfoldings, indicating a distinct pathology from Mtmr13 loss (Fig. 3.5C-E). Absence of Mtmr5 did not alter myelin thickness; g-ratios were not significantly different between *Mtmr5*$^{-/-}$ and wild type fibers (Fig. 3.5F). However, *Mtmr5*$^{-/-}$ mice had significantly fewer total myelinated axons compared to wild type control nerves (Fig. 3.5G). Consistently, the absence of Mtmr5 did not alter the diameter of myelinated axons, a feature of several mouse models of axonal CMT (Fig. 3.5H) (144, 145). These data demonstrate that Mtmr5 loss caused distinct nerve pathologies from Mtmr13 loss, despite sharing the same binding partner Mtmr2 and protein domains. In summary, Mtmr5 absence did not cause myelin defects but did lead to an overall reduction in myelinated axons.

Axonal sorting defects in the absence of Mtmr5

Incomplete radial sorting by immature Schwann cells can lead to the abnormal retention of large caliber axons in bundles, reducing the total number of myelinated axons in the nerve (146, 147). To determine whether loss of Mtmr5 caused abnormal Remak bundle development we assessed every bundle in ~40% of the sciatic nerve

area by EM. Nerves were characterized in wild type and *Mtmr5*$^{-/-}$ sciatic nerves at three months of age by quantifying the proportion of bundled axons whose diameter exceeded 1 μm, incomplete ensheathment of axons by Schwann cell processes, and the total number of axons per bundle. Wild type unmyelinated axons were surrounded by Schwann cell cytoplasm and only a small percentage of axons exceeded 1 μm in diameter (Fig. 3.6A). Loss of Mtmr5 caused a significant increase in the proportion of bundled axons that had a diameter >1 μm compared to controls (Fig. 3.6B, C). We observed a significant increase in single unmyelinated axons, and a decrease in the percentage of bundles containing between 11-20 axons (Fig. 3.6D). A significant proportion of *Mtmr5*$^{-/-}$ bundled axons were incompletely ensheathed, lacking Schwann cell processes between the axon and the basal lamina (Fig. 3.6E-H). Together these data indicate that Mtmr5 regulates late-stage radial sorting of large caliber axons. In contrast, *Mtmr13*$^{-/-}$ Remak bundles appear morphologically similar to wild type nerve bundles as our previous studies demonstrate (142). We hypothesize that Mtmr5 regulates steps critical for axon radial sorting and is dispensable during subsequent myelination.

Absence of both Mtmr5 and Mtmr13 is lethal in mice

Mtmr5 and Mtmr13 share 59% protein identity and are the only two proteins in the mammalian genome that share their unique set of protein domains (Fig. 3.1) (148). To determine whether Mtmr5 and Mtmr13 have partial redundant functions we generated *Mtmr5*$^{-/-}$; *Mtmr13*$^{-/-}$ double knockout mice (dKO). dKO animals were not viable; these mice died either during late stage gestation or within a few hours of birth (Fig. 3.7A, B). Embryos were observed at expected genotypic ratios from E13-E15 (data not shown). dKO P0 pups and E13 embryos were smaller than littermate controls but had no

developmental defects noticeable by the authors (Fig. 3.7A, C). Thus, both Mtmr5 and Mtmr13 were required for mouse survival.

Mtmr5 and Mtmr13 have critical roles in the PNS and are proposed to activate Rab21, a regulator of neurite growth and axon guidance (72, 149). We assessed whether loss of both proteins impacts axon guidance and/or peripheral nerve development during embryogenesis. Nerve branches in dKO mouse pinna, a region where axon guidance is well defined, showed no evidence of defects in axon branching or guidance at E13 (Fig. 3.7D, E). This does not preclude the idea that subtler axon guidance defects may occur in dKO mice which were not examined by the authors.

Myotubularin expression in peripheral nerves and Schwann cells

We assessed whether Mtmr5 and Mtmr13 are expressed at different stages of PNS development. Mouse sciatic nerve lysates were quantified for Mtmr2, Mtmr5, and Mtmr13 protein at distinct time points during mouse development. Mtmr5 levels were highest between P0 and P7, with a considerable decrease by P21 (Fig. 3.8A, B). Mtmr13 increased over time and peaked between P21 and 1 month. Mtmr2 was present throughout sciatic nerve development (Fig. 3.8A, B). This is consistent with the late stage radial sorting defects observed in *Mtmr5*$^{-/-}$ nerves, given that protein levels were highest during this phase (E17-P10). Mtmr13 levels correlated with PNS myelination, which begins at P0 and continues into adulthood.

We assessed the expression of all 14 myotubularin family members in adult mouse Schwann cells through analysis of a publicly available dataset (Fig. 3.8C) (150). RNA-seq analysis showed that *Mtmr2* and *Mtmr13* are highly expressed along with *Mtmr6* in Schwann cells isolated from adult mice. *Mtmr5* transcripts were at low levels in Schwann cells, consistent with our whole sciatic nerve protein analysis (Fig. 3.8C). We predicted that during radial sorting Mtmr2 functions in a complex with Mtmr5 to

determine which axons are sorted. Once the axons are sorted into a 1:1 association then Mtmr2 interacts with Mtmr13 to control myelination. The difference in *Mtmr5* and *Mtmr13* temporal expression may explain the unique PNS phenotypes observed in *Mtmr13*$^{-/-}$ and *Mtmr5*$^{-/-}$ animals.

DISCUSSION

Mtmr5-deficent mice have distinct nerve pathologies from other CMT4B mouse models

Nerve biopsies from CMT4B3 patients with *MTMR5* mutations show a range of phenotypes including myelin outfoldings, broad axon loss, thin myelin, and Schwann cell bands (67, 97, 98). Therefore, the disease pathology of Mtmr5 loss-of-function mutations was unclear compared to the other well-characterized CMT4B subtypes caused by MTMR2 or MTMR13 loss. We demonstrated that loss of Mtmr5 in mice led to axon radial sorting defects and fewer myelinated axons in the sciatic nerve. Myelin in *Mtmr5*$^{-/-}$ mouse PNS was normal. This is in contrast to the distinctive myelin abnormalities caused by either Mtmr2 or Mtmr13 knockout mouse models. Suggesting that Mtmr5 regulates axon radial sorting and is not required once the axons form a 1:1 relationship with myelinating Schwann cells.

Mtmr5-null mice as a model for CMT4B3 disease

Loss of *Mtmr5* in mice caused a ~10% reduction in myelinated axons due to radial sorting defects. Several patient families with loss-of-function mutations in *MTMR5* show moderate depletion in the number of myelinated axons without defects in myelin structure, suggesting primary axonal neuropathy (98, 140). Incomplete radial sorting can cause a reduction in the total number of myelinated axons, and results from either axonal or Schwann cell specific defects. Further conditional knockout mouse studies will

be required to elucidate whether Mtmr5 acts within the Schwann cell and/or the axon to ensure proper radial sorting.

We can only speculate why the neuropathy of *Mtmr5* mutant mice was milder than CMT patients. However, a milder phenotype is common for mouse models of axonal neuropathies, including neurofilament light chain mutants (*Nefl*$^{N98S/+}$, and *Nefl*$^{-/-}$), mitofusin 2 mutant (*Mfn2*^{R94W}), ganglioside-induced differentiation-associated protein 1 null (*Gdap1*$^{-/-}$), membrane metalloendopeptidase null (*Mme*$^{-/-}$), tripartite motif containing 2 null (*Trim2*$^{-/-}$), and histidine triad nucleotide binding protein 1 null (*Hint1*$^{-/-}$) mice (144, 151-155). A possible explanation is that mice do not live as long as humans and have less time to develop extensive axon loss. Additionally, human nerves are larger, which translates to an increase in the number of axons sorted for myelination.

Myelin in *Mtmr5*$^{-/-}$ mouse PNS was of normal thickness and structure. This is in contrast to the distinctive myelin abnormalities caused by either Mtmr2 or Mtmr13 loss, namely myelin outfoldings. One patient family with compound heterozygous mutations (M417V and T1590A) in *MTMR5* shows myelin outfoldings (67). T1590A mutation is located within the inactive phosphatase domain of MTMR5. It remains unclear how this particular mutation affects MTMR5 function. We predict that T1590A may be a gain of function mutation that enhances MTMR5's ability to interact with MTMR2. Sequestration of MTMR2 by mutant MTMR5 during myelination would cause a reduction in MTMR2-MTMR13 complex formation causing myelin abnormalities. This gain-of-function hypothesis may explain why only one *MTMR5*-mutant family shares similar nerve pathology to other CMT4B subtypes, but not our *Mtmr5*-null mice or other human mutations.

Mtmr5 and Mtmr13 form distinct protein complexes with Mtmr2 in the PNS

Both Mtmr5 and Mtmr13 protein levels increased when expressed with their binding partner Mtmr2 *in vitro* and in the PNS. We showed that Mtmr5 and Mtmr13 form a very weak interaction that was independent of Mtmr2. An Mtmr5-Mtmr13 complex would be unable to dephosphorylate PI3P or PI(3,5)P_2, key regulators of trafficking through early endosomes and lysosomes. Therefore, we hypothesized that two functional myotubularin protein complexes form in the PNS, an Mtmr2-Mtmr5 complex and an Mtmr2-Mtmr13 complex. These two complexes would have similar capacity to regulate endosomal trafficking by activating Rab proteins and dephosphorylating phosphoinositides. In tissues outside the PNS these two Mtmr complexes likely have overlapping or redundant function, because loss of both Mtmr5 and Mtmr13 protein was lethal in mice whereas the individual knockouts were viable.

In contrast to their redundant roles in embryo development, we determined that Mtmr5 and Mtmr13 have distinct nerve function because of differences in the developmental timing. Mtmr5 levels were highest during axon radial sorting, whereas Mtmr13 increased over the course of myelination and remained high in adult sciatic nerves. Mtmr2 was fairly constant throughout nerve development. Therefore, we predict that Mtmr2 and Mtmr5 function together in immature Schwann cells to control which axons are sorted for myelination, and Mtmr2-Mtmr13 function in a complex to regulate myelination. The lack of Mtmr5 protein expression after P7 may explain why loss of Mtmr5 had no impact on Mtmr2 protein levels in adult nerves. Expression of Mtmr2 during all stages of nerve development also explains why loss of this protein leads to a decrease in both Mtmr5 and Mtmr13 levels in mouse sciatic nerves. We demonstrated that in most tissues either Mtmr5 or Mtmr13 protein was sufficient for normal cell function due to shared protein expression. The PNS may require both proteins because of temporal differences in Mtmr5 and Mtmr13.

Control of endosomal trafficking by Mtmr5 and Mtmr13 during axon sorting and myelination

Schwann cells determine which axons are large enough to be myelinated through signaling from ErbB2/3 tyrosine kinase receptors on the cell surface. Abnormal trafficking of the ErbB2/3 receptor in Schwann cells has been proposed as a common mechanism linking demyelinating subtypes of CMT (66). Previous studies conducted by our lab and others have shown that maintenance of normal endosomal PI3P levels in Schwann cells is critical to controlling ErbB2/3 trafficking and downstream signaling (42, 43). Loss of Mtmr2 has been shown to cause increased pErbB2 levels during myelin initiation (42). Because Mtmr5 and Mtmr13 interact in a complex with Mtmr2, we predict that Mtmr5 and/or Mtmr13 loss may also lead to an increase in ErbB2/3 activation due to mistrafficking. This will be an interesting area of future study, which may help clarify the dual role of ErbB2/3 in controlling axon sorting and myelination.

Mtmr5 and Mtmr13 protein may also control the trafficking of β1-integrin, which binds to laminin 211 in the Schwann cell basal lamina. The trafficking of β1-integrin through early endosomes is controlled by Rab21, which the DENN domains of Mtmr5 and Mtmr13 are predicted to activate (72). β1-integrin is required for the extension and maintenance of Schwann cell processes around axons. Loss of β1-integrin leads to radial sorting defects and delayed myelination in conditional knockout mice (130). Interestingly, Mtmr5$^{-/-}$ unmyelinated axons had incomplete Schwann cell ensheathment between the axons and basal lamina. This could be caused by a reduction in β1-integrin on the plasma membrane of *Mtmr5*$^{-/-}$ Schwann cells due to reduced recycling from early endosomes. Although ErbB2/3 and integrin are the two receptors most likely to be controlled by Mtmr5 and Mtmr13 mediated endosomal trafficking, these pseudophosphatase may control multiple receptors during peripheral nerve development.

Understanding how Mtmr5 and Mtmr13 control the trafficking of receptors involved in mediating axo-glial interaction and pro-myelination signals will be critical to uncovering why loss of these proteins cause CMT. In conclusion we have shown for the first time that Mtmr5 controls axon radial sorting in mouse peripheral nerves, providing a model to study axon sorting defects and CMT4B3 disease.

MATERIALS AND METHODS

Mice - All animal work was approved by and conformed to the standards of the Oregon Health & Science University Animal Care and Use Committee. *Mtmr2*$^{-/-}$ and *Mtmr13*$^{-/-}$ mice have been previously described (94, 142). An *Mtmr5* null mouse was generated via CRISPR/Cas9 mutagenesis. Two guide RNAs were designed against exon 1 and exon 25 of the mouse *Mtmr5* gene using the online tool CRISPR Design. The following guide RNAs (gRNAs) were selected for their minimal off-target affects and potential to generate a large deletion beginning after the start-site (exon 1: GCTCGCGGACTACTTCGTGC) and ending after a putative internal initiation site (exon 25: CGTAAGAAGTATAACCCCCC). These *Mtmr5*-specific gRNA sequences were ligated into the *BbsI* restriction endonuclease site of px330 (addgene plasmid #42230) (156). Plasmids containing gRNAs plus Cas9 endonuclease were injected into the pronuclei of C57BL/6NJ mouse embryos. The embryo donors were oviduct transferred into CB6F1/J pseudopregnent recipient dams. *Mtmr5* founder mice were screen by PCR and Sanger sequencing to identify putative mutations in exon 1, exon 25, and large deletions between exon 1 and exon 25 using the following primers: forward exon 1 primer AMO-49 5’ CATGCGGAGTGGCCCAAT 3’, reverse exon 1 primer AMO-50 5’ GGATGTTTCTTACACAGGCCATGT 3’, forward exon 25 primer AMO-51 5’ CACGGGTTACCAAGGACAAGG 3’, reverse exon 25 primer AMO-56 5’ GTCAACTCTGATAGCGAGCACAG 3’. Mutations were confirmed by TOPO TA

(ThermoFisher) cloning and Sanger sequencing. Mice were breed to homozygosity and western blots were run to confirm Mtmr5 protein loss in brain and sciatic nerve tissue. To test male sterility, six *Mtmr5*$^{-/-}$ male mice were allowed to breed with C57BL/6 females for at least 21 days. Bred females were monitored for pregnancy and births for an additional three to four weeks.

Mtmr5$^{-/-}$; *Mtmr13*$^{-/-}$ (double knockout) mice were generated by crossing the *Mtmr5* CRISPR founder male with a single *Mtmr13*$^{-/-}$ female. *Mtmr5*$^{+/-}$; *Mtmr13*$^{+/-}$ progeny were screened by PCR and Sanger sequencing for the large deletion using the following primers: AMO-49 5' CATGCGGAGTGGCCCAAT 3' and AMO-56 5' GTCAACTCTGATAGCGAGCACAG 3'. The *Mtmr5*$^{+/-}$; *Mtmr13*$^{+/-}$ mice were crossed with *Mtmr13*$^{-/-}$ mice to generate *Mtmr5*$^{+/-}$; *Mtmr13*$^{-/-}$ progeny. The *Mtmr5*$^{+/-}$; *Mtmr13*$^{-/-}$ mice were interbred and their pups were genotyped at P0 to screen for dKO animals. 49 pups from 13 litters were genotyped to assess the viability of Mtmr5 and Mtmr13 loss.

Plasmid Constructs - Expression vector containing FLAG epitope-tagged human MTMR2 have been described previously (69), as well has vectors expressing human EGFP-tagged MTMR2 (79), EGFP-MTMR13, and myc-MTMR13 mutant constructs (70). Human FLAG epitope-tagged MTMR5 expression vector was previously described (69). However, this vector contained several mutations (Gln insertion between amino acid 93 and 94; K592M) that were fixed by the authors. To generate the wild type construct human pcNF-MTMR5 transcript variant 1 from NM-002972.3 was amplified using oligonucleotides: 5' GTTTAAACTTAAGCTTATGGCGCGGCTCGCGGAC 3' and 5' CCTGATGTCCGGCGGGTACCG 3'. The resulting PCR product was In-Fusion (Takara Bio) cloned into the FLAG-MTMR5 vector digested with KpnI and HindIII.

Cell Culture and Immunoprecipitation - HEK293 cells were cultured in Dulbecco's Modified Eagle's medium (Gibco 11995-065) with 10% fetal bovine serum and penicillin/streptomycin. Cells were between 70 – 80% confluent at the time of transfection. A 60-mm dish was transfected with 2.5 ug of plasmid DNA, 7.5 ul X-tremeGENE9 (Roche), and 250 ul of Opti-MEM (Gibco) according to manufacturer's instructions. 48h after transfection, cells were washed with 1x phosphate-buffered saline and lysed in 430 ul of ice-cold lysis buffer (120mM NaCl, 50 mM Tris (pH 8.0), 0.5% Triton X-100, 100 mM NaF, 1mM ortho-vanadate, 2mM EDTA, and proteinase inhibitor (Roche 11836153001)). Lysates were vortexed then cleared by centrifugation (15,000 x g for 15 min at 4°C). Myc-tagged proteins were immunoprecipitated using anti-c-Myc monoclonal antibody supernatant (9E10, DSHB) and protein A-agarose (Invitrogen). Flag-tagged proteins were immunoprecipitated using anti-Flag-M2 affinity gel (Sigma). Immunoprecipitations were incubated for at least 2 h at 4°C, and washed in 1ml lysis buffer twice, then three times with 1ml of lysis buffer contain 0.5 M NaCl, and a final wash in 1ml lysis buffer. Immunoprecipitates and lysates were suspended in NuPAGE LDS sample buffer and 10 mM DTT. Immunoprecipitates and lysates were run on SDS-PAGE 4 – 12% BisTris gels and transferred to polyvinglidene difluoride membranes prior to immunoblotting.

Immunoblotting - Immunoblotting of sciatic nerve, brain, HEK293 cell, and mouse embryonic fibroblast (MEF) extracts was performed as previously described (94). Rabbit antibodies anti-MTMR13 (116-AN) and anti-MTMR2 (119-AN) were generated as previously described (94). Mouse anti-FLAG (M2) and anti-c-myc (9E10) were from Sigma-Aldrich and Roche Applied Science respectively. Mouse anti-Mtmr5 (B-9) was from Santa Cruz Biotechnology. Mouse anti-GFP antibody (N86/8) was from NeuroMab. Mouse antibodies anti-β tubulin (E7) and anti-GAPDH (MAB374) were from DSHB and

Millipore respectively. For each P0, P3, and P7 nerve lysate three mice were pooled (6 nerves per lysate). For P21 and 1-month old mouse extracts nerves from two mice were pooled (4 nerves total) to generate each independent extract. Extracts from mice 3 months and older were generated from a single animal (2 nerves per lysate). For each immunoblot, 8 – 25 µm of protein per lane was resolved in 4-12% NuPAGE Bis-Tris gels (Invitrogen) and chemiluminescent quantitation was performed as previously described (95).

Sciatic nerve morphology - Mice were perfused with Karnovsky's EM fixative (4% paraformaldehyde, 2% glutaraldehyde and 0.1M sodium cacodylate buffer (pH 7.4)). Sciatic nerves were dissected and further fixed for at least 24 hours at 4°C. The nerves were washed three times in 0.1M sodium cacodylate (pH 7.4) and then washed three times in 0.1M sodium phosphate buffer (PB) (pH 7.4) at room temperature (RT). Nerves were postfixed and stained in 2% osmium tetraoxide in 0.1M PB buffer (pH 7.4) for 1hr. The nerves were washed three times in 0.1M PB at room temperature. Then underwent a series of ethanol dehydrations: 25%, 50%, 70%, 80%, and 95% EtOH diluted in ultra-pure water, 5 min incubations. A final dehydration was performed by incubating samples in 100% EtOH twice for 10 min, then two incubations in propylene oxide for 10 min each in scintillation vials. Tissues were infiltrated overnight in 1:1 propylene oxide:Embed 812 resin mixture then freshly-prepared 100% Embed 812 resin. Nerves were embedded in 60°C oven for 48h, the distal end was positioned towards the outside of the blocks to orient the nerves in the same direction.

Toluidine blue semi thin (200-500 µm) plastic cross-sections were prepared from the mid-sciatic nerve. Four non-overlapping images of Toluidine blue nerve sections were acquired at 63x on a Zeiss Axio imager.M2 ApoTome microscope with an AxioCam 512 color camera. The tile feature in Zeiss Zen 2 (blue edition) software was used to

capture the entire transverse fascicular area (TFA) for each nerve. To obtain total axon counts, 63x tiled Toluidine blue images were used. All myelinated axons in the TFA were marked and counted using Cell Counter plugin for Fiji (Fiji is just image-j). G-ratio was determined using the G ratio plugin for Fiji. 200 myelinated axons were randomly selected across 4 non-overlapping 63x Toluidine blue images of the TFA. In order to acquire an area-based g ratio measurement, the area of the axon was divided by the area of the myelined fiber. This measurement was then used to derive a diameter-based g ratio measurement.

EM images were obtained using a FEI Tecnai G2 operating at 80kV and an Advanced Microscopy Techniques camera. To analyze Remak bundles, 2900x EM images were used. All intact Remak axons in the large fascicle of each nerve were analyzed. Each Remak axon was counted and its area measure. Any axon with an area greater than 0.79 μm^2 (1 μm in diameter) was considered large. 2900x EM images were also used to count abnormally ensheathed axons. At least 42% of the nerve was exhaustively analyzed for each mouse.

Immunofluorescence - Whole-mount immunofluorescence of E13 mouse embryos with neurofilament medium chain (2H3) antibody was adapted from a previously described protocol (157). Individual embryos were stained in microcentrifuge tubes at room temp (RT) unless otherwise stated. Embryos were removed from their placenta in 1xPBS and 3mm of tail from each embryo was taken for genotyping. Embryos were fixed overnight at 4°C in 4% paraformaldehyde, 1xPBS solution (pH 7.4). After fixation, the embryos were washed with 1xPBS twice for 10 minutes. Then underwent a series of methanol (MeOH) dehydrations: 1hr in 50% MeOH (1xPBS), 2hr 80% MeOH (1xPBS), overnight in 100% MeOH. Embryos were bleached in 3% H_2O_2, 70% MeOH, 20% DMSO overnight, and washed five times at 45 minute intervals in 1xTNT (10mM Tris, 154mM NaCl, 0.1%

Triton X-100). Incubated in primary antibody for 2-3 days (1xTNT, 0.02% sodium azide, 4% nonfat milk, 5% DMSO, 2% normal goat serum (NGS), 0.37 ug/mL 2H3 antibody). Embryos were washed in 1xTNT five times, 45 minutes each. Followed by a 2-day incubation in secondary antibody solution (1xTNT, 4% bovine serum albumin, 0.02% sodium azide, 5% DMSO, 2% NGS, 6.4 ug/mL Cy3 goat-anti-mouse (115-175-205) from Jackson ImmunoResearch). In all subsequent steps the embryos were protected from light. Embryos are washed in 1xTBS (pH 7.4) four times for 45 minutes then overnight. Dehydrated by MeOH series: 1hr in 50% MeOH (1xPBS), 2hr 80% MeOH (1xPBS), overnight in 100% MeOH. The samples were cleared in 1:2 BABB solution (Benzyl:Benzyl benzoate). Whole embryo images were taken on Zeiss AxioCam MR microscope at 1x magnification prior to the 1:2 BABB clearing step. Images of the nerve branches were taken on a Zeiss ApoTome microscope 5x magnification in 1:2 BABB solution.

Statistics - Statistical analysis of immunoblots, weight, and morphology data were performed using a one-way ANOVA followed by a post-hoc Tukey's test when more than two groups of results were compared. A Student's t-test was used when two groups were compared. Chi-squared (χ^2) test was performed on genetic ratio data. The nonparametric Kolmogorov-Smirnov test (K-S test) was used for comparing the distribution of axon size. A probability value of ≤ 0.05 was used for declaring statistical significance. χ^2 and K-S tests were performed using R version 3.5.1. Prism software package (GraphPad) was used to perform ANOVA, Tukey multiple comparison, and Student's t-tests.

ACKNOWLEDGEMENTS

The authors wish to thank the OHSU Transgenic Mouse Core and Lev Fedorov for assistance with CRISPR-mutagenesis and expert advice. The authors would also like to thank Matthew Pomaville and Kevin Wright for expert advice on mouse whole embryo NF-M immunofluorescence. The authors would like to thank Jo Hill and Sue Aicher for EM preparation and processing. The EM microscope was purchased through a Murdock Charitable Trust grant to Sue Aicher. The E7 (β-tubulin) monoclonal antibody was developed by Dr. Michael Klymkowsky and obtained from Developmental Studies Hybridoma Bank (DSHB). The monoclonal antibody 2H3 (NF-M), developed by Drs. T.M. Jessell and J. Dodd, was obtained from the DSHB developed under the National Institutes of Health-National Institute of Child Health & Human Development and maintained by The University of Iowa, Department of Biology, Iowa City, IA 52242. This work was supported by National Institutes of Health – National Institute of Neurological Disorders and Stroke grants NS086812 (to F.L.R.) and the OHSU Neuroscience Imaging Center P30 grant (NS061800; To Sue Aicher), and through the philanthropy of Frank and Julie Jungers.

FIGURES AND LEGENDS

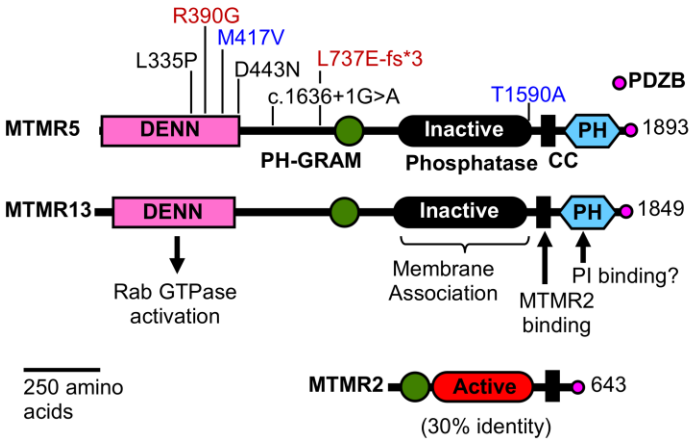

Figure 3.1: CMT-causing myotubularin proteins. All mutations are recessive, consistent with a loss of function mechanism. Functions attributed to specific domains of MTMR2, MTMR5, and MTMR13 are indicated. MTMR5 mutations M417V-T1590V and R390G-L737E-fs*s are shown in blue and red, respectively, to indicate compound heterozygosity. c.1636+1G>A is a splice site mutation predicted to cause non-sense mediate RNA decay. MTMR5 has a 59% identity with MTMR13 and a 30% identity with MTMR2 protein. *Abbreviations*: PH, pleckstrin homology; DENN, differentially expressed in neoplastic versus normal cells; GRAM, glucosyltransferase Rab activator myotubularins; PDZB, PDZ domain binding motif; CC, coiled-coil; PI, phosphoinositide.

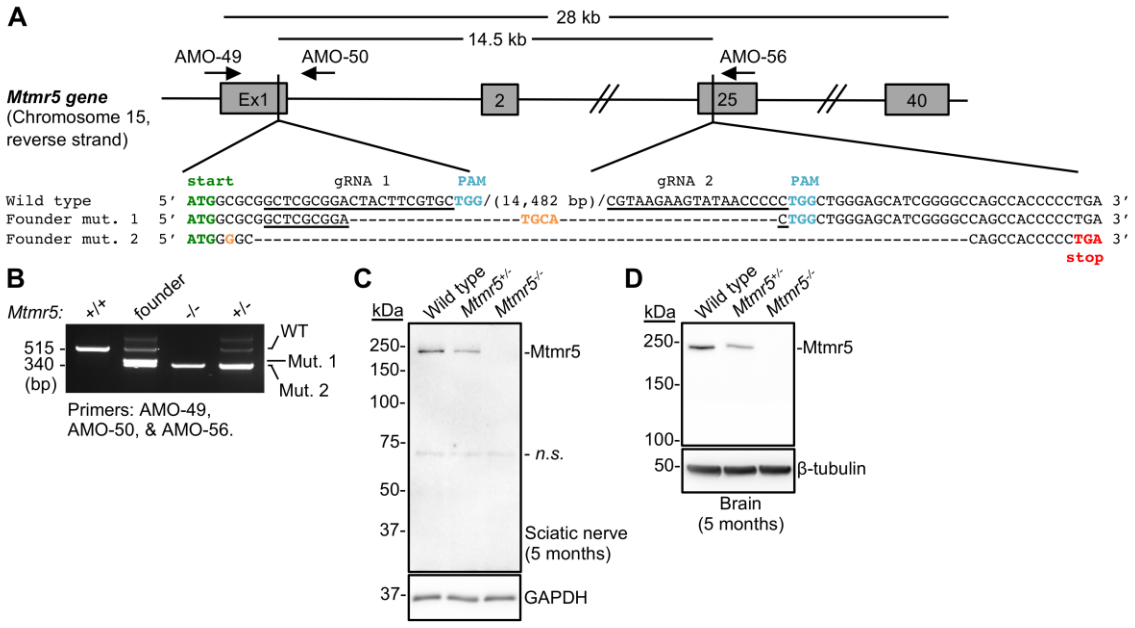

Figure 3.2: CRISPR/Cas9-mediated disruption of *Mtmr5*. (**A**) CRISPR-Cas9 mediated 14 kb deletion between exon 1 and exon 25 of *Mtmr5/Sbf1.* The following features are indicated: gRNA target sequences (underlined), transcription start site (green), PAM sequences (blue), premature stop codon (red), and additional mutations (orange). The CRISPR-Cas9 founder mouse was mosaic for two deletions indicated as mutation 1 (mut. 1) and mut. 2. Mice were genotyped using primers AMO-49, AMO-50, and AMO-56 at the indicated *Mtmr5* genomic locations and orientation. (**B**) Genotyping from a wild type mouse produces a 515 bp PCR fragment. The F1 generation and all subsequent intercrosses contained the mutation 2 deletion exclusively. (**C-D**) Immunoblot analysis of Mtmr5 protein levels from sciatic nerve and brain extracts of wild type, *Mtmr5*$^{+/-}$, and *Mtmr5*$^{-/-}$ 5 month old mice using a C-terminal Mtmr5 antibody. Each sciatic nerve extract was prepared by pooling two nerves (3 biological replicates). The protein loading controls were GAPDH and β-tubulin.

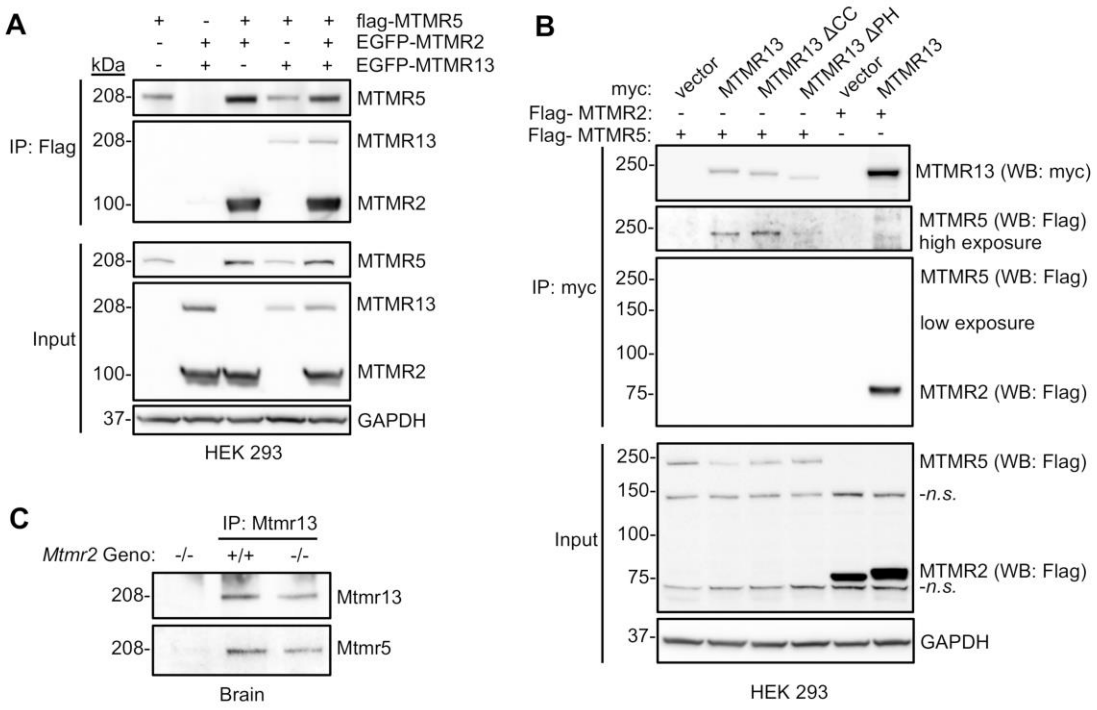

Figure 3.3: Physical association between CMT-linked myotubularin proteins. (**A**) HEK293 cells were transfected with FLAG-MTMR5 co-expressed with EGFP-MTMR2 and/or EGFP-MTMR13. After 48h, cell lysates were prepared and analyzed by FLAG immunoprecipitation (IP), SDS-PAGE, and western blotting (WB). Coexpression of EGFP-MTMR2 increases the amount of FLAG-MTMR5 protein in the lysate and IP. FLAG-MTMR5 immunoprecipitates EGFP-MTMR2 much more efficiently than EGFP-MTMR13. Representative images from one of two experiments are presented. (**B**) Coimmunoprecipitation of endogenous Mtmr13 and Mtmr5 from wild type and *Mtmr2*$^{-/-}$ mouse brains. Mtmr13 was detected using the 116-AP anti-MTMR13 antibody. The association between Mtmr5 and Mtmr13 was not altered by the absence of Mtmr2. (**C**) HEK293 cells were transfected with constructs encoding FLAG or c-Myc epitope-tagged versions of the indicated myotubularin proteins. The association between FLAG-MTMR5 and myc-MTMR13 does not require the coiled-coil (CC) or the c-terminal pleckstrin homology domain (PH) of MTMR13. Coexpression of FLAG-MTMR2 but not FLAG-

MTMR5 increased the recovery of immunoprecipitated myc-MTMR13 from HEK293 cells. Nonspecifc cross-reaction of the anti-FLAG antibody with proteins present in the cell lysates are indicated (*n.s.*). Representative images from one of two experiments.

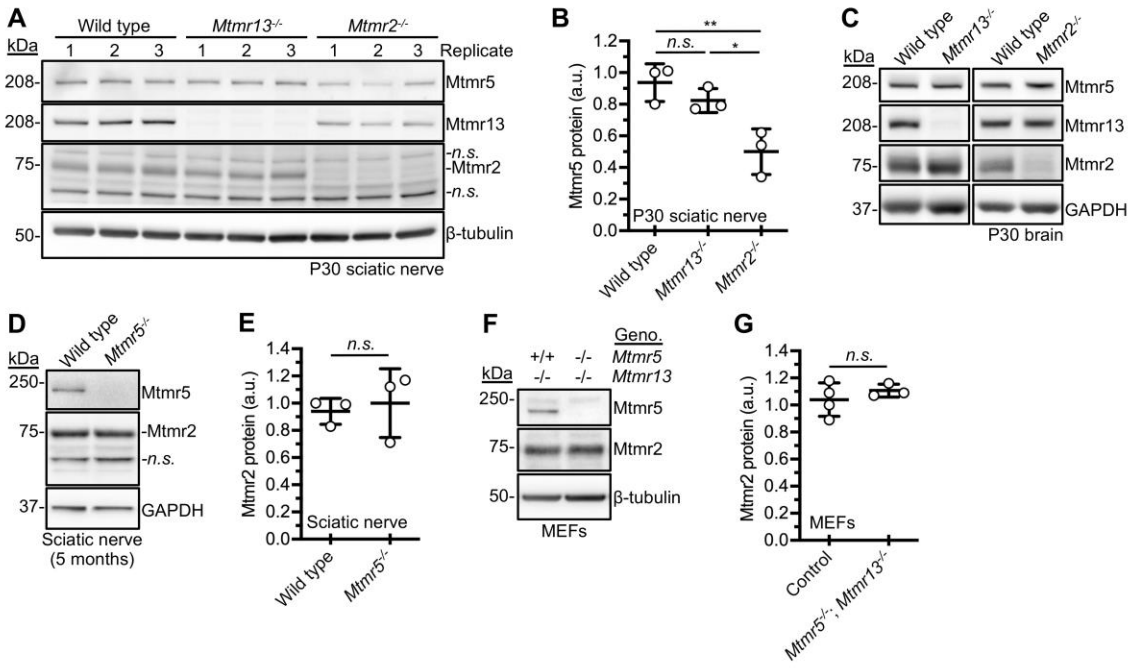

Figure 3.4: Loss-of-function relationships amongst CMT-linked myotubularin proteins. (**A**) Sciatic nerve lysates prepared from wild type, *Mtmr13*$^{-/-}$, and *Mtmr2*$^{-/-}$ P30 mice. Pools A, B, and C denote independent (replicate) pools of nerves of the same genotype (4 nerves per lysate). Non-specific bands are denoted (*n.s.*) in Mtmr2 blots. (**B**) Quantification of Mtmr5 protein levels: wild type 0.937 ± 0.115, *Mtmr13*$^{-/-}$ 0.825 ± 0.072, *Mtmr2*$^{-/-}$ 0.499 ± 0.147 arbitrary units (a.u.). These data are presented as mean ± SD; one-way ANOVA with post-hoc Tukey test (**p* < 0.05, ***p* < 0.01; *n.s.,* not significant; n = 3 for each genotype). (**C**) Protein extracts from wild type, *Mtmr13*$^{-/-}$, and *Mtmr2*$^{-/-}$ P30 brain lysates showed no difference in Mtmr5 protein levels. (**D**) Sciatic nerve lysates prepared from wild type and *Mtmr5*$^{-/-}$ animals at age 5 months (2 nerves per lysate). (**E**) Mtmr5 did not enhance the protein levels of Mtmr2 in mouse sciatic nerve: 0.937 ± 0.096 for wild type verse 1.003 ± 0.253 a.u. for *Mtmr5*$^{-/-}$ nerves (*p* = 0.697; n = 3 for each genotype). (**F**) Protein extracts from control *Mtmr5*$^{+/+}$; *Mtmr13*$^{-/-}$ and *Mtmr5*$^{-/-}$; *Mtmr13*$^{-/-}$ MEF cultures blotted for Mtmr2 protein. (**G**) No significant difference in Mtmr2 protein levels: 1.040 ± 0.122 for control (*Mtmr5*$^{+/+}$; *Mtmr13*$^{-/-}$ and *Mtmr5*$^{+/-}$; *Mtmr13*$^{-/-}$) verses

1.104 ± 0.048 a.u. for *Mtmr5*$^{-/-}$; *Mtmr13*$^{-/-}$ MEF lysates (p = 0.258; n = 3-4 per genotype). Two-sample Student's t-test of Mtmr2 protein levels data presented as mean ± SD*; n.s.,* not significant.

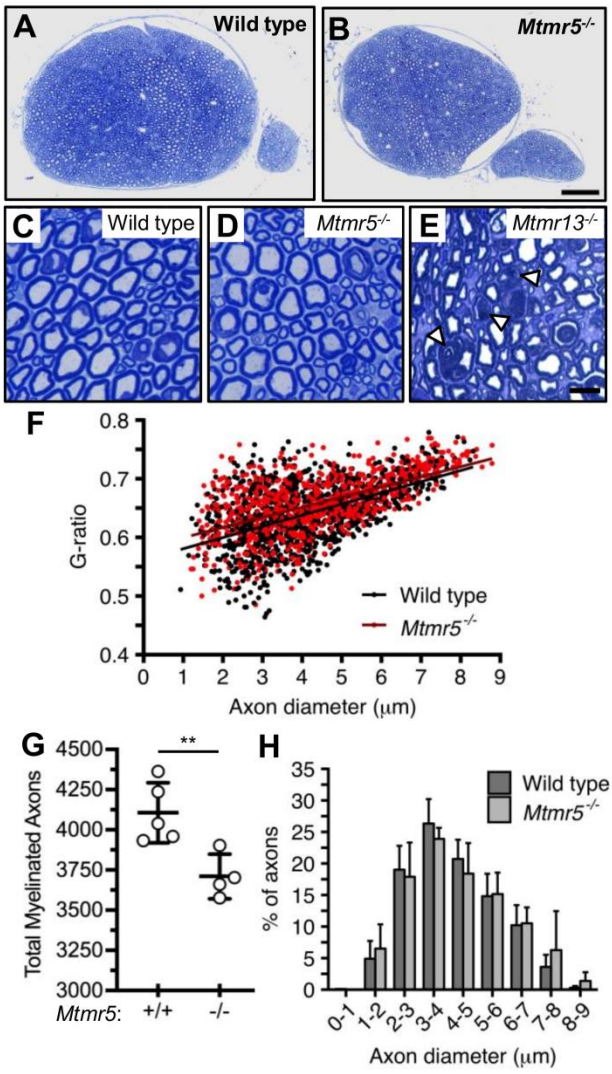

Figure 3.5: Sciatic nerve morphology in the absence of Mtmr5. (**A**) Comparable sciatic nerve morphology between wild type and *Mtmr5*$^{-/-}$ mice at 3 month. Scale bar = 100 μm. (**C, D**) Toluidine blue stained mid-sciatic nerve myelin appeared normal in *Mtmr5*$^{-/-}$ mice. Wildtype and *Mtmr13*$^{-/-}$ sciatic nerve cross-sections are shown for comparison. Arrowheads indicate myelin outfoldings. Scale bar = 10 μm. (**E**) G-ratio analysis of myelin thickness in wild type and *Mtmr5*$^{-/-}$ nerves, best-fit line shown (N = 4-5 mice, 200 myelin fibers per mouse). (**F**) The total number of myelinated sciatic nerve fibers were significantly reduced in *Mtmr5*$^{-/-}$ compared to wild type nerves. Data represented as mean ± SD; two-sample Student's t-test (n = 4-5 mice). (**G**) Similar axon

size distribution between wild type and *Mtmr5*$^{-/-}$ nerves. Two-sample Kolmogorov-Smirnov test (p = 0.16; wild type N = 5 mice, n = 999 axons; and *Mtmr5*$^{-/-}$ N = 4 mice, n = 799 axons).

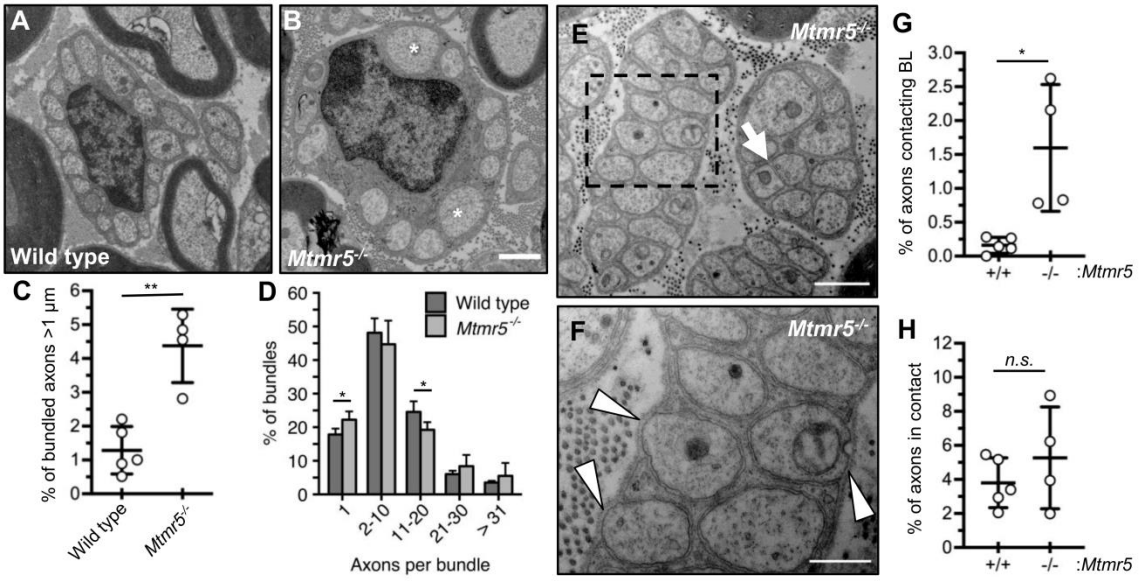

Figure 3.6: Mtmr5 absence alters axon radial sorting and ensheathment. (**A, B**) EM images of sciatic nerve cross sections from wild type and *Mtmr5*$^{-/-}$ mice. Asterisks indicate axons >1 µm in diameter. Scale bar: 1 µm. (**C**) Percentage of unmyelinated axons greater than >1 µm diameter was significantly increased in *Mtmr5*$^{-/-}$ sciatic nerves bundles at 3 months: 1.29 ± 0.70% wild type verses 4.37 ± 1.09% *Mtmr5*$^{-/-}$ (n = 4-5 mice). (**D**) Number of axons per bundle expressed as a percentage. Categories are distinguished by the number of ensheathed axons. (**E**) EM of two bundles from a transverse *Mtmr5*$^{-/-}$ sciatic nerve section. Arrow indicates an area without Schwann cell cytoplasm between axons. Scale bar: 1 µm. (**F**) Higher magnification image from the section boxed in image (E). Arrowheads identify points of direct contact between the basal lamina (BL) and axons. Scale bar: 500 nm. (**G, H**) Axons lacking full Schwann cell ensheathment were counted and expressed as a percentage of the total bundled axons per mouse. (**G**) Quantification of the percentage of axons abnormally contacting the Schwann cell BL. (**H**) Quantification of the percentage of axons in direct contact with another axon. Data represented as mean ± SD; Two-sample Student's t-test (*$p \leq 0.05$; **$p \leq 0.01$; n = 5 wild type and n = 4 *Mtmr5*$^{-/-}$ mice).

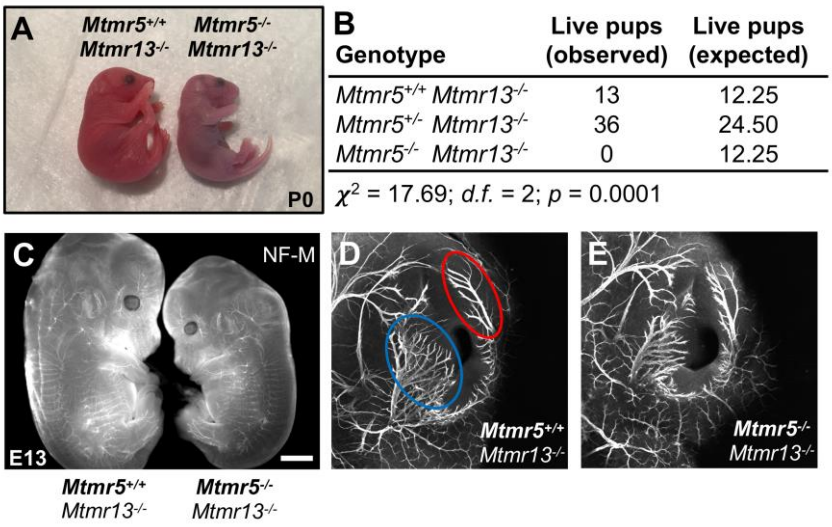

Figure 3.7: *Mtmr5-Mtmr13* double-knockout mice are not viable beyond birth and showed normal axon guidance at E13. (**A**) Images of *Mtmr5*$^{-/-}$; *Mtmr13*$^{-/-}$ mice found dead at P0, littermate controls are shown in each image. (**B**) *Mtmr5*$^{-/-}$; *Mtmr13*$^{-/-}$ double knockout animals were not represented at expected ratios; Chi-squared (χ^2) 17.69; p = 0.0001; n = 49 live pups total. (**C**) Representative images of *Mtmr5*$^{+/+}$; *Mtmr13*$^{-/-}$ control and *Mtmr5*$^{-/-}$; *Mtmr13*$^{-/-}$ mouse embryos immunostained with neurofilament medium chain (NF-M) antibody to label axons. Scale bar: 2000 μm. (**D-E**) Corresponding higher magnification images of *Mtmr5*$^{+/+}$; *Mtmr13*$^{-/-}$ control and *Mtmr5*$^{-/-}$; *Mtmr13*$^{-/-}$ embryo ears. No difference in the morphology of two major nerve branches around the ear: The Great Auricular Nerve (red) and the Auriculotemporal Nerve (blue). These nerve branches form between embryonic day 12 (E12) and E13.

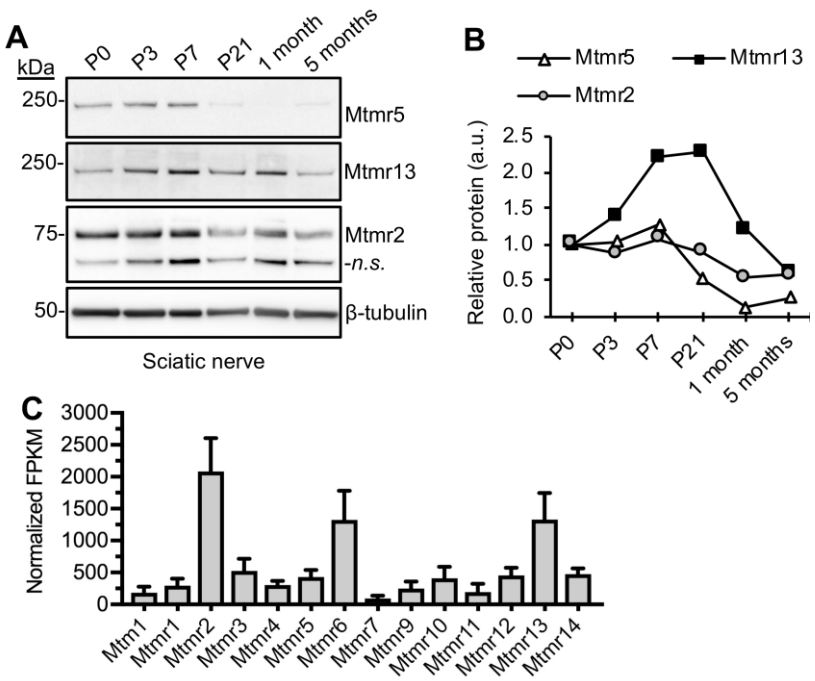

Figure 3.8: Myotubularin proteins in mouse sciatic nerve and Schwann cells. (**A**) Immunoblot of Mtmr5, Mtmr13, and Mtmr2 protein from wild type mouse sciatic nerve protein extracts at P0, P3, P7, P21, 1 month, and 5 months of age. β-tubulin immunoblot and a total protein stain are shown as loading controls. (**B**) Relative protein abundance of Mtmr5, Mtmr13, and Mtmr2 normalized to a total protein stain. (**C**) RNAseq FPKM expression of all 14 Mtmr transcripts for pooled Schwann cells isolated from wild type mouse sciatic nerves. Graph generated from the publically available *Clements M.P. et al* data (GSE103039) (150).

TABLES

Table 3.1: Loss of Mtmr5 caused male sterility

Breeding Pair M X F	Pairs mated (no.)	Litters (no.)	Litter size
+/+ +/-	3	3	6 ± 2
+/- +/-	9	9	6 ± 1
+/- -/-	3	3	3 ± 1
-/- +/+	6	0	0

SUPPLEMENTARY DATA

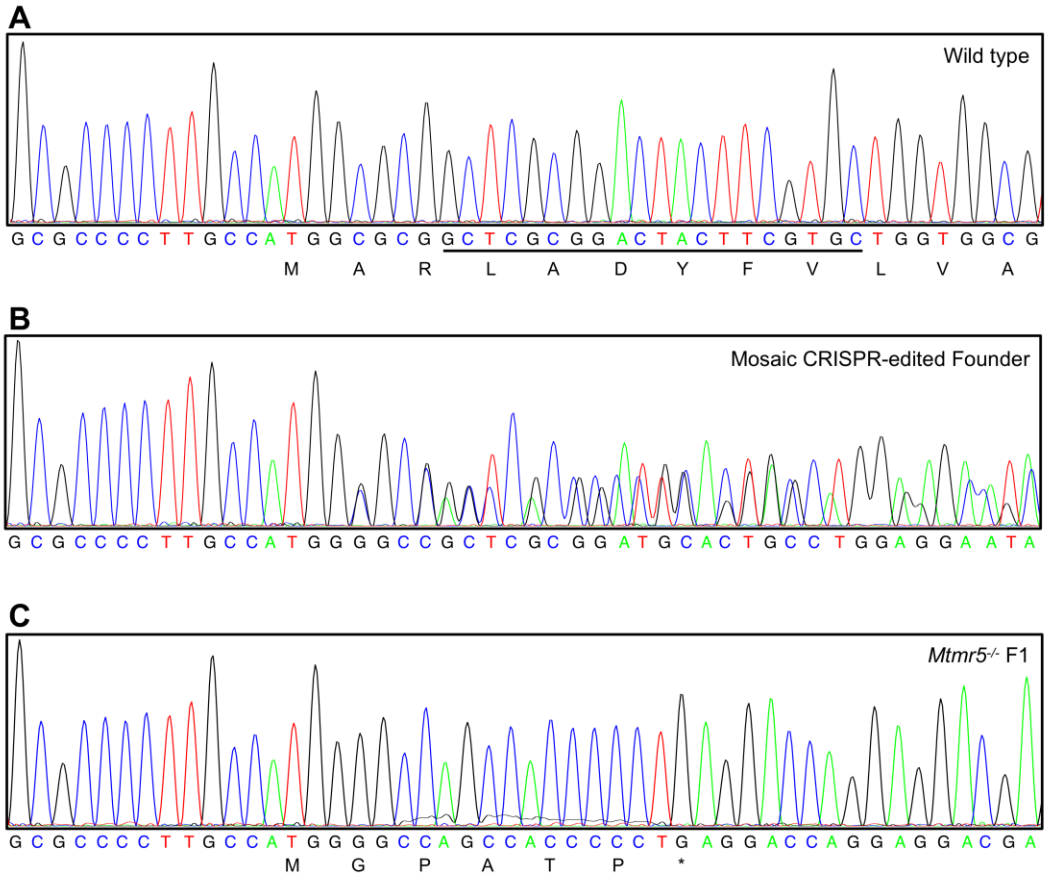

Supplemental figure 3.9: Sequencing CRISPR/Cas9-edited *Mtmr5* alleles. Example chromatograms obtained by Sanger sequencing genomic PCR fragments containing the *Mtmr5* exon 1 gRNA target sequence. (**A**) Wild type mouse ID #696 chromatogram with gRNA sequence underlined and coding frame indicated. (**B**) CRISPR-Cas9 founder mouse ID #684 chromatogram. Note the altered peaks resulting from two mosaic deletions between *Mtmr5* exon 1 and exon 25 gRNA sequences. The two deletions were identified using Poly Peak Parser to separate the double peaks. (**C**) Mutant *Mtmr5*$^{-/-}$ mouse ID #992 sequence with coding frame indicated and pre-mature stop codon identified (*)).

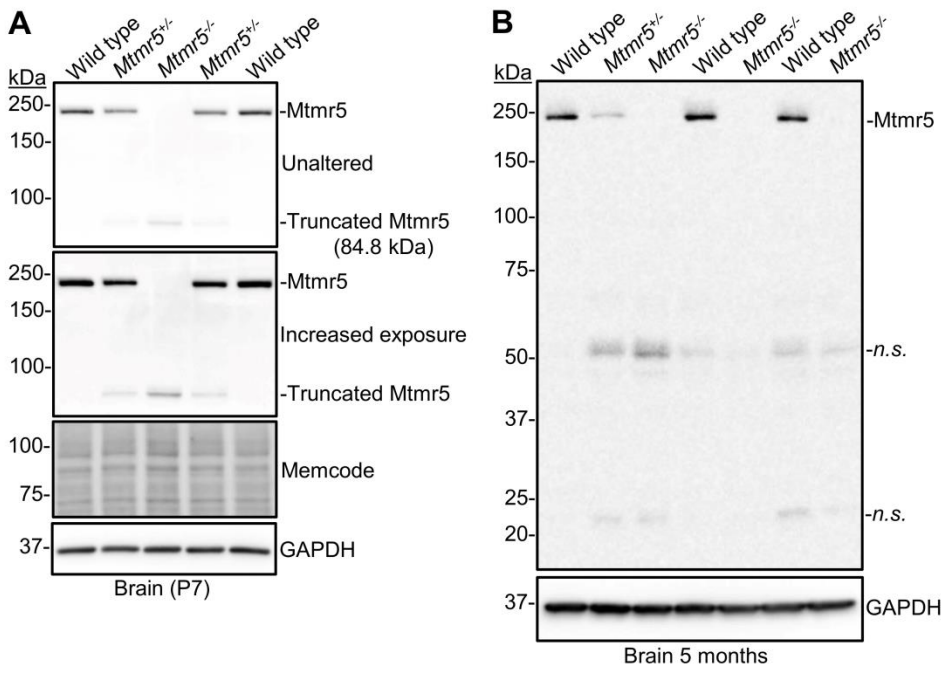

Supplemental figure 3.10: Immunoblot of Mtmr5 protein levels from wild type, *Mtmr5*$^{+/-}$, and *Mtmr5*$^{-/-}$ mouse brains. The protein loading controls were Memcode total protein stain and GAPDH. (**A**) At P7 a protein band was detected in *Mtmr5*-null allele mouse brains between 75 kDa and 100 kDa with the Mtmr5 C-terminal antibody. An unaltered and a gain-adjusted version of the Mtmr5 immunoblot are shown to clearly identify the truncated protein. The truncated Mtmr5 (84.8 kDa) had a protein level of 0.17 a.u. compared to full-length protein with a mean of 1.03 ± 0.04 a.u. (n = 2 wild type, and n = 1 *Mtmr5*$^{-/-}$; mean ± SD). (**B**) At age 5 months the truncated Mtmr5 protein product was not detected in mutant mouse brains (n = 3 wild type, n = 1 *Mtmr5*$^{+/-}$, and n = 3 *Mtmr5*$^{-/-}$ mice; *n.s.*, non-specific protein bands).

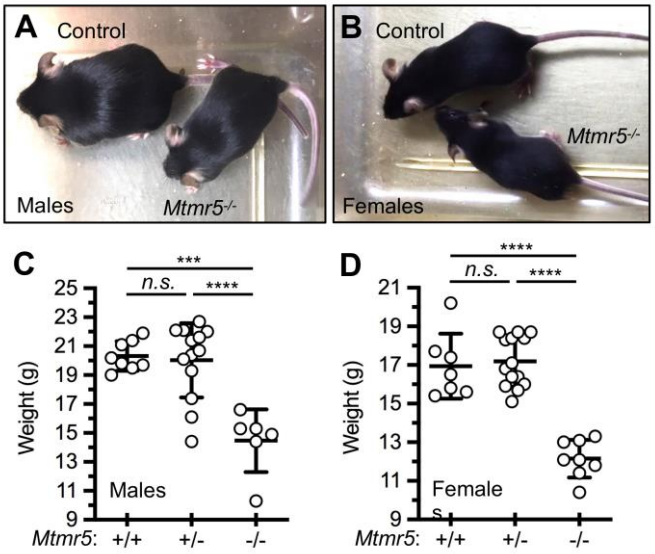

Supplemental figure 3.11: Reduced weight in the absence of Mtmr5. (**A - B**) An *Mtmr5*$^{-/-}$ male and female alongside an *Mtmr5*$^{+/+}$ and *Mtmr5*$^{+/-}$ littermate control respectively at 38 days old (P38). (**C**) At P38, *Mtmr5*$^{-/-}$ male mice were significantly smaller than controls. Average weights: 20.33 ± 1.03 g, 20.02 ± 2.57 g, and 14.47 ± 2.17 g (n = 8, 13, and 6 for *Mtmr5*$^{+/+}$, *Mtmr5*$^{+/-}$, and *Mtmr5*$^{-/-}$, respectively). (**D**) Female *Mtmr5*$^{-/-}$ mice were significantly smaller than controls at P38. Average weights: 16.94 ± 1.69 g, 17.19 ± 1.30 g, 12.15 ± 0.98 g (n = 7, 14, and 8 for *Mtmr5*$^{+/+}$, *Mtmr5*$^{+/-}$, and *Mtmr5*$^{-/-}$, respectively). These data are presented as mean ± SD; one-way ANOVA with post-hoc Tukey test (***$p \leq 0.001$; ****$p \leq 0.0001$; *n.s.*, not significant).

Chapter 4

Role of RhoA/ROCK and ERM during Schwann cell myelination and CMT4B2-like dysmyelination

Anna E. Mammel[1,2] and Fred L. Robinson[1,3]

[1]The Jungers Center for Neurosciences Research, Department of Neurology, Oregon Health & Science University, 3181 SW Sam Jackson Park Road, Portland, OR 97239, USA.

[2]Cell, Developmental & Cancer Biology Graduate Program, Oregon Health & Science University

[3]Vollum Institute, Oregon Health & Science University

PREFACE

This work is unpublished

Anna Mammel designed and performed all experiments and wrote the manuscript. Fred Robinson contributed to the concept of the project and experiment design.

ABSTRACT

Schwann cell (SC) myelination requires the regulation of pro-myelination signals, controlled membrane production/transport, and changes in the SC cytoskeleton to move the growing sheath around an axon. Loss of function mutations in Myotubularin-related protein 13 (Mtmr13), cause SC myelin to over-grow longitudinally and fold back on itself to generated “myelin outfoldings” in both Charcot-Marie-Tooth disease type 4B2 (CMT4B2) patients and knockout mouse models. Mtmr13 controls endosomal trafficking together with its binding partner Mtmr2. However, it has yet to be determined how loss of Mtmr13 disrupts endosome trafficking and leads to SC dysmyelination. We found that *Mtmr13*$^{-/-}$ sciatic nerves have elevated levels of the pro-myelination signal ErbB2/3 and activated Ezrin Radixin Moesin (ERM). ERM attaches actin to the plasma membrane to control cell mobility and polarization. We determined that ERM activation was essential for SC myelin *in vitro* but does not contribute to myelin outfoldings in *Mtmr13*$^{-/-}$ cultures. ERM activity is controlled by the Rho-associated protein kinase (ROCK). Our results suggest that inhibition of ROCK reduced myelin outfoldings caused by Mtmr13 loss. We hypothesize that Mtmr13 controls RhoA/ROCK activation by tightly regulating the trafficking of receptors such as β1-integrin and ErbB2/3, thereby controlling actin assembly and pro-myelination signals.

INTRODUCTION

Myelin is a specialized multilayer membrane produced by oligodendrocytes in the central nervous system (CNS) and SCs in the peripheral nervous system (PNS). Myelin functions by providing trophic support and insulating axons to make possible rapid, saltatory conduction (59). Glial cells produce myelin by spirally wrapping around an axon under layers of compacting membrane. This process requires coordinated actin

polymerization/disassembly, membrane trafficking, and receptor signaling at the leading edge of the enwrapping glial cell (29, 30). In oligodendrocytes actin disassembly is the driving force required for myelin wrapping and compaction. A similar mechanism has been proposed during PNS myelination (29, 30). SCs control pro-myelination signals by internalizing receptors and recycling them back to the plasma membrane or to lysosomes for degradation (66). However, it remains unclear how SC receptor endosome trafficking and cytoskeleton rearrangements coordinate to produce a functional myelin sheath.

Myelin outfoldings are abnormalities that occur when myelin folds back on itself due to excess longitudinal growth. Myelin outfoldings lead to demyelination, secondary axon loss, and neuropathy in humans and mouse models. Nearly all the genes known to cause abnormal SC myelin outfoldings when mutated regulate actin dynamics and/or endosome trafficking. These include: cell division cycle 42 (Cdc42), inverted formin 2 (Inf2), FGD1-related F-actin-binding protein (Frabin), neural Wiskott–Aldrich syndrome protein (N-Wasp), cell adhesion molecule 4 (Cadm4), lymphoid cell kinase (Lck), myotubularin-related 2 (Mtmr2), and Mtmr13 (Table 4.1) (36, 37, 89, 142, 158-161). There is a clear link between endosome trafficking and actin regulation in cell biology, but how these two processes work together to control SC myelination lacks investigation.

Loss-of-function mutations in the endosomal regulator MTMR13 cause the inherited peripheral neuropathy CMT4B2, with distinctive myelin outfoldings and subsequent demyelination (68, 142). Mtmr13 interacts with the PI 3-phosphatase Mtmr2 to control endosome trafficking though PI3P hydrolysis and Rab activation. *Drosophila* ortholog of Mtmr13 functions in a complex with Mtmr2 and Rab21 to promote the recycling of integrin from endosomes back to the plasma membrane, regulating the formation of actin-rich filipodia by Rho GTPases in macrophages (72). Whether mammalian Mtmr13 regulates endosomal trafficking of particular receptors to control

Rho GTPase mediated actin dynamics during SC myelination has yet to be elucidated. Therefore, we assessed whether loss of Mtmr13 affects pro-myelination and actin-associated protein receptor signaling during myelination. And whether there is a correlation between actin cytoskeleton rearrangements and *Mtmr13*-mediated receptor endosome trafficking in SCs.

It is well established that Rho GTPases are required for proper SC myelination (33, 35, 36). RhoA signals through the Rho-kinase ROCK to mediate actin cytoskeleton rearrangements and endocytosis. ROCK is a serine-threonine kinase that activates the downstream effectors: Ezrin Radixin Moesin (ERM), LIM kinases, Adducin, Myosin light chain II (MLC), and Myosin light chain kinase (MLCK) (33). ROCK is activated at the onset of SC myelination, and pharmacological inhibition of ROCK results in the formation of numerous short myelin segments (33). We hypothesize that Mtmr13-mediated endosomal trafficking controls myelin formation by maintaining the correct levels of pro-myelination signals and downstream RhoA/ROCK activation in SCs. Our work supports a critical link between endosome trafficking and RhoA/ROCK mediated actin rearrangement to prevent the formation of myelin outfoldings.

RESULTS

Abnormal actin accumulation in Mtmr13-null myelin outfoldings

Genetic studies suggest that correct myelin sheath formation requires coordinated cytoskeleton rearrangements and endosome trafficking. Therefore, we ascertained whether loss of Mtmr13 leads to abnormal F-actin assembly in PNS nerve fibers. Wild type mouse sciatic nerve fibers showed normal F-actin enrichment in regions of non-compact myelin at the glial paranodes, Schmidt-Lanterman incisures (SLIs), and around the nucleus (Fig. 4.1A). Mouse sciatic nerve fibers lacking Mtmr13 still showed normal F-actin accumulation in paranodes, SLIs, and near the Schwann cell nucleus.

However, all identified myelin outfoldings contained proximal F-actin accumulations (Fig. 4.1B). The actin associated with myelin outfoldings resembled the structure of cortical-actin that lies underneath the plasma membrane during bleb formation and cell migration (Fig. 4.1C). This suggests a correlation between the formation of *Mtmr13*$^{-/-}$ myelin outfoldings and cortical F-actin assembly underneath the myelin membrane.

Loss of Mtmr13 alters ErbB2/3 and actin associated protein signaling at the onset of PNS myelination

PNS myelination begins at post-natal day 0 (P0) in mice. Myelin outfoldings begin to appear at P3 in Mtmr13 null mice and accumulate over time. Therefore, Mtmr13 is required to regulate the myelination process. Previous work has shown that Mtmr13's binding partner Mtmr2 controls the activation state of the major pro-myelination signal ErbB2/3 at the onset of PNS myelination (42). We determined whether Mtmr13 also controls ErbB2/3 activity. Loss of Mtmr13 caused a significant increase in ErbB3 protein activation at P3 (Fig. 4.2A, B). We propose that Mtmr2 and Mtmr13 work together to control the endosomal trafficking of ErbB2/3 to modulate the abundance of this pro-myelination signal.

We have previously shown that loss of Mtmr13 does not alter the activation state of downstream ErbB2/3 effectors ERK1/2 or AKT in P4 or 4-month-old mouse sciatic nerves (94). We assessed the activation state of the focal adhesion kinase (FAK), a signaling protein downstream of ErbB2/3 and $\alpha 6\beta 1$ integrin known to modulate actin assembly. While FAK signaling was unaltered in P3 Mtmr13-null sciatic nerves, we did observe a significant decrease in total FAK protein (Fig. 4.2C, D). The decrease in FAK could have been in response to overactivation caused by aberrant ErbB2/3 signaling in Mtmr13-null nerves. Therefore, FAK levels may be reduced to compensate for overactivation.

ERM proteins mediate membrane-to-actin attachment and are key regulators of bleb-based cell migration (162). Myelin outfoldings are a blebbing outwards of the SC plasma membrane. The presence of cortical F-actin structures in *Mtmr13*-null myelin outfoldings led us to assess the activation state of ERM proteins in mouse sciatic nerves at the onset of myelination. We observed a significant increase in activated ERM (pERM) proteins in mouse sciatic nerves lacking Mtmr13 (Fig. 4.2E, F). ERM phosphorylation induces a structural change from a closed to an open conformation to allow membrane and actin binding. Mounting evidence suggests that cycles of ERM phosphorylation and dephosphoylation are essential for ERM activity, though little is known about how this is regulated *in vivo* (163). In conclusion, we determined that Mtmr13 controls a subset of protein signals critical to both myelination and cortical actin architecture at the onset of myelination.

Requirement of Ezrin Radixin Moesin (ERM) activation for Schwann cell myelination

ERM is localized to actin-rich regions of the SC paranodal microvilli, but whether ERM activation is required for myelination remains unknown (164). We uncovered the role of ERM during myelination by inhibiting ERM activation with the molecule NSC668394 in wild type myelinating SC-dorsal root ganglion (SC-DRG) cultures. SC-DRG explants were switched to media containing ascorbic acid to induce myelination with or without a range of NSC668394 inhibitor concentrations (5 μM, 10 μM, or 20 μM) for 2 weeks. While the drug was well tolerated at 5 μM or 10 μM concentrations, 20 μM ERM inhibitor led to widespread cell death 4 days post treatment (Supplemental Fig. 4.7A).

Two striking, reproducible, and concentration dependent effects were observed in cultures treated with NSC668394: a dramatic decrease in the number and length of myelin segments compared to cultures treated with a DMSO (0.1%) control media (Fig. 4.3). This was observed in both wild type and *Mtmr13*$^{-/-}$ SC-DRG explants (Supplemental Fig. 4.7B, Supplemental Fig. 4.8). Bulk myelination was inhibited over the entire culture, as observed by a decrease in total myelin associated glycoprotein (MAG) and myelin basic protein (MBP) in treated cultures (Supplemental Fig. 4.8B). The reduction in myelination was not caused by a reduction in SCs or axon development as assessed by DAPI nuclei staining and anti-neurofilament antibodies (Fig. 4.3A).

Quantitation of the length of myelin segments demonstrated that ERM inhibited cultures were on average 20-27% shorter than control culture segments. While treated cultures still contained myelin segments of normal length the overall size distribution was skewed towards shorter segments, and control cultures had a normal Gaussian distribution. This was observed in both wild type and *Mtmr13*-null cultures (Fig. 4.3C, Supplemental Fig. 4.8D). It should be noted that the distribution of myelin segment lengths were not significantly different between untreated wild type and *Mtmr13*$^{-/-}$ cultures. However, explants lacking Mtmr13 had segments as long as 263 μm whereas the longest segment in wild type cultures was 202 μm. This anecdotal evidence may correlate with the hypothesis that loss of Mtmr13 leads to longitudinal myelin overgrowth.

Requirement of RhoA/ROCK activation for Schwann cell myelination in Mtmr13-null cultures

The Rho kinase (ROCK) is a serine-threonine kinase that regulates cortical actin assembly by activating downstream effectors: LIM kinase, MLC, MLCK, Adducin, and ERM (33). Previous studies have demonstrated that pharmacological ROCK inhibition

leads to the formation of numerous short myelin segments in wild type SC-DRG explants (33). We confirmed that the addition of the ROCK inhibitor Y27632 (20 μM or 30 μM) and myelin-inducing ascorbic acid caused numerous short myelin segments in our wild type SC-DRG cultures (*data not shown*). We observed a similar result in cultures lacking Mtmr13. We supplemented *Mtmr13*$^{-/-}$ SC-DRG culture media with 30 μM of Y27632 on day 8 when myelination was induced through addition of ascorbic acid. The cultures were allowed to myelinate in treatment media for 2 weeks. Y27632 treatment had no impact on the number of myelin segments, but a significant decrease in segment length in cultures lacking Mtmr13 (Fig. 4.4). *Mtmr13*-null cultures treated with 30 μM ROCK inhibitor had a 25% decrease in myelin segment length on average compared DMSO (0.1%) treated controls. Similar to ERM inhibition, treatment with Y27632 shifted the distribution of segment lengths towards shorter segments, whereas control cultures had a Gaussian distribution (Fig. 4.4C).

Contribution of ERM and ROCK activation to CMT4B2-like myelin outfoldings

We considered whether the outfoldings caused by Mtmr13 loss may be modified by inhibition of ERM or upstream ROCK. We determined that despite regulating SC myelin formation and having increased activation in *Mtmr13*$^{-/-}$ sciatic nerves, inhibition of ERM with 5 μM NSC66894 did not have a significant impact on the percentage of myelin segments that contain one or more outfoldings in *Mtmr13*$^{-/-}$ SC-DRG cultures (Fig. 4.5A, B). However, inhibition of ROCK with Y27632 modestly reduced myelin outfoldings caused by Mtmr13 loss by 34% (Fig. 4.5C, D). Therefore, overactivation of ROCK but not ERM contributes to myelin outfolding formation. This suggests that overactivation of ERM may be a symptom of increased RhoA/ROCK activation when Mtmr13 was lost. We hypothesize that Mtmr13 controls RhoA/ROCK activation by tightly regulating the

trafficking of Rho activators such as β1-integrin or ErbB2/3, thereby controlling cortical actin assembly and pro-myelination signals (Fig. 4.6).

DISCUSSION

Loss of Mtmr13 causes abnormal SC myelin outfoldings resulting in demyelination and secondary axon degeneration (68). We previously determined that Mtmr13 works together with Mtmr2 to control endosome trafficking through phosphoinositide hydrolysis and Rab activation (94). The role of Mtmr13 in regulating both actin dynamics and endosome trafficking has been established in *Drosophila* macrophages where it is required for endosome recycling and filipodia formation (72). However, the role of MTMR13-mediated endosomal trafficking and actin remodeling during SC myelination has yet to be established. We showed that loss of Mtmr13 led to abnormal cortical actin accumulation in SC myelin outfoldings. We determined that Mtmr13 controls the abundance of the pro-myelination signal ErbB2/3, and the actin associated signaling proteins FAK and ERM in mouse sciatic nerves. Decreased RhoA/ROCK activation was able to partially rescue myelin defects in *Mtmr13*$^{-/-}$ cultures. This work supports a model where both endosome receptor trafficking and actin restructuring is required for proper SC myelination.

Relationship between myelin outfoldings, actin assembly, and endosomal trafficking

Myelin is essential for the rapid propagation of action potentials along an axon and is one of the most specialized features in cell biology. Myelin is generated by glial cells that circumferentially wrap around an axon to generate layers of myelin membrane (4). Even though myelinating cells remain stationary, the process of extending their inner membrane around an axon has similar properties to the leading edge of a cell during

migration. The complex process of myelination requires coordinated receptor signaling, membrane trafficking, and cytoskeleton rearrangements at the leading edge during SC myelination. Endosome trafficking of receptors regulate myelination by fine-tuning the signals that SCs receive from axons and the basal lamina.

Myelin outfoldings are a specific defect caused by myelin folding back on itself due to longitudinal overgrowth. The underlying pathology of myelin outfoldings has been attributed to phosphoinositide dysregulation and impaired endosomal trafficking (37, 91, 142). In oligodendrocytes, myelin outfoldings occur naturally during myelin formation (165). It has been proposed that these outfoldings serve as membrane reservoirs for lateral growth while preserving radial thickness. Outfoldings result from the delivery of myelin membrane through cytoplasmic channels to the oligodendrocyte inner tongue. Interestingly, deletion of the actin assembly protein Arp2/3 in oligodendrocytes causes increased myelin outfoldings in mice. Cytoskeleton rearrangements have a critical role in limiting membrane growth and outfoldings during myelination (166).

We determined that F-actin accumulates in SC myelin outfoldings when the endosomal regulator Mtmr13 was lost. F-actin was localized directly underneath myelin outfoldings and was reminiscent of cortical actin. We could not determine whether the actin accumulation was causative or consequential. It could be the case that myelin outfoldings arise then actin accumulates in these cytoplasmic regions. However, our data along with other genetic studies provide a correlation between F-actin assembly and the generation of myelin outfoldings in SC.

Role of cortical actin proteins ERM and RhoA/ROCK in myelin sheath formation

RhoA is a small GTPase that regulates cortical actin assembly through downstream effectors ROCK and formins (167). ERM proteins are activated downstream of ROCK which phosphorylates a C-terminal threonine located at the interface between

the C-terminal actin-binding domain and the N-terminal $PI(4,5)P_2$ binding FERM domain of ERM (163). Cycles of ERM activation and deactivation are required for membrane blebbing, in which a patch of membrane detaches from the actin cortex to form a spherical protrusion which is 1-10 μm in diameter and filled with cytosol (167). When the bleb stops expanding, cortical actin reassembles and the membrane bleb is contracted by actomyosin. Membrane blebbing is often observed during apoptosis, cytokinesis, and cell migration.

ERM is known to be enriched in SC microvilli at the paranodes of mature myelin sheaths, and we determined that its activation was critical for SC myelination. Decreased ERM activation led to a decrease in total myelination and myelin segment length without disrupting SC number or axon density. This suggests that ERM activation is required for both myelin initiation and elongation. In SCs, non-phosphorylated ERM is diffusely cytoplasmic while activated ERM is enriched at the bipolar tips of SCs where actin and RhoA/ROCK accumulate (168). Therefore, reduced ERM activation may lead to loss of SC bipolar morphology and impaired SC-axon contact. Correct glial polarity and axon contact are required for myelination to occur.

Inhibition of either ERM or ROCK caused a decrease in segment length, but only inhibition of ERM decreased the number of myelin segments in SC-DRG explants. Additionally, inhibition of ROCK but not ERM protein activation suppressed CMT4B-like myelin outfoldings suggesting that increased ERM activity is a symptom of increased RhoA/ROCK overactivation rather than directly contributing to myelin outfolding formation in Mtmr13-null nerves. ROCK and ERM may actually have distinct mechanisms by which they control myelination. ROCK activates several downstream effectors that are known to have various roles during myelination including myosin light chain II and LIMK which suppresses cofilin. Inhibition of myosin II activity in SC-DRG cultures lead to multipolar SCs that fail to completely ensheath axons (169). The actin

severing protein cofilin is required for SC alignment along axons and myelination in SC-DRG cultures (170). Therefore, inhibition of ROCK has several pathways by which it can control SC myelination compared to ERM inhibition.

Effect of receptor trafficking through endosomes by Mtmr13 on downstream RhoA/ROCK activation

Endosomal trafficking is essential for cortical actin assembly and formation of actin-rich cell protrusions. We proposed that Mtmr13, in concert with its active binding partner Mtmr2, controls the endosome trafficking of receptors critical for myelination and actin dynamics. We demonstrated that loss of Mtmr13 caused an increase in activated ErbB2/3, and a decrease in total FAK protein which is activated downstream of ErbB2/3 and $\alpha 6\beta 1$-integrin. ErbB2/3 recruits PI 3-kinases to produce the singling lipid $PI(3,4,5)P_3$ which is known to play a role in establishing cell polarity, myelination, and recruiting Rho GTPases (165). Therefore, Mtmr13 may result in increased RhoA/ROCK activation through defects in ErbB2/3 endosome trafficking.

Alternatively, Mtmr13 may control the endosomal trafficking of $\alpha 6\beta 1$-integrin from the early endosome back to the abaxonal SC plasma membrane. Sbf, the *Drosophila* ortholog of Mtmr13, controls endosomal recycling of integrin through Rab21 activation (72). This endosome recycling is thought to influence macrophage cell shape in *Drosophila* through Rho GTPase control of actin remodeling (72). We proposed that Mtmr13 may regulate RhoA/ROCK activation through early endosome recycling of β1-integrin to the SC plasma membrane. In SCs, $\alpha 6\beta 1$-integrin binds to laminin 2 in the basal lamina then associates with integrin-linked kinase (ILK) to negatively regulate RhoA/ROCK activation (129). Loss of Mtmr13 could lead to increased retention of inactive cellular $\alpha 6\beta 1$-integrin due to impaired early endosome recycling (Fig. 4.6). We

predict this will lead to increased RhoA/ROCK activation due to loss of ILK recruitment. Increased RhoA/ROCK results in disorganized actin assembly/contractility generating myelin outfoldings during myelination (Fig. 4.6). In conclusion, we have demonstrated that Mtmr13 functions to control both endosomal trafficking and actin dynamics to prevent SC dysmyelination.

MATERIALS AND METHODS

Mice - All animal work was approved by and conformed to the Institutional Animal Care and Use Committee at Oregon Health and Science University. C57BL/6 mice were obtained from Charles River. *Mtmr13*$^{-/-}$ mice have been previously characterized and described (94, 142).

Immunoblotting - Preparation of protein extracts from myelinated SC-DRG explants, immunoblotting, and quantitation using chemiluminescence imaging was carried out as previously described (95). Primary antibodies used for SC-DRG explant immunoblotting were a rabbit pAb to MAG and a rat mAb to MBP from Santa Cruz Biotechnology and Millipore respectively. Protein extracts from P3 mouse sciatic nerves were generated using the previously described protocol (43). Six nerves from three mice were pooled per lysate. Primary antibodies used for P3 nerve immunoblots were the rabbit mAbs to Ezrin/Radixin/Moesin (ERM), pEzrin(Thr567)/Radixin(Thr564)/Moesin(Thr558), ErbB3, and pErbB3(Tyr1289) (Cell Signaling). Additional antibodies used were mouse mAbs to FAK (BD Bioscience) and GAPDH (Millipore), as well as the rabbit pAb to pFAK(Tyr397) (Millipore).

Teased sciatic nerve fiber isolation and immunofluorescence - Sciatic nerves from P21 mice were dissected and fixed in ice-cold 4% PFA for 30 minutes. Nerves were washed

three times at room temperature (RT) in 1xPBS for five minute intervals. Fixed nerves were transferred to a 60mm Petri dish filled with 1xPBS and the perineurial sheath was gently removed using forceps. The unsheathed nerves were transferred to a positively charged microscope slide. Using forceps and 23G needles individual fibers were separated out taking care not to stretch any fibers. The slides were allowed to air-dry overnight at RT. A pap-pen was used to create a barrier around the isolated fibers. Slides were washed once in 1xPBS for 5 minutes, then permeabilized for 15 minutes in 0.2% Triton-X 100. Slides were washed twice for five minutes in 1xPBS at RT. Phalloidin Alexa-594 was added at a concentration of 1:500 in 1xPBS for 40 minutes. Slides were washed three times in 1xPBS then stained with DAPI (1:40,000) in 1xPBST for one minute. Slides were washed twice in 1xPBS then a final rinse in DI-H_2O before being mounted in an Elvanol solution.

Schwann cell myelinating explants and immunofluorescence - Wild type (C57BL/6) and *Mtmr13*$^{-/-}$ Dorsal Root Ganglia were dissected, cultured, and induced to myelinate as previously described (95). Neuronal growth factor (NGF) was added with each media change at a concentration of 50 ng/ml. Schwann cell-dorsal root ganglion (SC-DRG) explants were treated with the following pharmacological inhibitors: ERM inhibitor, NSC668394 (Cat# 341216, Millipore) or a ROCK inhibitor, Y27632 (Cat# S1049, Selleck Chemical). Inhibitors were added at a range of concentrations on culture day 8 when SC myelination was induced through the addition of 50 µg/ml ascorbic acid. Fresh drug was added with each media change on culture days 11, 14, 17, and 20.

SC-DRG explants were fixed in 4% PFA for 15 minutes and permeabilized in ice-cold methanol for 5 minutes, protocol has been described in full (95). Primary antibodies used for immunofluorescence were a rat mAb against myelin basic protein (MBP) (Millipore) and mouse mAb to neurofilament medium chain (NF-M) (Cat# 2H3-s, DSHB).

After an overnight incubation in primary antibody solution at 4°C (1xPBS with 0.1% Tween-20 (PBST), 2% NGS, and diluted antibodies) explants were washed 3 times for 10 minutes in PBST. Cultures were incubated for 1 hour at RT with the following fluorescent secondary antibodies: Cy3-goat-anti-rat (Cat # 112-165-143, Jackson ImmunoResearch Labs) and 488-goat-anti-mouse (Cat# 115-545-062, Jackson ImmunoResearch Labs) diluted in PBST containing 2% NGS. Cultures were washed 3 times for 10 minutes in PBST, then nuclei were labels with 0.36 µM DAPI in PBST for 1 minute at RT. Cultures were washed for five minutes twice in PBST then rinsed in distilled deionized water. Cultures were mounted on slides using Elvanol mounting medium and allowed to solidify overnight at 4°C.

Image acquisition and analysis - The extent to which SC-DRG cultures myelinated was determined for each explant by acquiring 4 images using Zeiss Axio ApoTome Image M2 microscope (5x objective). To avoid bias, an image was taken from the center of each quadrant of the coverslip/explant. The number of myelin basic protein (MBP)-positive segments was determined for each image using the 3D Objects Counter plug-in for Fiji (Fiji is just ImageJ). These totals were used to determine the density of myelinated segments (per mm^2) within an explant. The length of myelin segments was measured from a single image per coverslip acquired using Zeiss Axio ApoTome Image M2 microscope (5x objective). Each full myelin segment length was measured using the Simple Neurite Tracer in the FIJI Segmentation plug-in.

To determine the percentage of myelin segments that contained outfoldings we acquired images using a Nikon CSU-W1 spinning disk microscope (60x Nikon Plan Apo VC OFN 25 objective). Twenty images from each coverslip were randomly acquired from the most highly myelinated areas (five images per quadrant). This method was used to sample across the entire coverslip area. Using the Fiji processing package Z-stacked

images were projected into a single image using the max projection of each pixel. The total number of complete myelin segments were counted. A myelin segment was determine to have an irregularity if it met the criteria previously described (95).

Statistics - Statistical analysis was performed using R version 3.3.1 (https://www. -project.org/). Unless otherwise stated in the figure legend, an unpaired t-test was used to evaluate significance ($p \leq 0.05$), Welch's correction was applied when unequal variance was observed. Two sample Kolmogorov-Smirnov was used to compared distribution differences in myelin segment length between treatment conditions. For SC-DRG explant analysis n = 3 to 7 coverslips were derived from at least 2 independent (pregnant) female mice per genotype and treatment condition.

ACKNOWLEDGEMENTS

Microscopy and analysis were carried out in OHSU's Advanced Light Microscopy Core at the Jungers Center for Neurosciences Research. The authors wish to thank Aurelie Snyder and Stefanie Kaech Petrie of the Advanced Light Microscopy Core for expert advice. The monoclonal antibody 2H3 (NF-M), developed by Drs. T.M. Jessell and J. Dodd, was obtained from the Developmental Studies Hybridoma Bank developed under the auspices of the National Institutes of Health-National Institute of Child Health & Human Development and maintained by The University of Iowa, Department of Biology, Iowa City, IA 52242. This work was supported by National Institutes of Health – National Institute of Neurological Disorders and Stroke grant (NS086812 to F.L.R.) and the OHSU Neuroscience Imaging Center P30 grant (NS061800 to Sue Aicher), and through the philanthropy of Frank and Julie Jungers.

FIGURES & LEGENDS

Table 4.1: Mutations that cause myelin outfoldings in Schwann cells

gene ID	Protein Function	Actin dynamics	Endosome trafficking	Additional PNS defects	Disease	Mouse Model	Reference
Cdc42	Filopodia formation	x	x	Axon radial sorting defects	--	*DHH-Cre/Cdc42fl/fl*	Guo L *et al. Glia* 2015
Inf2	Cdc24 effector	x	x	Hypomyelination	CMTDIE	--	Roos A *et al.* JPNS 2015
Fgd4	Cdc24 GEF, endocytosis	x	x	--	CMT4H	Frabin-/-	Horn M *et al. Brain* 2012
N-Wasp	Promotes actin assembly, endocytosis/phagocytosis	x	x	Hypomyelination	--	*DHH-Cre/N-Waspfl/fl*	Novak N *et al. JCB* 2011
Mtmr2	PI - 3 phosphatase, endosome trafficking		x	--	CMT4B1	Mtmr2-/-	Bolis A *et al. JNeuro 2005*
Mtmr13	Pseudophosphatase, Rab - GEF, endosome trafficking		x	--	CMT4B2	Mtmr13-/-	Robinson *et al. PNAS* 2008
Miz1	transcription factor, cell cycle regulator			Demyelination	--	*Miz1ΔPOZ*	Sanz-Moreno *et al. JBC* 2015
Cadm4/ Necl4	Schwann cell-axon interaction, regulates actin cytoskeleton	x		Axon ion channel redistribution	--	*DHH-Cre/Cadm4fl/fl*	Golan N *et al JNeuro* 2013
Lck	Integrin signalling / cytoskeletal rearrangments	x		Schwann cell migration defects, hypomyelination	--	Lck-/-	Ness JK *et al Nature* 2013

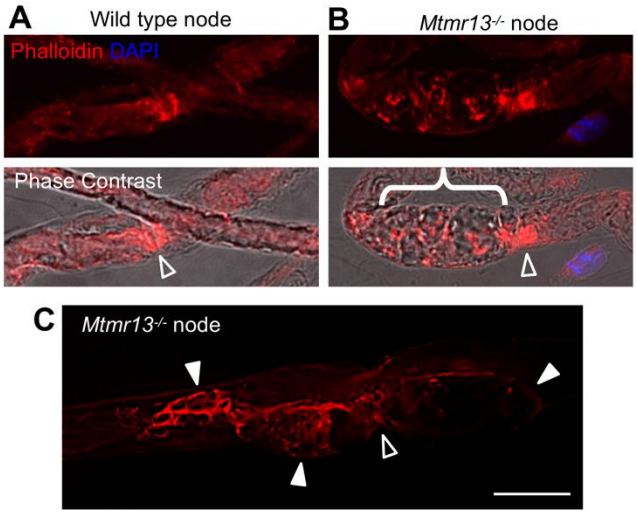

Figure 4.1: **Cortical F-actin distribution in Mtmr13-null myelin outfoldings**. P21 mice teased nerve fibers were labeled with DAPI to identify nuclei and phalloidin to label F-actin. Phase contrast images were used to identify myelin outfoldings. Unfilled arrowheads indicate Nodes of Ranvier. (**A**) Example of a wild type node containing F-actin rich microvilli at SC paranodes. (**B**) Example of a *Mtmr13*$^{-/-}$ node. Bracket denotes a region of myelin outfoldings on one side of the node. N = 2 mice per genotype, qualitatively assessed for aberrant F-actin distribution. (**C**) Higher magnification image of *Mtmr13*$^{-/-}$ stained with phalloidin to label F-actin. Submembranous F-actin forms a continuous rim with the myelin outfolding, reminiscent of cortical actin (filled arrowheads). Node of Ranvier specified by unfilled arrowhead and was identified from phase-contrast image (not shown). Scale bar = 10 μm.

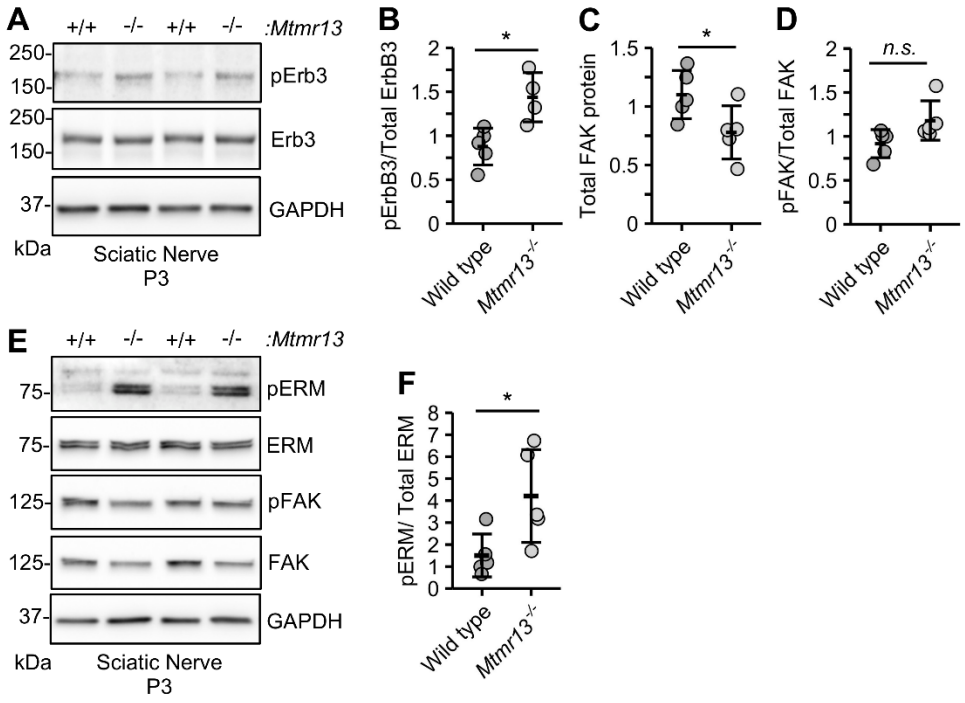

Figure 4.2: **Altered ErbB3 activation and actin associated protein signaling in the absence of Mtmr13.** (**A, E**) The activation of the pro-myelination and actin protein signals were determined by immunoblotting P3 sciatic nerve lysates (6 nerves pooled per lysate) and quantifying the relative amount of activated (phosphorylated) protein. (**B**) The ratio of activated ErbB3 (pY-1289) to total protein was significantly increased in *Mtmr13*$^{-/-}$ nerves at P3. (**C**) Total FAK levels were significantly decreased in nerves lacking Mtmr13. (**D**) The ratio of pFAK (pY-397) to total protein was unaltered in the absence of Mtmr13. These data are presented as mean ± SD; Student's two-sample t-test. (**F**) At P3, the ratio of pERM to total ERM protein was significantly increased in *Mtmr13*$^{-/-}$ lysates. Welsh's unpaired t-tests were used to evaluate significance. Wild type n = 5 and *Mtmr13*$^{-/-}$ n = 4-5 nerve lysates (*$p < 0.05$; *n.s,* not significant).

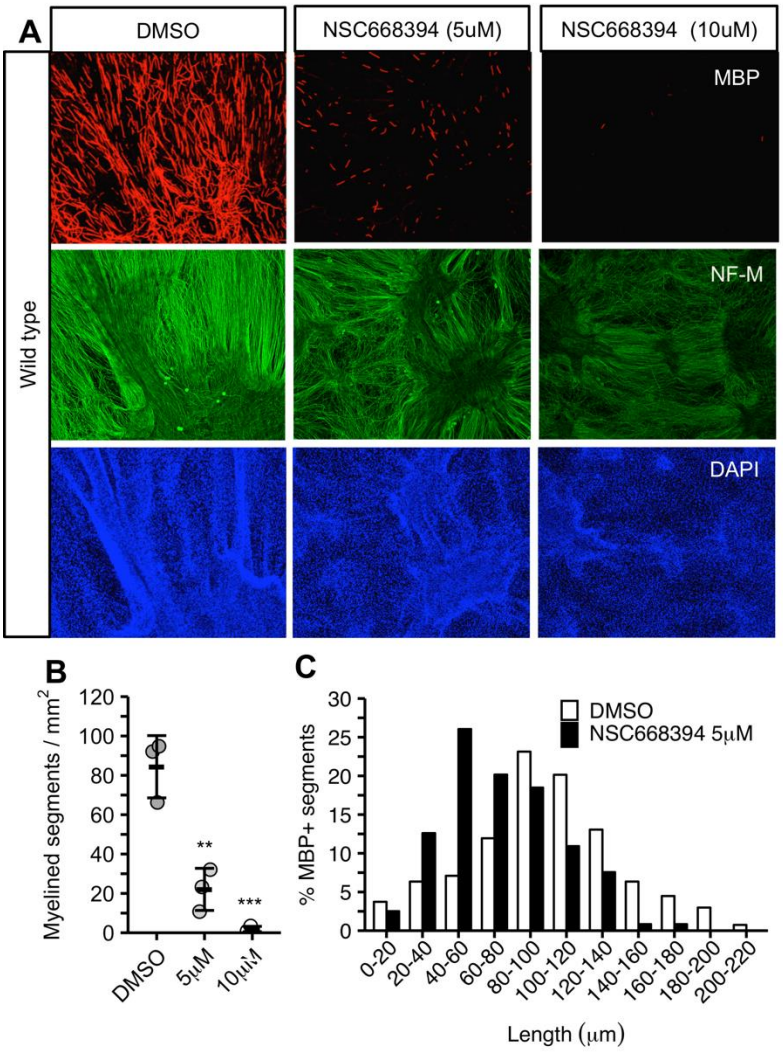

Figure 4.3: ERM activation regulates Schwann cell myelination *in vitro.* (**A**) Representative images of SC-DRG explants treated with 5 μM or 10 μM NSC668394, a pharmacological inhibitor of ERM phosphorylation preventing the conformation charge required for actin binding. 0.1% DMSO was used as a treatment control. Myelin, axons, and nuclei were visualized via immunofluorescence with antibodies to myelin basic protein (MBP; red), neurofilament medium chain (NF-M; green), and DAPI stain (blue) respectively. Scale bar: 500 μm. (**B**) Dose dependent decrease in the density of MBP-positive myelinated segments in wild type SC-DRG explants treated with NSC668394. Quantified from n = 3 explants/coverslips per treatment condition, 4 low magnification

images per explant. One-way ANOVA with Tukey post-hoc test; mean ± SD; **p ≤ 0.01; ***p ≤ 0.001 (**C**) Decrease in wild type MBP-positive segment length with 5 μM NSC668394 treatment. Kolmogorov-Smirnov test ****p = 4.04x10^{-9}; DMSO treatment n = 248, 5 μM NSC668394 treatment n = 153 myelin segments quantified from three explants/coverslips per condition.

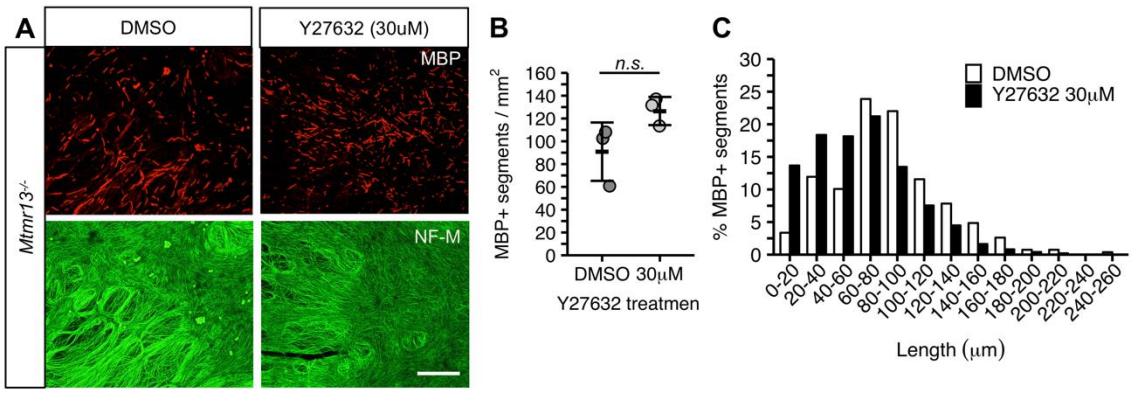

Figure 4.4: ROCK activation controls myelin length in *Mtmr13*$^{-/-}$ SC-DRG explants. (**A**) Representative images of SC-DRG explants treated with Y27632 30 μM or 0.1% DMSO control starting at culture day 8. Myelin segments and axons were visualized via immunofluorescence with antibodies to myelin basic protein (MBP; red) and neurofilament medium chain (NF-M; green). Scale bar: 500 μm. (**B**) Inhibition of ROCK had no effect on MBP-positive myelin density in *Mtmr13*$^{-/-}$ SC-DRG explants. Quantified from n = 3 explants/coverslips per treatment condition. Student's two-sample t-test; mean ± SD; *n.s.* not significant. (**D**) Decrease in wild type MBP-positive segment length with Y27632 30 μM treatment. Kolmogorov-Smirnov test ****p = 5.03x10^{-11}; DMSO treatment n = 268, Y27632 30 μM treatment n = 490 MBP-positive segments quantified from 4 explants/coverslips per condition.

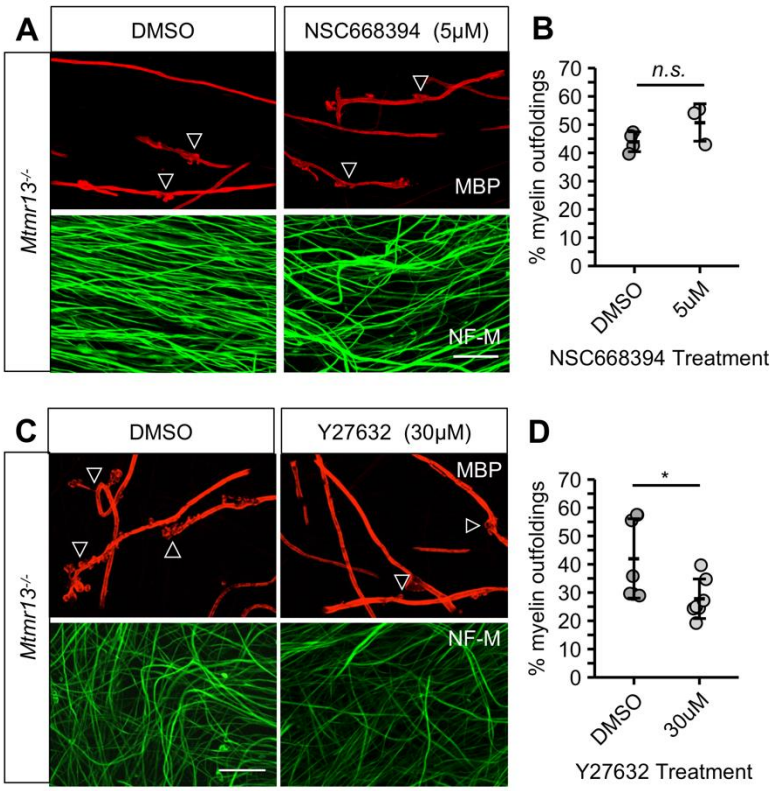

Figure 4.5: **Inhibiting ROCK decreases CMT4B2-like myelin outfoldings in *Mtmr13*$^{-/-}$ explants.** *Mtmr13*$^{-/-}$ SC-DRG explants were treated pharmacologically with an ERM inhibitor (NSC668394) or a ROCK inhibitor (Y27632) beginning at culture day 8 when myelination was induced. Drugs or 0.1% DMSO control were added with each media change at the indicated concentrations. At Day 21, cultures were visualized with myelin basic protein (MBP; red) and neurofilament medium chain (NF-M; green) immunofluorescence. Arrowheads indicate MBP-positive segments that contain one or more myelin outfolding. (**A**) Representative images of *Mtmr13*$^{-/-}$ explants treated with 5 μM ERM inhibitor or DMSO control. Scale bar = 20 μm. (**B**) Percentage of myelin segments that contained one or more myelin outfoldings was not significantly different in *Mtmr13*$^{-/-}$ explants treated with NSC668394. Student's two-sample t-test $p = 0.135$; DMSO n = 3 and NSC668394 n = 4 coverslips/explants; data represented as mean ± SD. (**C**) Representative images of *Mtmr13*$^{-/-}$ explants treated with 30 μM ROCK inhibitor or

DMSO control. Scale bar = 20 μm. (**D**) Percentage of myelin segments that contained one or more outfolding was significantly decreased in in *Mtmr13*$^{-/-}$ explants treated with Y27632. Welch two-sample t-test for unequal variances; *$p \leq 0.05$; n = 7 coverslips/explants per treatment condition; data represented as mean ± SD.

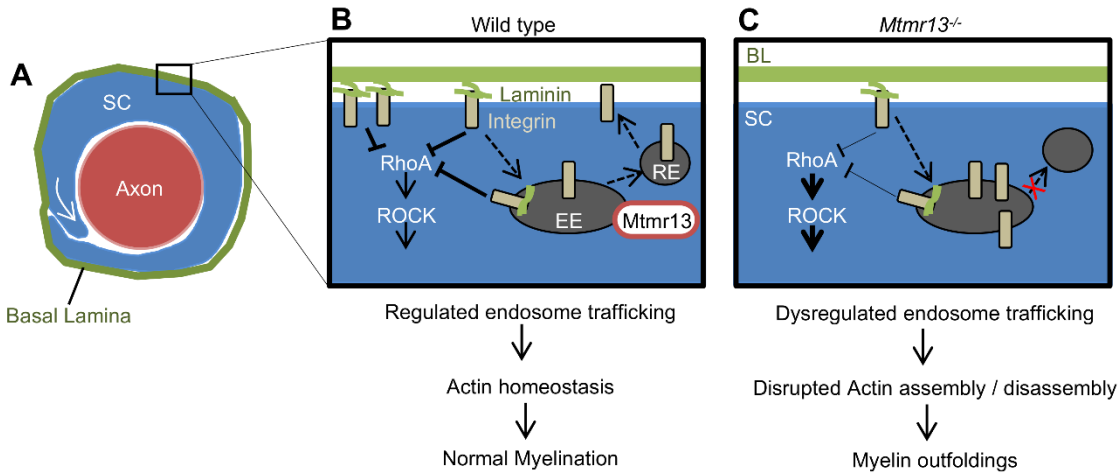

Figure 4.6: **Proposed model for the role of Mtmr13 in regulating RhoA activation through early endosome recycling of β1-integrin to the Schwann cell plasma membrane.** (**A**) Depiction of a promyelinating Schwann cell (SC) beginning to enwrap an axon. Myelin extends through the movement of the leading edge of the SC between the axon and myelin layers (white arrow). Transmembrane receptors on both the abaxonal and adaxonal SC interface promote activation of actin polymerization and actomyosin contractility proteins required for SC leading edge motility. (**B**) At the SC abaxonal face, α6β1-integrin binds to laminin 2 in the basal lamina (BL). Through the association with integrin-linked kinase (ILK), integrin negatively regulates RhoA/ROCK activation in SC (129). Mtmr13 is predicted to mediate endosomal membrane exit of integrin by activating Rab21 (72). (**C**) Loss of Mtmr13 may lead to increased retention of inactive integrin receptors in early endosomes resulting in increased RhoA/ROCK activation due to loss of ILK recruitment. Increased RhoA/ROCK could result in disorganized actin assembly/contractility generating myelin outfoldings as the myelin sheath grows.

SUPPLEMENTARY DATA

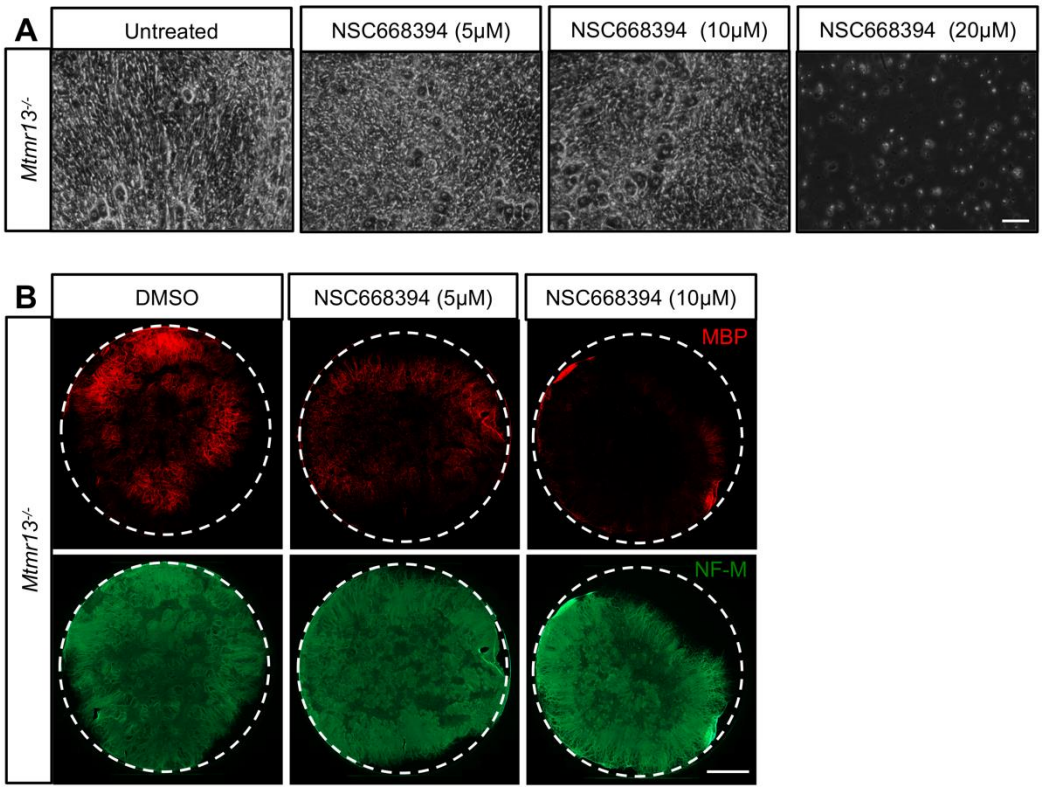

Supplemental Figure 4.7: Treatment with the ERM inhibitor NSC668394 causes dose dependent cell death and myelin disruption in SC-DRG explants. (**A**) Representative phase-contrast images of untreated control and SC-DRG explants treated with 5 μM, 10 μM, or 20 μM NSC668394. Images were taken on culture day 14 and cell death was observed in all 20 μM treated cultures starting 4 days after treatment (n = 3). Scale bar: 500 μm (**B**) Low magnification images of whole *Mtmr13*$^{-/-}$ SC-DRG explants treated with 0.1% DMSO, 5 μM, or 10 μM NSC668394. Myelin and axons were visualized with antibodies to myelin basic protein (MBP; red) and neurofilament medium chain (NF-M; green) respectively. Scale bar: 5 mm.

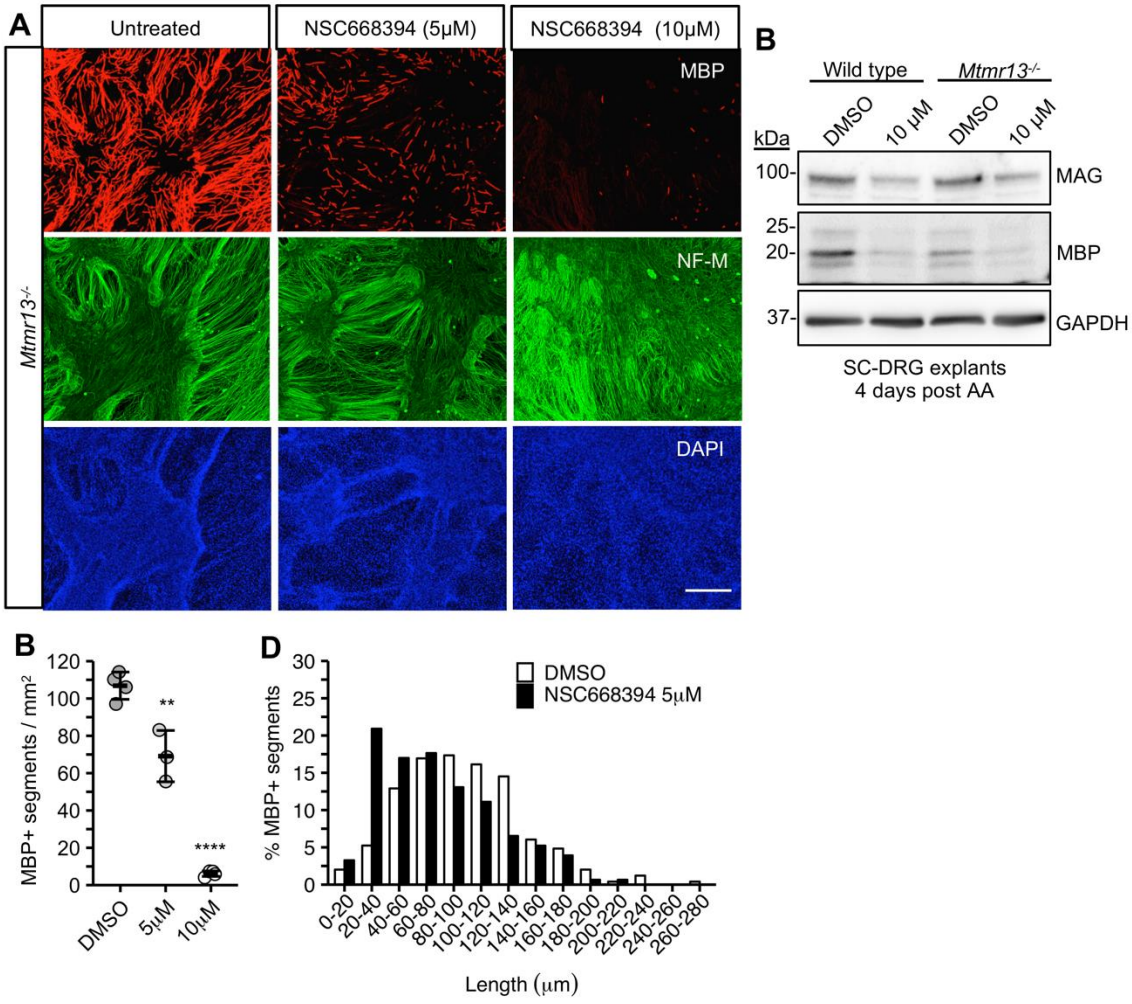

Supplemental Figure 4.8: **ERM activation regulates Schwann cell myelination in *Mtmr13*$^{-/-}$ explants.** (**A**) Representative images of SC-DRG explants treated with 5 μM or 10 μM NSC668394, 0.1% DMSO was a treatment control. Myelin, axons, and nuclei were visualized via immunofluorescence with antibodies to myelin basic protein (MBP; red), neurofilament medium chain (NF-M; green), and DAPI stain (blue). Scale bar: 500 μm. (**B**) After 12 days in culture (4 days post ascorbic acid + inhibitor treatment) protein extracts were prepared from SC-DRG explants and analyzed for myelin protein abundance. Myelin associated glycoprotein (MAG) and Myelin Basic Protein (MBP) levels are decreased in wild type and *Mtmr13*$^{-/-}$ explants treated with 10 μM NSC668394. GAPDH was a protein loading control. (**C**) Dose dependent decrease in the density of

MBP-positive myelinated segments in *Mtmr13*$^{-/-}$ SC-DRG explants treated with NSC668394. Quantified from n = 3-4 explants/coverslips per treatment condition from 4 low magnification images per explant. One-way ANOVA with Tukey post-hoc test; mean ± SD; ***p ≤ 0.001; ****p ≤ 0.0001 (**D**) Decrease in *Mtmr13*$^{-/-}$ explants MBP-positive segment length with 5 μM NSC668394 treatment. Kolmogorov-Smirnov test ****p = 8.33×10^{-5}; DMSO treatment n = 268, 5 μM NSC668394 treatment n = 119 myelin segments quantified from 3 explants/coverslips per condition.

Chapter 5

Conclusions and Future Directions

SIGNIFICANCE

Myelin is an incredible biological structure, composed of specialized proteins and lipids exclusively produced in myelinating glial cells. A myelinating glial cell spirally wraps around an axon and each adaxonal membrane layer compacts to form a condensed multilayer sheath. Myelination is a complex process that requires precise control of receptor signals, cytoskeletal changes, and membrane production in the glial cell. How oligodendrocytes in the CNS and Schwann cells (SCs) in the PNS determine which axons to myelinate, how they enwrap these axons, and produce the correct amount of myelin is still heavily studied. This dissertation work sought to determine how SCs regulate signals critical to axon sorting and myelination by endocytosing, recycling, and/or degrading transmembrane receptors. This work focused on four endosomal regulatory proteins Vps34, Mtmr2, Mtmr5, and Mtmr13. We showed that these proteins are essential for axon sorting and/or SC myelination. Vps34 generates the early endosomal signaling lipid PI3P. We demonstrated that loss of Vps34 caused axon radial sorting defects, arrested myelination, and impaired ErbB2/3 receptor trafficking and signaling in SCs. Loss of either Mtmr2 or Mtmr13 causes myelin to overgrow longitudinally generating abnormal myelin outfoldings and peripheral neuropathy, due in part to increased ErbB2/3 signaling and RhoA activation. Lastly, we showed for the first time that loss of Mtmr5 did not affect myelination but instead led to axon radial sorting defects. Taken together, these results demonstrate that regulation of endo-lysosomal trafficking is critical for SCs to sort and myelinate axons.

The majority of the proteins linked to demyelinating forms of the inherited peripheral neuropathy CMT regulate endo-lysosomal trafficking (64). These proteins are broadly expressed in human tissues, but phenotypic defects caused by loss-of-function mutations are largely isolated to the PNS (64). Why SCs are particularly vulnerable to endosomal trafficking defects is unclear. The work presented in this dissertation

demonstrates that endosomal trafficking is essential for SCs to control the pro-myelination signal ErbB2/3 and coordinate cytoskeletal changes required for radial sorting and myelination. The conclusions presented provide a valuable insight into why SC endosomal trafficking disruptions cause demyelinating CMT and a framework for future therapeutic studies.

CONCLUSIONS AND FUTURE DIRECTIONS

Determining how ErbB2/3 endosomal trafficking is controlled by PI 3-kinases and phosphatases in Schwann cells

In vitro studies have shown that Nrg1-III activation of ErbB2/3 triggers receptor internalization by clathrin-mediated endocytosis. ErbB2/3 may continue to signal from early endosomes before being dephosphorylated and recycled back to the plasma membrane. Ubiquitination of internalized ErbB2/3 targets the receptor for sorting into multivesicular bodies (MVBs), thus terminating this signaling pathway. Fusion of MVBs with lysosomes degrades the ErbB2/3 receptors. PI3P is an early endosome signature known to regulate early endosome receptor sorting, MVB formation, and endo-lysosome fusion. We have demonstrated that the PI 3-kinase Vps34 is essential for normal ErbB2/3 signaling during radial sorting and SC myelination of axons (43). Conditional deletion of *Vps34* in SCs caused enlarged vacuoles, stalled endo-lysosome trafficking, delayed radial sorting, and arrested myelination (43). Stalled endosomal trafficking may account for the abnormal post-translational modifications observed in the ErbB2/3 receptor and reduced myelination signals in *Vps34*-null SCs. In summary, this work highlighted the essential role of the early endosomal lipid PI3P during SC myelination. *Vps34*-null mice also provide a model to study how ErbB2/3 and other critical receptor signaling are controlled by endosomal trafficking during SC development and myelination.

PI 3-phosphatases are also required for normal ErbB2/3 signaling. We and others have demonstrated that loss of the PI 3-phosphatase Mtmr2 or its binding partner Mtmr13 leads to an increase in activated ErbB2/3 at the onset of myelination (42) (Chapter 4). Myelin abnormalities caused by loss of Mtmr2 are reduced when ErbB2/3 activation is suppressed pharmacologically *in vitro* (42). It has yet to be determined whether suppression of ErbB2/3 activation also alleviates *Mtmr13*$^{-/-}$ dysmyelination. This may be a future direction for the lab. We propose that Mtmr2 and Mtmr13 work together to control ErbB2/3 receptor endosomal recycling to maintain myelin homeostasis.

A future direction of this work would be to determine exactly how ErbB2/3 trafficking is controlled in SCs through the use of our mouse models that disrupt various stages of endosomal trafficking. PI3P generated by Vps34 controls receptor endocytosis, early endosome sorting, MVB/late endosome formation, and endosome-lysosome fusion. Mtmr2, along with binding partners Mtmr5 and Mtmr13, is proposed to control the recycling of receptors from early endosomes back to the plasma membrane through PI3P dephosphorylation and Rab activation. Our lab has knockout mouse models for all of these proteins and mutant cultured SCs ready for these studies. To determine the subcellular localization of internalized ErbB2/3, we would infect primary mutant mouse SCs with epitope tagged ErbB2/3 (Flag-ErbB2) which we would label at the cell surface before inducing receptor internalization with Nrg1. We would use various membrane compartment markers (early endosome, EEA1; late endosome, Rab7; and lysosome, Lamp1) to determine where ErbB2/3 accumulates when endosomal regulators are deleted. We predict that loss of Vps34 will lead to an accumulation of ErbB2/3 in MVBs, and loss of either Mtmr2, Mtmr5, or Mtmr13 will lead to increased ErbB2/3 in early endosomes. In a broader context these results would identify how SCs utilized membrane trafficking to fine tune ErbB2/3 signaling. Precise ErbB2/3 signaling is

required for SCs to determine which axon to myelinate and how much myelin to produce for sufficient nerve conduction.

Evolution of Mtmr5 and Mtmr13: why do vertebrates require both proteins?

Myelin evolved in vertebrates along with hinged jaw formation. Lamprey are jawless vertebrate fish that express a subset of myelin proteins, but do not produce myelin sheaths (1). Interestingly, sea lamprey (*P. marinus*) genomes contain orthologous genes to the majority of human myotubularins, including Mtmr5 and Mtmr13. Invertebrates have a single ortholog of Mtmr5 and Mtmr13, this includes octopuses (*O. bimaculoides*) which have six myotubularin proteins including a single Mtmr5/13 gene. This suggests that a duplication from a single Mtmr5/13 gene occurred when vertebrates evolved. Our genetic studies have demonstrated that both Mtmr5 and Mtmr13 are required in the PNS. Mtmr5 controls axon radial sorting and Mtmr13 regulates SC myelination. Their unique roles in the PNS supports the hypothesis that Mtmr5 and Mtmr13 evolved from a single gene which allowed SCs to express Mtmr5 during radial sorting and Mtmr13 during myelination, compartmentalizing these two processes.

We demonstrated that Mtmr5 and Mtmr13 have comparable function in tissues outside the PNS, but it is unclear whether they can compensate for one another in this tissue. We showed that Mtmr5 protein levels correlates with axon radial sorting and Mtmr13 levels were highest during SC myelination (Fig. 5.1). The future direction for this work will be to determine whether differences in expression timing alone explain the distinct roles of Mtmr5 and Mtmr13 in the PNS. To answer this question, we would overexpress Mtmr5 protein exogenously in *Mtmr13*$^{-/-}$ myelinating SC-DRG cultures. This experiment would determine whether Mtmr5 is able to rescue the dysmyelination that results from lack of Mtmr13. If Mtmr5 and Mtmr13 have an analogous function, then exogenous expression of Mtmr5 should substantially reduce the abundance of CMT4B2-

like myelin outfoldings in *Mtmr13*$^{-/-}$ cultures. However, if Mtmr5 and Mtmr13 have unique protein properties, then Mtmr5 would be unable to rescue myelin outfoldings. These studies would increase our understanding of how Mtmr5 and Mtmr13 function in the PNS, and clarify why loss of either protein causes peripheral neuropathy.

Mtmr13 controls endosomal trafficking and cytoskeletal dynamics to regulate Schwann cell myelination

Loss-of-function mutations in Mtmr13 cause demyelinating peripheral neuropathy and abnormal myelin outfoldings (68). The *Drosophila* ortholog of Mtmr5/13 functions to regulate endosome recycling and actin-rich filipodia formation in macrophages (72). However, the role of Mtmr5 or Mtmr13-mediated endosomal trafficking and actin remodeling during axon radial sorting and myelination has yet to be established. We showed that loss of Mtmr13 led to abnormal cortical actin accumulation in SC myelin outfoldings. Mtmr13 regulates actin-associated signaling proteins FAK and ERM in mouse sciatic nerves. We determined that ERM activation was essential for SC myelin but did not contribute to dysmyelination caused by Mtmr13 loss. ERM is activated by the Rho-associated protein kinase (ROCK). Decreased RhoA/ROCK activation partially rescued myelin outfoldings in *Mtmr13*$^{-/-}$ cultures. We hypothesize that Mtmr13 controls RhoA/ROCK actin dynamics indirectly by coordinating the endosomal recycling of receptors such as β1-integrin and ErbB2/3.

Future studies will determine how Mtmr13 loss affects RhoA activation directly, and whether RhoA overactivation drives myelin outfolding formation. We showed indirectly that loss of Mtmr13 causes increased RhoA activation, assessed by downstream ERM phosphorylation. However, there are other kinases that can phosphorylate and activate ERM. Therefore, RhoA activation should be measured directly in *Mtmr13*$^{-/-}$ mouse sciatic nerves and myelinating cultures. This can be

assessed using a pull-down assay with the RhoA-binding-domain of Rhotekin protein, which interacts directly and specifically with activated RhoA. We would compare the amount of activated RhoA in sciatic nerves from *Mtmr13*$^{-/-}$ mice and littermate controls, with the prediction that loss of Mtmr13 leads to increased activated RhoA levels. We and others have shown that suppressing RhoA/ROCK activation shortens myelin segments but does not inhibit total myelin abundance. Endogenous RhoA activity can be stimulated by adding activator proteins (e.g. calpeptin) to myelinating SC-DRG cultures. This experiment would test the hypothesis that increased RhoA activation causes abnormal myelin outfoldings similar to those observed in *Mtmr2* and *Mtmr13*-null models. These data would provide critical evidence that SCs require RhoA/ROCK activation and downstream cytoskeletal changes to control longitudinal myelin growth and prevent myelin outfolding formation.

Identifying the mechanism by which Mtmr5 controls axon radial sorting

During PNS development SCs extend actin-rich lamellipodia into axon bundles to determine which axons should be sorted into a 1:1 relationship for myelination. Axon radial sorting is regulated in part by extra cellular matrix and axonal signals that mediate downstream intracellular cytoskeleton rearrangements. We have demonstrated that loss of Mtmr5 in mice caused abnormal retention of large axons in unmyelinated Remak bundles. However, loss of Mtmr5 had no impact on myelination once a 1:1 SC to axon association was formed. Mtmr5 was expressed during axon radial sorting and turned off by P21, suggesting that Mtmr5 is required for the very specific glial process of determining which axons require myelin.

ErbB2/3 signaling is critical for axon radial sorting and myelination. Nrg1 heterozygous mice have radial sorting defects along with myelin abnormalities. Abnormal endosomal trafficking of the ErbB2/3 receptor has been proposed as a

common mechanism linking demyelinating subtypes of CMT (66). Loss of Mtmr2 or Mtmr13 cause increased pErbB2 levels during myelin initiation (42) (Chapter 4). We predict that Mtmr5 loss also leads to increased ErbB2/3 activation, actin dysregulation, and radial sorting defects. ErbB2/3 activation can be assessed by western blotting *Mtmr5*$^{-/-}$ sciatic nerve lysates for total and pErbB2/3 at various time points during radial sorting. These results may clarify the dual role of ErbB2/3 in controlling axon sorting and myelination. This dissertation work suggests that maintaining the correct ErbB2/3 activation during peripheral development may provide a convergent method to treat multiple CMT4B disease subtypes.

FIGURES AND LEGENDS

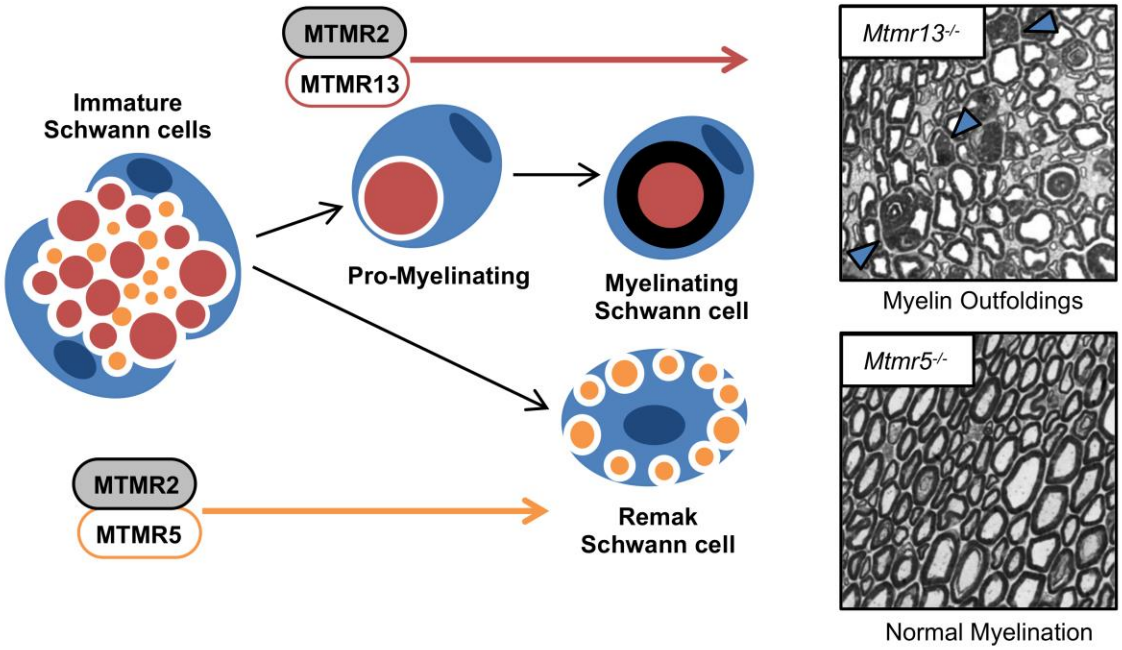

Figure 5.1: **Proposed model for the role of Mtmr5 and Mtmr13 in the PNS.** We predict that two CMT4B-causing myotubularin protein complexes form in the PNS: an Mtmr2-Mtmr5 complex and an Mtmr2-Mtmr13 complex. Mtmr2-Mtmr5 protein complex regulates late stage axon radial sorting (E17-P10). Mtmr2-Mtmr13 protein complex functions to maintain myelin homeostasis once large axons form a 1:1 relationship with a pro-myelinating Schwann cell (P0-adult). Timing differences may explain why loss of Mtmr13 generate outfoldings whereas Mtmr5 loss causes Remak defects and no effect on subsequent myelination.

REFERENCES

1 Weil, M.T., Heibeck, S., Topperwien, M., Tom Dieck, S., Ruhwedel, T., Salditt, T., Rodicio, M.C., Morgan, J.R., Nave, K.A., Mobius, W. *et al.* (2018) Axonal Ensheathment in the Nervous System of Lamprey: Implications for the Evolution of Myelinating Glia. *J Neurosci*, **38**, 6586-6596.

2 Zalc, B. (2016) The acquisition of myelin: An evolutionary perspective. *Brain Res*, **1641**, 4-10.

3 Yoshida, M. and Colman, D.R. (1996) Parallel evolution and coexpression of the proteolipid proteins and protein zero in vertebrate myelin. *Neuron*, **16**, 1115-1126.

4 Sherman, D.L. and Brophy, P.J. (2005) Mechanisms of axon ensheathment and myelin growth. *Nat Rev Neurosci*, **6**, 683-690.

5 Kleopa, K.A. and Sargiannidou, I. (2015) Connexins, gap junctions and peripheral neuropathy. *Neurosci Lett*, **596**, 27-32.

6 Salzer, J.L. (2015) Schwann cell myelination. *Cold Spring Harb Perspect Biol*, **7**, a020529.

7 Baumann, N. and Pham-Dinh, D. (2001) Biology of oligodendrocyte and myelin in the mammalian central nervous system. *Physiol Rev*, **81**, 871-927.

8 Lee, S., Leach, M.K., Redmond, S.A., Chong, S.Y., Mellon, S.H., Tuck, S.J., Feng, Z.Q., Corey, J.M. and Chan, J.R. (2012) A culture system to study oligodendrocyte myelination processes using engineered nanofibers. *Nat Methods*, **9**, 917-922.

9 Mei, F., Fancy, S.P.J., Shen, Y.A., Niu, J., Zhao, C., Presley, B., Miao, E., Lee, S., Mayoral, S.R., Redmond, S.A. *et al.* (2014) Micropillar arrays as a high-throughput screening platform for therapeutics in multiple sclerosis. *Nat Med*, **20**, 954-960.

10 Harty, B.L. and Monk, K.R. (2017) Unwrapping the unappreciated: recent progress in Remak Schwann cell biology. *Curr Opin Neurobiol*, **47**, 131-137.

11 Quarles R.H., M.W.B., and Morell P. (2006), In *Basic Neurochemistry: Molecular, Cellular and Medical Aspects*. Elsevier Academic Press, in press., pp. 51-70.

12 Snaidero, N., Velte, C., Myllykoski, M., Raasakka, A., Ignatev, A., Werner, H.B., Erwig, M.S., Mobius, W., Kursula, P., Nave, K.A. *et al.* (2017) Antagonistic Functions of MBP and CNP Establish Cytosolic Channels in CNS Myelin. *Cell Rep*, **18**, 314-323.

13 Stassart, R.M., Mobius, W., Nave, K.A. and Edgar, J.M. (2018) The Axon-Myelin Unit in Development and Degenerative Disease. *Front Neurosci*, **12**, 467.

14 Feltri, M.L., Poitelon, Y. and Previtali, S.C. (2016) How Schwann Cells Sort Axons: New Concepts. *Neuroscientist*, **22**, 252-265.

15 Newbern, J. and Birchmeier, C. (2010) Nrg1/ErbB signaling networks in Schwann cell development and myelination. *Semin Cell Dev Biol*, **21**, 922-928.

16 Stolt, C.C. and Wegner, M. (2016) Schwann cells and their transcriptional network: Evolution of key regulators of peripheral myelination. *Brain Res*, **1641**, 101-110.

17 Britsch, S., Goerich, D.E., Riethmacher, D., Peirano, R.I., Rossner, M., Nave, K.A., Birchmeier, C. and Wegner, M. (2001) The transcription factor Sox10 is a key regulator of peripheral glial development. *Genes Dev*, **15**, 66-78.

18 Riethmacher, D., Sonnenberg-Riethmacher, E., Brinkmann, V., Yamaai, T., Lewin, G.R. and Birchmeier, C. (1997) Severe neuropathies in mice with targeted mutations in the ErbB3 receptor. *Nature*, **389**, 725-730.

19 Jacob, C., Christen, C.N., Pereira, J.A., Somandin, C., Baggiolini, A., Lotscher, P., Ozcelik, M., Tricaud, N., Meijer, D., Yamaguchi, T. *et al.* (2011) HDAC1 and HDAC2 control the transcriptional program of myelination and the survival of Schwann cells. *Nat Neurosci*, **14**, 429-436.

20 Mogha, A., Benesh, A.E., Patra, C., Engel, F.B., Schoneberg, T., Liebscher, I. and Monk, K.R. (2013) Gpr126 functions in Schwann cells to control differentiation and myelination via G-protein activation. *J Neurosci*, **33**, 17976-17985.

21 Taveggia, C., Zanazzi, G., Petrylak, A., Yano, H., Rosenbluth, J., Einheber, S., Xu, X., Esper, R.M., Loeb, J.A., Shrager, P. *et al.* (2005) Neuregulin-1 type III determines the ensheathment fate of axons. *Neuron*, **47**, 681-694.

22 Weider, M., Kuspert, M., Bischof, M., Vogl, M.R., Hornig, J., Loy, K., Kosian, T., Muller, J., Hillgartner, S., Tamm, E.R. *et al.* (2012) Chromatin-remodeling factor Brg1 is required for Schwann cell differentiation and myelination. *Dev Cell*, **23**, 193-201.

23 Ryu, E.J., Wang, J.Y., Le, N., Baloh, R.H., Gustin, J.A., Schmidt, R.E. and Milbrandt, J. (2007) Misexpression of Pou3f1 results in peripheral nerve hypomyelination and axonal loss. *J Neurosci*, **27**, 11552-11559.

24 Birchmeier, C. and Nave, K.A. (2008) Neuregulin-1, a key axonal signal that drives Schwann cell growth and differentiation. *Glia*, **56**, 1491-1497.

25 Morris, J.K., Lin, W., Hauser, C., Marchuk, Y., Getman, D. and Lee, K.F. (1999) Rescue of the cardiac defect in ErbB2 mutant mice reveals essential roles of ErbB2 in peripheral nervous system development. *Neuron*, **23**, 273-283.

26 Michailov, G.V., Sereda, M.W., Brinkmann, B.G., Fischer, T.M., Haug, B., Birchmeier, C., Role, L., Lai, C., Schwab, M.H. and Nave, K.A. (2004) Axonal neuregulin-1 regulates myelin sheath thickness. *Science*, **304**, 700-703.

27 Beirowski, B. (2019) The LKB1-AMPK and mTORC1 Metabolic Signaling Networks in Schwann Cells Control Axon Integrity and Myelination: Assembling and upholding nerves by metabolic signaling in Schwann cells. *Bioessays*, **41**, e1800075.

28 Viader, A., Golden, J.P., Baloh, R.H., Schmidt, R.E., Hunter, D.A. and Milbrandt, J. (2011) Schwann cell mitochondrial metabolism supports long-term axonal survival and peripheral nerve function. *J Neurosci*, **31**, 10128-10140.

29 Brown, T.L. and Macklin, W.B. (2019) The Actin Cytoskeleton in Myelinating Cells. *Neurochem Res*, in press.

30 Nawaz, S., Sanchez, P., Schmitt, S., Snaidero, N., Mitkovski, M., Velte, C., Bruckner, B.R., Alexopoulos, I., Czopka, T., Jung, S.Y. *et al.* (2015) Actin filament turnover drives leading edge growth during myelin sheath formation in the central nervous system. *Dev Cell*, **34**, 139-151.

31 Hu, B., Arpag, S., Zhang, X., Mobius, W., Werner, H., Sosinsky, G., Ellisman, M., Zhang, Y., Hamilton, A., Chernoff, J. *et al.* (2016) Tuning PAK Activity to Rescue Abnormal Myelin Permeability in HNPP. *PLoS Genet*, **12**, e1006290.

32 Etienne-Manneville, S. and Hall, A. (2002) Rho GTPases in cell biology. *Nature*, **420**, 629-635.

33 Melendez-Vasquez, C.V., Einheber, S. and Salzer, J.L. (2004) Rho kinase regulates schwann cell myelination and formation of associated axonal domains. *J Neurosci*, **24**, 3953-3963.

34 Melendez-Vasquez, C.V., Rios, J.C., Zanazzi, G., Lambert, S., Bretscher, A. and Salzer, J.L. (2001) Nodes of Ranvier form in association with ezrin-radixin-moesin (ERM)-positive Schwann cell processes. *Proc Natl Acad Sci U S A*, **98**, 1235-1240.

35 Guo, L., Moon, C., Niehaus, K., Zheng, Y. and Ratner, N. (2012) Rac1 controls Schwann cell myelination through cAMP and NF2/merlin. *J Neurosci*, **32**, 17251-17261.

36 Guo, L., Moon, C., Zheng, Y. and Ratner, N. (2013) Cdc42 regulates Schwann cell radial sorting and myelin sheath folding through NF2/merlin-dependent and independent signaling. *Glia*, **61**, 1906-1921.

37 Horn, M., Baumann, R., Pereira, J.A., Sidiropoulos, P.N., Somandin, C., Welzl, H., Stendel, C., Luhmann, T., Wessig, C., Toyka, K.V. *et al.* (2012) Myelin is dependent on the Charcot-Marie-Tooth Type 4H disease culprit protein FRABIN/FGD4 in Schwann cells. *Brain*, **135**, 3567-3583.

38 Boyer, O., Nevo, F., Plaisier, E., Funalot, B., Gribouval, O., Benoit, G., Huynh Cong, E., Arrondel, C., Tete, M.J., Montjean, R. *et al.* (2011) INF2 mutations in Charcot-Marie-Tooth disease with glomerulopathy. *N Engl J Med*, **365**, 2377-2388.

39 Sidiropoulos, P.N., Miehe, M., Bock, T., Tinelli, E., Oertli, C.I., Kuner, R., Meijer, D., Wollscheid, B., Niemann, A. and Suter, U. (2012) Dynamin 2 mutations in Charcot-Marie-Tooth neuropathy highlight the importance of clathrin-mediated endocytosis in myelination. *Brain*, **135**, 1395-1411.

40 Gouttenoire, E.A., Lupo, V., Calpena, E., Bartesaghi, L., Schupfer, F., Medard, J.J., Maurer, F., Beckmann, J.S., Senderek, J., Palau, F. *et al.* (2013) Sh3tc2 deficiency affects neuregulin-1/ErbB signaling. *Glia*, **61**, 1041-1051.

41 Schink, K.O., Tan, K.W. and Stenmark, H. (2016) Phosphoinositides in Control of Membrane Dynamics. *Annu Rev Cell Dev Biol*, **32**, 143-171.

42 Bolino, A., Piguet, F., Alberizzi, V., Pellegatta, M., Rivellini, C., Guerrero-Valero, M., Noseda, R., Brombin, C., Nonis, A., D'Adamo, P. *et al.* (2016) Niacin-mediated Tace activation ameliorates CMT neuropathies with focal hypermyelination. *EMBO Mol Med*, **8**, 1438-1454.

43 Logan, A.M., Mammel, A.E., Robinson, D.C., Chin, A.L., Condon, A.F. and Robinson, F.L. (2017) Schwann cell-specific deletion of the endosomal PI 3-kinase Vps34 leads to delayed radial sorting of axons, arrested myelination, and abnormal ErbB2-ErbB3 tyrosine kinase signaling. *Glia*, **65**, 1452-1470.

44 Simons, M. and Trotter, J. (2007) Wrapping it up: the cell biology of myelination. *Curr Opin Neurobiol*, **17**, 533-540.

45 Trajkovic, K., Dhaunchak, A.S., Goncalves, J.T., Wenzel, D., Schneider, A., Bunt, G., Nave, K.A. and Simons, M. (2006) Neuron to glia signaling triggers myelin membrane exocytosis from endosomal storage sites. *J Cell Biol*, **172**, 937-948.

46 Chen, G., Zhang, Z., Wei, Z., Cheng, Q., Li, X., Li, W., Duan, S. and Gu, X. (2012) Lysosomal exocytosis in Schwann cells contributes to axon remyelination. *Glia*, **60**, 295-305.

47 Krauss, M. and Haucke, V. (2007) Phosphoinositides: regulators of membrane traffic and protein function. *FEBS Lett*, **581**, 2105-2111.

48 Alvarez-Prats, A., Bjelobaba, I., Aldworth, Z., Baba, T., Abebe, D., Kim, Y.J., Stojilkovic, S.S., Stopfer, M. and Balla, T. (2018) Schwann-Cell-Specific Deletion of Phosphatidylinositol 4-Kinase Alpha Causes Aberrant Myelination. *Cell Rep*, **23**, 2881-2890.

49 Domenech-Estevez, E., Baloui, H., Meng, X., Zhang, Y., Deinhardt, K., Dupree, J.L., Einheber, S., Chrast, R. and Salzer, J.L. (2016) Akt Regulates Axon Wrapping and Myelin Sheath Thickness in the PNS. *J Neurosci*, **36**, 4506-4521.

50 Hasegawa, J., Strunk, B.S. and Weisman, L.S. (2017) PI5P and PI(3,5)P2: Minor, but Essential Phosphoinositides. *Cell Struct Funct*, **42**, 49-60.

51 Vaccari, I., Carbone, A., Previtali, S.C., Mironova, Y.A., Alberizzi, V., Noseda, R., Rivellini, C., Bianchi, F., Del Carro, U., D'Antonio, M. *et al.* (2015) Loss of Fig4 in both Schwann cells and motor neurons contributes to CMT4J neuropathy. *Hum Mol Genet*, **24**, 383-396.

52 Bolino, A., Muglia, M., Conforti, F.L., LeGuern, E., Salih, M.A., Georgiou, D.M., Christodoulou, K., Hausmanowa-Petrusewicz, I., Mandich, P., Schenone, A. *et al.* (2000) Charcot-Marie-Tooth type 4B is caused by mutations in the gene encoding myotubularin-related protein-2. *Nat Genet*, **25**, 17-19.

53 Vaccari, I., Dina, G., Tronchere, H., Kaufman, E., Chicanne, G., Cerri, F., Wrabetz, L., Payrastre, B., Quattrini, A., Weisman, L.S. *et al.* (2011) Genetic interaction between MTMR2 and FIG4 phospholipid phosphatases involved in Charcot-Marie-Tooth neuropathies. *PLoS Genet*, **7**, e1002319.

54 Jessen, K.R. and Mirsky, R. (2019) The Success and Failure of the Schwann Cell Response to Nerve Injury. *Front Cell Neurosci*, **13**, 33.

55 Arthur-Farraj, P.J., Latouche, M., Wilton, D.K., Quintes, S., Chabrol, E., Banerjee, A., Woodhoo, A., Jenkins, B., Rahman, M., Turmaine, M. *et al.* (2012) c-Jun reprograms Schwann cells of injured nerves to generate a repair cell essential for regeneration. *Neuron*, **75**, 633-647.

56 Gomez-Sanchez, J.A., Carty, L., Iruarrizaga-Lejarreta, M., Palomo-Irigoyen, M., Varela-Rey, M., Griffith, M., Hantke, J., Macias-Camara, N., Azkargorta, M., Aurrekoetxea, I. *et al.* (2015) Schwann cell autophagy, myelinophagy, initiates myelin clearance from injured nerves. *J Cell Biol*, **210**, 153-168.

57 Gomez-Sanchez, J.A., Pilch, K.S., van der Lans, M., Fazal, S.V., Benito, C., Wagstaff, L.J., Mirsky, R. and Jessen, K.R. (2017) After Nerve Injury, Lineage Tracing Shows That Myelin and Remak Schwann Cells Elongate Extensively and Branch to Form Repair Schwann Cells, Which Shorten Radically on Remyelination. *J Neurosci*, **37**, 9086-9099.

58 Love, S. (2006) Demyelinating diseases. *J Clin Pathol*, **59**, 1151-1159.

59 Nave, K.A. and Werner, H.B. (2014) Myelination of the nervous system: mechanisms and functions. *Annu Rev Cell Dev Biol*, **30**, 503-533.

60 Saporta, M.A. and Shy, M.E. (2013) Inherited peripheral neuropathies. *Neurol Clin*, **31**, 597-619.

61 Jerath, N.U. and Shy, M.E. (2015) Hereditary motor and sensory neuropathies: Understanding molecular pathogenesis could lead to future treatment strategies. *Biochim Biophys Acta*, **1852**, 667-678.

62 Bird, T.D. (1993) Adam, M.P., Ardinger, H.H., Pagon, R.A., Wallace, S.E., Bean, L.J.H., Stephens, K. and Amemiya, A. (eds.), In *GeneReviews((R))*, Seattle (WA), in press.

63 Bird, T.D. (1993) Adam, M.P., Ardinger, H.H., Pagon, R.A., Wallace, S.E., Bean, L.J.H., Stephens, K. and Amemiya, A. (eds.), In *GeneReviews((R))*, Seattle (WA), in press.

64 Brennan, K.M., Bai, Y. and Shy, M.E. (2015) Demyelinating CMT--what's known, what's new and what's in store? *Neurosci Lett*, **596**, 14-26.

65 King, R.H., Chandler, D., Lopaticki, S., Huang, D., Blake, J., Muddle, J.R., Kilpatrick, T., Nourallah, M., Miyata, T., Okuda, T. *et al.* (2011) Ndrg1 in development and maintenance of the myelin sheath. *Neurobiol Dis*, **42**, 368-380.

66 Lee, S.M., Chin, L.S. and Li, L. (2017) Dysregulation of ErbB Receptor Trafficking and Signaling in Demyelinating Charcot-Marie-Tooth Disease. *Mol Neurobiol*, **54**, 87-100.

67 Nakhro, K., Park, J.M., Hong, Y.B., Park, J.H., Nam, S.H., Yoon, B.R., Yoo, J.H., Koo, H., Jung, S.C., Kim, H.L. *et al.* (2013) SET binding factor 1 (SBF1) mutation causes Charcot-Marie-Tooth disease type 4B3. *Neurology*, **81**, 165-173.

68 Senderek, J., Bergmann, C., Weber, S., Ketelsen, U.P., Schorle, H., Rudnik-Schoneborn, S., Buttner, R., Buchheim, E. and Zerres, K. (2003) Mutation of the SBF2 gene, encoding a novel member of the myotubularin family, in Charcot-Marie-Tooth neuropathy type 4B2/11p15. *Hum Mol Genet*, **12**, 349-356.

69 Kim, S.A., Vacratsis, P.O., Firestein, R., Cleary, M.L. and Dixon, J.E. (2003) Regulation of myotubularin-related (MTMR)2 phosphatidylinositol phosphatase by MTMR5, a catalytically inactive phosphatase. *Proc Natl Acad Sci U S A*, **100**, 4492-4497.

70 Robinson, F.L. and Dixon, J.E. (2005) The phosphoinositide-3-phosphatase MTMR2 associates with MTMR13, a membrane-associated pseudophosphatase also mutated in type 4B Charcot-Marie-Tooth disease. *J Biol Chem*, **280**, 31699-31707.

71 Yoshimura, S., Gerondopoulos, A., Linford, A., Rigden, D.J. and Barr, F.A. (2010) Family-wide characterization of the DENN domain Rab GDP-GTP exchange factors. *J Cell Biol*, **191**, 367-381.

72 Jean, S., Cox, S., Schmidt, E.J., Robinson, F.L. and Kiger, A. (2012) Sbf/MTMR13 coordinates PI(3)P and Rab21 regulation in endocytic control of cellular remodeling. *Mol Biol Cell*, **23**, 2723-2740.

73 Taylor, G.S., Maehama, T. and Dixon, J.E. (2000) Myotubularin, a protein tyrosine phosphatase mutated in myotubular myopathy, dephosphorylates the lipid second messenger, phosphatidylinositol 3-phosphate. *Proc Natl Acad Sci U S A*, **97**, 8910-8915.

74 Blondeau, F., Laporte, J., Bodin, S., Superti-Furga, G., Payrastre, B. and Mandel, J.L. (2000) Myotubularin, a phosphatase deficient in myotubular myopathy, acts on phosphatidylinositol 3-kinase and phosphatidylinositol 3-phosphate pathway. *Hum Mol Genet*, **9**, 2223-2229.

75 Walker, D.M., Urbe, S., Dove, S.K., Tenza, D., Raposo, G. and Clague, M.J. (2001) Characterization of MTMR3. an inositol lipid 3-phosphatase with novel substrate specificity. *Curr Biol*, **11**, 1600-1605.

76 Begley, M.J., Taylor, G.S., Brock, M.A., Ghosh, P., Woods, V.L. and Dixon, J.E. (2006) Molecular basis for substrate recognition by MTMR2, a myotubularin family phosphoinositide phosphatase. *Proc Natl Acad Sci U S A*, **103**, 927-932.

77 Schaletzky, J., Dove, S.K., Short, B., Lorenzo, O., Clague, M.J. and Barr, F.A. (2003) Phosphatidylinositol-5-phosphate activation and conserved substrate specificity of the myotubularin phosphatidylinositol 3-phosphatases. *Curr Biol*, **13**, 504-509.

78 Tsujita, K., Itoh, T., Ijuin, T., Yamamoto, A., Shisheva, A., Laporte, J. and Takenawa, T. (2004) Myotubularin regulates the function of the late endosome through

the gram domain-phosphatidylinositol 3,5-bisphosphate interaction. *J Biol Chem*, **279**, 13817-13824.

79 Kim, S.A., Taylor, G.S., Torgersen, K.M. and Dixon, J.E. (2002) Myotubularin and MTMR2, phosphatidylinositol 3-phosphatases mutated in myotubular myopathy and type 4B Charcot-Marie-Tooth disease. *J Biol Chem*, **277**, 4526-4531.

80 Berger, P., Berger, I., Schaffitzel, C., Tersar, K., Volkmer, B. and Suter, U. (2006) Multi-level regulation of myotubularin-related protein-2 phosphatase activity by myotubularin-related protein-13/set-binding factor-2. *Hum Mol Genet*, **15**, 569-579.

81 Lorenzo, O., Urbe, S. and Clague, M.J. (2006) Systematic analysis of myotubularins: heteromeric interactions, subcellular localisation and endosome related functions. *J Cell Sci*, **119**, 2953-2959.

82 Zou, J., Chang, S.C., Marjanovic, J. and Majerus, P.W. (2009) MTMR9 increases MTMR6 enzyme activity, stability, and role in apoptosis. *J Biol Chem*, **284**, 2064-2071.

83 Zou, J., Zhang, C., Marjanovic, J., Kisseleva, M.V., Majerus, P.W. and Wilson, M.P. (2012) Myotubularin-related protein (MTMR) 9 determines the enzymatic activity, substrate specificity, and role in autophagy of MTMR8. *Proc Natl Acad Sci U S A*, **109**, 9539-9544.

84 Gupta, V.A., Hnia, K., Smith, L.L., Gundry, S.R., McIntire, J.E., Shimazu, J., Bass, J.R., Talbot, E.A., Amoasii, L., Goldman, N.E. *et al.* (2013) Loss of catalytically inactive lipid phosphatase myotubularin-related protein 12 impairs myotubularin stability and promotes centronuclear myopathy in zebrafish. *PLoS Genet*, **9**, e1003583.

85 Zou, J., Majerus, P.W., Wilson, D.B., Schrade, A., Chang, S.C. and Wilson, M.P. (2012) The role of myotubularin-related phosphatases in the control of autophagy and programmed cell death. *Adv Biol Regul*, **52**, 282-289.

86 Hnia, K., Vaccari, I., Bolino, A. and Laporte, J. (2012) Myotubularin phosphoinositide phosphatases: cellular functions and disease pathophysiology. *Trends Mol Med*, **18**, 317-327.

87 Raess, M.A., Cowling, B.S., Bertazzi, D.L., Kretz, C., Rinaldi, B., Xuereb, J.M. and Kessler, P. (2017) Expression of the neuropathy-associated MTMR2 gene rescues MTM1-associated myopathy. **26**, 3736-3748.

88 Uhlen, M., Fagerberg, L., Hallstrom, B.M., Lindskog, C., Oksvold, P., Mardinoglu, A., Sivertsson, A., Kampf, C., Sjostedt, E., Asplund, A. *et al.* (2015) Proteomics. Tissue-based map of the human proteome. *Science*, **347**, 1260419.

89 Bolino, A., Bolis, A., Previtali, S.C., Dina, G., Bussini, S., Dati, G., Amadio, S., Del Carro, U., Mruk, D.D., Feltri, M.L. *et al.* (2004) Disruption of Mtmr2 produces CMT4B1-like neuropathy with myelin outfolding and impaired spermatogenesis. *J Cell Biol*, **167**, 711-721.

90 Bolis, A., Coviello, S., Bussini, S., Dina, G., Pardini, C., Previtali, S.C., Malaguti, M., Morana, P., Del Carro, U., Feltri, M.L. *et al.* (2005) Loss of Mtmr2 phosphatase in Schwann cells but not in motor neurons causes Charcot-Marie-Tooth type 4B1 neuropathy with myelin outfoldings. *J Neurosci*, **25**, 8567-8577.

91 Bolis, A., Coviello, S., Visigalli, I., Taveggia, C., Bachi, A., Chishti, A.H., Hanada, T., Quattrini, A., Previtali, S.C., Biffi, A. *et al.* (2009) Dlg1, Sec8, and Mtmr2 regulate membrane homeostasis in Schwann cell myelination. *J Neurosci*, **29**, 8858-8870.

92 Azzedine, H., Bolino, A., Taieb, T., Birouk, N., Di Duca, M., Bouhouche, A., Benamou, S., Mrabet, A., Hammadouche, T., Chkili, T. *et al.* (2003) Mutations in MTMR13, a new pseudophosphatase homologue of MTMR2 and Sbf1, in two families with an autosomal recessive demyelinating form of Charcot-Marie-Tooth disease associated with early-onset glaucoma. *Am J Hum Genet*, **72**, 1141-1153.

93 Lassuthova, P., Vill, K., Erdem-Ozdamar, S., Schroder, J.M., Topaloglu, H., Horvath, R., Muller-Felber, W., Bansagi, B., Schlotter-Weigel, B., Glaser, D. *et al.* (2018) Novel SBF2 mutations and clinical spectrum of Charcot-Marie-Tooth neuropathy type 4B2. *Clin Genet*, **94**, 467-472.

94 Ng, A.A., Logan, A.M., Schmidt, E.J. and Robinson, F.L. (2013) The CMT4B disease-causing phosphatases Mtmr2 and Mtmr13 localize to the Schwann cell cytoplasm and endomembrane compartments, where they depend upon each other to achieve wild-type levels of protein expression. *Hum Mol Genet*, **22**, 1493-1506.

95 Robinson, D.C., Mammel, A.E., Logan, A.M., Larson, A.A., Schmidt, E.J., Condon, A.F. and Robinson, F.L. (2018) An In Vitro Model of Charcot-Marie-Tooth Disease Type 4B2 Provides Insight Into the Roles of MTMR13 and MTMR2 in Schwann Cell Myelination. *ASN Neuro*, **10**, 1759091418803282.

96 Bohlega, S., Alazami, A.M., Cupler, E., Al-Hindi, H., Ibrahim, E. and Alkuraya, F.S. (2011) A novel syndromic form of sensory-motor polyneuropathy is linked to chromosome 22q13.31-q13.33. *Clin Genet*, **79**, 193-195.

97 Flusser, H., Halperin, D., Kadir, R., Shorer, Z., Shelef, I. and Birk, O.S. (2018) Novel SBF1 splice-site null mutation broadens the clinical spectrum of Charcot-Marie-Tooth type 4B3 disease. *Clin Genet*, **94**, 473-479.

98 Manole, A., Horga, A., Gamez, J., Raguer, N., Salvado, M., San Millan, B., Navarro, C., Pittmann, A., Reilly, M.M. and Houlden, H. (2017) SBF1 mutations associated with autosomal recessive axonal neuropathy with cranial nerve involvement. *Neurogenetics*, **18**, 63-67.

99 Megarbane, A., Dorison, N., Rodriguez, D. and Tamraz, J. (2010) Multiple cranial nerve neuropathies, microcephaly, neurological degeneration, and "fork and bracket sign" in the MRI: a distinct syndrome. *Am J Med Genet A*, **152A**, 2297-2300.

100 Firestein, R., Nagy, P.L., Daly, M., Huie, P., Conti, M. and Cleary, M.L. (2002) Male infertility, impaired spermatogenesis, and azoospermia in mice deficient for the pseudophosphatase Sbf1. *J Clin Invest*, **109**, 1165-1172.

101 Liska, F., Chylikova, B., Janku, M., Seda, O., Vernerova, Z., Pravenec, M. and Kren, V. (2016) Splicing mutation in Sbf1 causes nonsyndromic male infertility in the rat. *Reproduction*, **152**, 215-223.

102 Balla, T. (2013) Phosphoinositides: tiny lipids with giant impact on cell regulation. *Physiol Rev*, **93**, 1019-1137.

103 Goebbels, S., Oltrogge, J.H., Kemper, R., Heilmann, I., Bormuth, I., Wolfer, S., Wichert, S.P., Mobius, W., Liu, X., Lappe-Siefke, C. *et al.* (2010) Elevated phosphatidylinositol 3,4,5-trisphosphate in glia triggers cell-autonomous membrane wrapping and myelination. *J Neurosci*, **30**, 8953-8964.

104 Sherman, D.L., Krols, M., Wu, L.M., Grove, M., Nave, K.A., Gangloff, Y.G. and Brophy, P.J. (2012) Arrest of myelination and reduced axon growth when Schwann cells lack mTOR. *J Neurosci*, **32**, 1817-1825.

105 Chow, C.Y., Zhang, Y., Dowling, J.J., Jin, N., Adamska, M., Shiga, K., Szigeti, K., Shy, M.E., Li, J., Zhang, X. *et al.* (2007) Mutation of FIG4 causes neurodegeneration in the pale tremor mouse and patients with CMT4J. *Nature*, **448**, 68-72.

106 Roberts, R. and Ktistakis, N.T. (2013) Omegasomes: PI3P platforms that manufacture autophagosomes. *Essays Biochem*, **55**, 17-27.

107 Raiborg, C., Schink, K.O. and Stenmark, H. (2013) Class III phosphatidylinositol 3-kinase and its catalytic product PtdIns3P in regulation of endocytic membrane traffic. *FEBS J*, **280**, 2730-2742.

108 Devereaux, K., Dall'Armi, C., Alcazar-Roman, A., Ogasawara, Y., Zhou, X., Wang, F., Yamamoto, A., De Camilli, P. and Di Paolo, G. (2013) Regulation of

mammalian autophagy by class II and III PI 3-kinases through PI3P synthesis. *PLoS One*, **8**, e76405.

109 Backer, J.M. (2008) The regulation and function of Class III PI3Ks: novel roles for Vps34. *Biochem J*, **410**, 1-17.

110 Zhou, X., Wang, L., Hasegawa, H., Amin, P., Han, B.X., Kaneko, S., He, Y. and Wang, F. (2010) Deletion of PIK3C3/Vps34 in sensory neurons causes rapid neurodegeneration by disrupting the endosomal but not the autophagic pathway. *Proc Natl Acad Sci U S A*, **107**, 9424-9429.

111 Jaber, N., Dou, Z., Lin, R.Z., Zhang, J. and Zong, W.X. (2012) Mammalian PIK3C3/VPS34: the key to autophagic processing in liver and heart. *Autophagy*, **8**, 707-708.

112 Willinger, T. and Flavell, R.A. (2012) Canonical autophagy dependent on the class III phosphoinositide-3 kinase Vps34 is required for naive T-cell homeostasis. *Proc Natl Acad Sci U S A*, **109**, 8670-8675.

113 Bechtel, W., Helmstadter, M., Balica, J., Hartleben, B., Kiefer, B., Hrnjic, F., Schell, C., Kretz, O., Liu, S., Geist, F. *et al.* (2013) Vps34 deficiency reveals the importance of endocytosis for podocyte homeostasis. *J Am Soc Nephrol*, **24**, 727-743.

114 Feltri, M.L., D'Antonio, M., Quattrini, A., Numerato, R., Arona, M., Previtali, S., Chiu, S.Y., Messing, A. and Wrabetz, L. (1999) A novel P0 glycoprotein transgene activates expression of lacZ in myelin-forming Schwann cells. *Eur J Neurosci*, **11**, 1577-1586.

115 Beirowski, B., Babetto, E., Golden, J.P., Chen, Y.J., Yang, K., Gross, R.W., Patti, G.J. and Milbrandt, J. (2014) Metabolic regulator LKB1 is crucial for Schwann cell-mediated axon maintenance. *Nat Neurosci*, **17**, 1351-1361.

116 Nodari, A., Zambroni, D., Quattrini, A., Court, F.A., D'Urso, A., Recchia, A., Tybulewicz, V.L., Wrabetz, L. and Feltri, M.L. (2007) Beta1 integrin activates Rac1 in

Schwann cells to generate radial lamellae during axonal sorting and myelination. *J Cell Biol*, **177**, 1063-1075.

117 Jang, S.Y., Shin, Y.K., Park, S.Y., Park, J.Y., Rha, S.H., Kim, J.K., Lee, H.J. and Park, H.T. (2015) Autophagy is involved in the reduction of myelinating Schwann cell cytoplasm during myelin maturation of the peripheral nerve. *PLoS One*, **10**, e0116624.

118 Grove, M., Komiyama, N.H., Nave, K.A., Grant, S.G., Sherman, D.L. and Brophy, P.J. (2007) FAK is required for axonal sorting by Schwann cells. *J Cell Biol*, **176**, 277-282.

119 Schu, P.V., Takegawa, K., Fry, M.J., Stack, J.H., Waterfield, M.D. and Emr, S.D. (1993) Phosphatidylinositol 3-kinase encoded by yeast VPS34 gene essential for protein sorting. *Science*, **260**, 88-91.

120 Futter, C.E., Collinson, L.M., Backer, J.M. and Hopkins, C.R. (2001) Human VPS34 is required for internal vesicle formation within multivesicular endosomes. *J Cell Biol*, **155**, 1251-1264.

121 Johnson, E.E., Overmeyer, J.H., Gunning, W.T. and Maltese, W.A. (2006) Gene silencing reveals a specific function of hVps34 phosphatidylinositol 3-kinase in late versus early endosomes. *J Cell Sci*, **119**, 1219-1232.

122 Sorkin, A. and Goh, L.K. (2009) Endocytosis and intracellular trafficking of ErbBs. *Exp Cell Res*, **315**, 683-696.

123 Norrmen, C. and Suter, U. (2013) Akt/mTOR signalling in myelination. *Biochem Soc Trans*, **41**, 944-950.

124 Wood, T.L., Bercury, K.K., Cifelli, S.E., Mursch, L.E., Min, J., Dai, J. and Macklin, W.B. (2013) mTOR: a link from the extracellular milieu to transcriptional regulation of oligodendrocyte development. *ASN Neuro*, **5**, e00108.

125 Monk, K.R., Feltri, M.L. and Taveggia, C. (2015) New insights on Schwann cell development. *Glia*, **63**, 1376-1393.

126 Scherer, S.S. and Wrabetz, L. (2008) Molecular mechanisms of inherited demyelinating neuropathies. *Glia*, **56**, 1578-1589.

127 Alanko, J., Mai, A., Jacquemet, G., Schauer, K., Kaukonen, R., Saari, M., Goud, B. and Ivaska, J. (2015) Integrin endosomal signalling suppresses anoikis. *Nat Cell Biol*, **17**, 1412-1421.

128 Berti, C., Bartesaghi, L., Ghidinelli, M., Zambroni, D., Figlia, G., Chen, Z.L., Quattrini, A., Wrabetz, L. and Feltri, M.L. (2011) Non-redundant function of dystroglycan and beta1 integrins in radial sorting of axons. *Development*, **138**, 4025-4037.

129 Pereira, J.A., Benninger, Y., Baumann, R., Goncalves, A.F., Ozcelik, M., Thurnherr, T., Tricaud, N., Meijer, D., Fassler, R., Suter, U. *et al.* (2009) Integrin-linked kinase is required for radial sorting of axons and Schwann cell remyelination in the peripheral nervous system. *J Cell Biol*, **185**, 147-161.

130 Feltri, M.L., Graus Porta, D., Previtali, S.C., Nodari, A., Migliavacca, B., Cassetti, A., Littlewood-Evans, A., Reichardt, L.F., Messing, A., Quattrini, A. *et al.* (2002) Conditional disruption of beta 1 integrin in Schwann cells impedes interactions with axons. *J Cell Biol*, **156**, 199-209.

131 Simonsen, A., Lippe, R., Christoforidis, S., Gaullier, J.M., Brech, A., Callaghan, J., Toh, B.H., Murphy, C., Zerial, M. and Stenmark, H. (1998) EEA1 links PI(3)K function to Rab5 regulation of endosome fusion. *Nature*, **394**, 494-498.

132 Fernandez-Borja, M., Wubbolts, R., Calafat, J., Janssen, H., Divecha, N., Dusseljee, S. and Neefjes, J. (1999) Multivesicular body morphogenesis requires phosphatidyl-inositol 3-kinase activity. *Curr Biol*, **9**, 55-58.

133 Poteryaev, D., Datta, S., Ackema, K., Zerial, M. and Spang, A. (2010) Identification of the switch in early-to-late endosome transition. *Cell*, **141**, 497-508.

134 Grove, M. and Brophy, P.J. (2014) FAK is required for Schwann cell spreading on immature basal lamina to coordinate the radial sorting of peripheral axons with myelination. *J Neurosci*, **34**, 13422-13434.

135 Rasband, M.N. and Peles, E. (2015) The Nodes of Ranvier: Molecular Assembly and Maintenance. *Cold Spring Harb Perspect Biol*, **8**, a020495.

136 Pooya, S., Liu, X., Kumar, V.B., Anderson, J., Imai, F., Zhang, W., Ciraolo, G., Ratner, N., Setchell, K.D., Yoshida, Y. *et al.* (2014) The tumour suppressor LKB1 regulates myelination through mitochondrial metabolism. *Nat Commun*, **5**, 4993.

137 Shy, M.E. (2011) Inherited peripheral neuropathies. *Continuum (Minneap Minn)*, **17**, 294-315.

138 Amoasii, L., Hnia, K. and Laporte, J. (2012) Myotubularin phosphoinositide phosphatases in human diseases. *Curr Top Microbiol Immunol*, **362**, 209-233.

139 Firestein, R. and Cleary, M.L. (2001) Pseudo-phosphatase Sbf1 contains an N-terminal GEF homology domain that modulates its growth regulatory properties. *J Cell Sci*, **114**, 2921-2927.

140 Alazami, A.M., Alzahrani, F., Bohlega, S. and Alkuraya, F.S. (2014) SET binding factor 1 (SBF1) mutation causes Charcot-Marie-tooth disease type 4B3. *Neurology*, **82**, 1665-1666.

141 Romani, M., Mehawej, C., Mazza, T., Megarbane, A. and Valente, E.M. (2016) "Fork and bracket" syndrome expands the spectrum of SBF1-related sensory motor polyneuropathies. *Neurol Genet*, **2**, e61.

142 Robinson, F.L., Niesman, I.R., Beiswenger, K.K. and Dixon, J.E. (2008) Loss of the inactive myotubularin-related phosphatase Mtmr13 leads to a Charcot-Marie-Tooth 4B2-like peripheral neuropathy in mice. *Proc Natl Acad Sci U S A*, **105**, 4916-4921.

143 Tersar, K., Boentert, M., Berger, P., Bonneick, S., Wessig, C., Toyka, K.V., Young, P. and Suter, U. (2007) Mtmr13/Sbf2-deficient mice: an animal model for CMT4B2. *Hum Mol Genet*, **16**, 2991-3001.

144 Lancaster, E., Li, J., Hanania, T., Liem, R., Scheideler, M.A. and Scherer, S.S. (2018) Myelinated axons fail to develop properly in a genetically authentic mouse model of Charcot-Marie-Tooth disease type 2E. *Exp Neurol*, **308**, 13-25.

145 Kudryashova, E., Wu, J., Havton, L.A. and Spencer, M.J. (2009) Deficiency of the E3 ubiquitin ligase TRIM32 in mice leads to a myopathy with a neurogenic component. *Hum Mol Genet*, **18**, 1353-1367.

146 Poitelon, Y., Bogni, S., Matafora, V., Della-Flora Nunes, G., Hurley, E., Ghidinelli, M., Katzenellenbogen, B.S., Taveggia, C., Silvestri, N., Bachi, A. *et al.* (2015) Spatial mapping of juxtacrine axo-glial interactions identifies novel molecules in peripheral myelination. *Nat Commun*, **6**, 8303.

147 Poitelon, Y., Lopez-Anido, C., Catignas, K., Berti, C., Palmisano, M., Williamson, C., Ameroso, D., Abiko, K., Hwang, Y., Gregorieff, A. *et al.* (2016) YAP and TAZ control peripheral myelination and the expression of laminin receptors in Schwann cells. *Nat Neurosci*, **19**, 879-887.

148 Robinson, F.L. and Dixon, J.E. (2006) Myotubularin phosphatases: policing 3-phosphoinositides. *Trends Cell Biol*, **16**, 403-412.

149 Burgo, A., Sotirakis, E., Simmler, M.C., Verraes, A., Chamot, C., Simpson, J.C., Lanzetti, L., Proux-Gillardeaux, V. and Galli, T. (2009) Role of Varp, a Rab21 exchange factor and TI-VAMP/VAMP7 partner, in neurite growth. *EMBO Rep*, **10**, 1117-1124.

150 Clements, M.P., Byrne, E., Camarillo Guerrero, L.F., Cattin, A.L., Zakka, L., Ashraf, A., Burden, J.J., Khadayate, S., Lloyd, A.C., Marguerat, S. *et al.* (2017) The Wound Microenvironment Reprograms Schwann Cells to Invasive Mesenchymal-like Cells to Drive Peripheral Nerve Regeneration. *Neuron*, **96**, 98-114 e117.

151 Auer-Grumbach, M., Toegel, S., Schabhuttl, M., Weinmann, D., Chiari, C., Bennett, D.L.H., Beetz, C., Klein, D., Andersen, P.M., Bohme, I. *et al.* (2016) Rare Variants in MME, Encoding Metalloprotease Neprilysin, Are Linked to Late-Onset Autosomal-Dominant Axonal Polyneuropathies. *Am J Hum Genet*, **99**, 607-623.

152 Balastik, M., Ferraguti, F., Pires-da Silva, A., Lee, T.H., Alvarez-Bolado, G., Lu, K.P. and Gruss, P. (2008) Deficiency in ubiquitin ligase TRIM2 causes accumulation of neurofilament light chain and neurodegeneration. *Proc Natl Acad Sci U S A*, **105**, 12016-12021.

153 Barneo-Munoz, M., Juarez, P., Civera-Tregon, A., Yndriago, L., Pla-Martin, D., Zenker, J., Cuevas-Martin, C., Estela, A., Sanchez-Arago, M., Forteza-Vila, J. *et al.* (2015) Lack of GDAP1 induces neuronal calcium and mitochondrial defects in a knockout mouse model of charcot-marie-tooth neuropathy. *PLoS Genet*, **11**, e1005115.

154 Strickland, A.V., Rebelo, A.P., Zhang, F., Price, J., Bolon, B., Silva, J.P., Wen, R. and Zuchner, S. (2014) Characterization of the mitofusin 2 R94W mutation in a knock-in mouse model. *J Peripher Nerv Syst*, **19**, 152-164.

155 Zhu, Q., Lindenbaum, M., Levavasseur, F., Jacomy, H. and Julien, J.P. (1998) Disruption of the NF-H gene increases axonal microtubule content and velocity of neurofilament transport: relief of axonopathy resulting from the toxin beta,beta'-iminodipropionitrile. *J Cell Biol*, **143**, 183-193.

156 Cong, L., Ran, F.A., Cox, D., Lin, S., Barretto, R., Habib, N., Hsu, P.D., Wu, X., Jiang, W., Marraffini, L.A. *et al.* (2013) Multiplex genome engineering using CRISPR/Cas systems. *Science*, **339**, 819-823.

157 Merte, J., Wang, Q., Vander Kooi, C.W., Sarsfield, S., Leahy, D.J., Kolodkin, A.L. and Ginty, D.D. (2010) A forward genetic screen in mice identifies Sema3A(K108N), which binds to neuropilin-1 but cannot signal. *J Neurosci*, **30**, 5767-5775.

158 Ness, J.K., Snyder, K.M. and Tapinos, N. (2013) Lck tyrosine kinase mediates beta1-integrin signalling to regulate Schwann cell migration and myelination. *Nat Commun*, **4**, 1912.

159 Novak, N., Bar, V., Sabanay, H., Frechter, S., Jaegle, M., Snapper, S.B., Meijer, D. and Peles, E. (2011) N-WASP is required for membrane wrapping and myelination by Schwann cells. *J Cell Biol*, **192**, 243-250.

160 Roos, A., Weis, J., Korinthenberg, R., Fehrenbach, H., Hausler, M., Zuchner, S., Mache, C., Hubmann, H., Auer-Grumbach, M. and Senderek, J. (2015) Inverted formin 2-related Charcot-Marie-Tooth disease: extension of the mutational spectrum and pathological findings in Schwann cells and axons. *J Peripher Nerv Syst*, **20**, 52-59.

161 Golan, N., Kartvelishvily, E., Spiegel, I., Salomon, D., Sabanay, H., Rechav, K., Vainshtein, A., Frechter, S., Maik-Rachline, G., Eshed-Eisenbach, Y. *et al.* (2013) Genetic deletion of Cadm4 results in myelin abnormalities resembling Charcot-Marie-Tooth neuropathy. *J Neurosci*, **33**, 10950-10961.

162 Chugh, P. and Paluch, E.K. (2018) The actin cortex at a glance. *J Cell Sci*, **131**.

163 McClatchey, A.I. (2014) ERM proteins at a glance. *J Cell Sci*, **127**, 3199-3204.

164 Gatto, C.L., Walker, B.J. and Lambert, S. (2003) Local ERM activation and dynamic growth cones at Schwann cell tips implicated in efficient formation of nodes of Ranvier. *J Cell Biol*, **162**, 489-498.

165 Snaidero, N., Mobius, W., Czopka, T., Hekking, L.H., Mathisen, C., Verkleij, D., Goebbels, S., Edgar, J., Merkler, D., Lyons, D.A. *et al.* (2014) Myelin membrane wrapping of CNS axons by PI(3,4,5)P3-dependent polarized growth at the inner tongue. *Cell*, **156**, 277-290.

166 Zuchero, J.B., Fu, M.M., Sloan, S.A., Ibrahim, A., Olson, A., Zaremba, A., Dugas, J.C., Wienbar, S., Caprariello, A.V., Kantor, C. *et al.* (2015) CNS myelin wrapping is driven by actin disassembly. *Dev Cell*, **34**, 152-167.

167 Charras, G.T., Hu, C.K., Coughlin, M. and Mitchison, T.J. (2006) Reassembly of contractile actin cortex in cell blebs. *J Cell Biol*, **175**, 477-490.

168 Scherer, S.S., Xu, T., Crino, P., Arroyo, E.J. and Gutmann, D.H. (2001) Ezrin, radixin, and moesin are components of Schwann cell microvilli. *J Neurosci Res*, **65**, 150-164.

169 Wang, H., Tewari, A., Einheber, S., Salzer, J.L. and Melendez-Vasquez, C.V. (2008) Myosin II has distinct functions in PNS and CNS myelin sheath formation. *J Cell Biol*, **182**, 1171-1184.

170 Sparrow, N., Manetti, M.E., Bott, M., Fabianac, T., Petrilli, A., Bates, M.L., Bunge, M.B., Lambert, S. and Fernandez-Valle, C. (2012) The actin-severing protein cofilin is downstream of neuregulin signaling and is essential for Schwann cell myelination. *J Neurosci*, **32**, 5284-5297.